A TOG:αβ-TUBULIN COMPLEX STRUCTURE REVEALS

CONFORMATION-BASED MECHANISMS FOR

A MICROTUBULE POLYMERASE

APPROVED BY SUPERVISORY COMMITTEE

Luke M. Rice, Ph.D.

Joseph P. Albanesi, Ph.D.

Michael K. Rosen, Ph.D.

Hongtao Yu, Ph.D.

DEDICATION

This dissertation is dedicated to the two amazing men in my life,

my son Arda and my husband Ulas

A TOG:αβ-TUBULIN COMPLEX STRUCTURE REVEALS CONFORMATION-BASED MECHANISMS FOR A MICROTUBULE POLYMERASE

by

PELIN AYAZ

DISSERTATION

Presented to the Faculty of the Graduate School of Biomedical Sciences

The University of Texas Southwestern Medical Center at Dallas

In Partial Fulfillment of the Requirements

For the Degree of

DOCTOR OF PHILOSOPHY

The University of Texas Southwestern Medical Center at Dallas

Dallas, Texas

December, 2012

ACKNOWLEDGEMENTS

First and foremost, I would like to express my profound gratitude to Dr. Luke Rice, my advisor and mentor, for the opportunity to start this exciting project. I am very lucky to be the first Ph.D. student in his lab and I am grateful for the time and effort he invested to work with me and advise me along the course of my studies. I thank him for the exciting discussions we had, for challenging me, for teaching me to be rigorously critical and accepting me to his lab as an engineer and guiding me along the way to graduate as a scientist.

Second, I want to thank my committee members, Drs. Joseph Albanesi, Michael Rosen and Hongtao Yu for taking the time to review my work and offer their guidance and support and raising challenging questions to improve it for better.

I would also like to thank all past and present members of the Rice Lab, Dr. Xuecheng Ye, Dr. Vinu Johnson, Felipe Piedra, Patrick Huddleston, Lingyan Anderson, and Emily Garza. I have learnt a lot from them.

Next, I would like to thank Dr. Dominika Borek for helping me with the crystallization, the X-Ray data processing, model building and being very generous with sharing material and experience. I also thank Dr. Shae Padrick for helping me with the fluorescence anisotropy and the FPLC.

I would like to thank Dr. Chad Brautigam for the amazing AUC experiments, and Dr. Diana Tomchick, Dr. Zhe Chen, Helen Aronovich in the Univ. of Texas Southwestern Structural Biology Core Facility for advice and assistance.

I thank Drs. Michael Rosen, Youxing Jiang, for sharing equipment and reagents.

I would also like to extend my sincere gratitude to my family; my mother Aysen Armutlu, my father Muharrem Armutlu and my brother Emre Armutlu for their support and love, they always encouraged me and supported me in everything I decided to do. Finally, I dedicate this work to my own family that we have just started; my husband Ulas Ayaz, and my three month old son Arda Ayaz. I am very fortunate to have them by my side.

A TOG:αβ-TUBULIN COMPLEX STRUCTURE REVEALS

CONFORMATION-BASED MECHANISMS FOR

A MICROTUBULE POLYMERASE

PELIN AYAZ, Ph.D.

The University of Texas Southwestern Medical Center at Dallas, 2012

LUKE M. RICE, Ph.D.

Stu2p/XMAP215/Dis1 family proteins are evolutionarily conserved regulatory factors that use αβ-tubulin-interacting TOG (tumor overexpressed gene) domains to catalyze fast microtubule growth. Catalysis requires that these polymerases discriminate between unpolymerized and polymerized forms of αβ-tubulin, but how they do so has remained unclear. In this study, we first introduce the polymerization blocked mutants of αβ-tubulins that we developed as unique tools for biochemical studies of αβ-tubulins to avoid the difficulties that has arisen from the self-assembly tendency of tubulins, then we report the structure of the TOG1 domain from Stu2p bound to the plus end

polymerization blocked yeast αβ-tubulin we created to facilitate crystallization. Our structure and further biochemical characterizations of the TOG1:αβ-tubulin complex showed that TOG1 binds αβ-tubulin in a way that excludes equivalent binding of a second TOG domain. Furthermore, TOG1 preferentially binds a "curved" conformation of αβ-tubulin that cannot be incorporated into microtubules, contacting α- and β-tubulin surfaces that do not participate in microtubule assembly. Conformation-selective interactions with αβ-tubulin explain how TOG-containing polymerases discriminate between unpolymerized and polymerized forms of αβ-tubulin, and how they selectively recognize the growing end of the microtubule.

TABLE OF CONTENTS

PRIOR PUBLICATIONS

Ayaz P, Ye X, Huddleston P, Brautigam CA, Rice LM. A TOG:alpha/beta-tubulin Complex Structure Reveals Conformation-Based Mechanisms For a Microtubule Polymerase. **Science**. 2012; 337(6096):857-60

Johnson V, Ayaz P, Huddleston P, Rice LM. Design, Overexpression, and Purification of Polymerization-Blocked Yeast αβ-Tubulin Mutants. **Biochemistry**. 2011;50(40):8636-44

Armutlu P, Ozdemir ME, Ozdas S, Kavakli IH, Turkay M. Discovery of Novel CYP17 Inhibitors for the Treatment of Prostate Cancer with Structure-Based Drug Design. **Lett Drug Des Discov**. 2009;6(5):337-44.

Armutlu P, Ozdemir ME, Uney-Yuksektepe F, Kavakli IH, Turkay M. Classification of drug molecules considering their IC50 values using mixed-integer linear programming based hyper-boxes method. **Bmc Bioinformatics**. 2008;9:-.

LIST OF FIGURES

LIST OF TABLES

LIST OF DEFINITIONS

Alp14 – Altered polarity protein 14

AUC – Analytical ultracentrifugation

Bik1p – Nuclear fusion protein BIK1

CD – Circular dichroism

Ch-TOG – Colonic and hepatic tumor over-expressed gene

CLASP – Cytoplasmic linker-associated proteins

CLIP-170 – Cytoplasmic linker protein 170

DNA – Deoxyribonucleic acid

Dis1 – Distorted Trichomes 1

GDP – Guanosine diphosphate

GTP – Guanosine-5'-triphosphate

EB1– End binding 1

HEAT – Huntington, elongation factor 2, phosphatase A2, TOR PI-3 kinase

Kd – Equilibrium dissociation constant

kDa – Kilo dalton

M – molar

Mal3 – Microtubule integrity protein mal3

MAPs – Microtubule-associated proteins

MOR1 – Microtubule organization 1

MSPS – Mini spindles

MT – Microtubule

MTOC – Tumor overexpressed gene

PEG – Poly ethylene glycol

Stu2p – Suppressor of Tubulin 2

TACC – Transforming acidic coiled-coil

TOG – Tumor overexpressed gene

TOGL – Tumor overexpressed gene like

Tub1 – alpha-tubulin

Tub2 – beta-tubulin

Xmap215 – Microtubule Associated Protein 215 kDa

Zyg9 – Zygote defective protein 9

CHAPTER ONE

INTRODUCTION

Microtubules and dynamic instability

Microtubules are dynamic polymers that are essential in vital cell processes and that are targeted for anti-cancer therapy

Microtubules (MTs) are dynamics protein polymers that are made out of hetero-dimeric protein αβ-tubulin. Vital cellular processes such as cell division, membrane trafficking and cell morphogenesis depend on the rapid reorganization of the MT network (1). MTs facilitate this by stochastically switching between growing and shrinking at their ends. The combination of growth, shrinkage and the rapid transitions between the two is known as dynamic instability (2) and, it can be reconstituted in vitro (3). Many current anti-cancer drugs that target microtubules affect MT dynamics (reviewed in (4)).

The conformational state (the curvature) of αβ-tubulin affects MT dynamics by affecting the biochemistry of the interactions of neighboring αβ-tubulins in the lattice

The αβ-tubulins assemble in a head-to-tail fashion to form protofilaments with distinct polarity (Figure 1.1.) (5, 6). Typically, 13 protofilaments associate laterally to compose the hollow cylindrical tube polymer MT, which has a diameter of approximately 25 nm. (Figure 1.1.) (7). During a catastrophe event, the MT stops growing and shrinks very rapidly as the protofilaments peel off from the MT plus ends (5), whereas during a rescue event MTs stop shrinking and start to grow again. The dynamic instability requires

energy and this energy cost is paid by the energy release resulting from the GTP (Guanosine-5'-triphosphate) hydrolysis. The GTP bound to the α-tubulin is non-hydrolysable and the GTP bound to β-tubulin is hydrolyzed to GDP during -or soon after - longitudinal assembly (Figure 1.2.).

The body of the MT, and the plus ends of growing and shrinking MTs have distinct structures (8-11). The body of the MT is made out of straight protofilaments, whereas the shrinking MT ends show strongly curved protofilament extensions as they peel off. Partially curved, sheet-like extensions of multiple protofilaments are observed at the growing ends of the MTs. (Figure 1.2.) Crystallographic studies of αβ-tubulin only provide atomic models for the 'straight' (12, 13) and 'curved' (14) conformations (Figure 1.3.). These studies used drugs, regulatory proteins or manipulated solution conditions to trap αβ-tubulin assemblies to promote crystallization and the solution conformation of unpolymerized αβ-tubulin and the question of whether the nucleotide bound to β-tubulin (GDP- Guanosine diphosphate /GTP) affects this conformation of unpolymerized αβ-tubulin or not remains under debate (15-19, 68). One model suggests that GDP-bound unpolymerized αβ-tubulin has a curved conformation and GTP-bound unpolymerized αβ-tubulin has a straight conformation, and the other model suggests an induced fit mechanism where the allosteric effects of lattice incorporation result in the straightening of the naturally curved GTP-bound αβ-tubulin. However, neither two models nor their supporting evidence can rule out the possibility of an equilibrium of curved and straight conformations of unpolymerized αβ-tubulin, where one of the conformations might be more populated than the other, and ratio of their populations might be affected by the

GTP/GDP nucleotide state. There is also evidence suggesting nucleotide-dependent effects on lateral contacts when αβ–tubulins are part of the MT lattice (69, 70).

The conformational state (the curvature) of αβ-tubulin affects the longitudinal and lateral MT polymerization surfaces, presumably affecting the biochemistry of the interactions of neighboring αβ-tubulins in the lattice. Ultimately, the lack of structural insight on αβ-tubulins undermines our understanding of the molecular details of dynamic instability, how MTs interact with regulatory proteins and the molecular mechanisms by which MT dynamics are regulated.

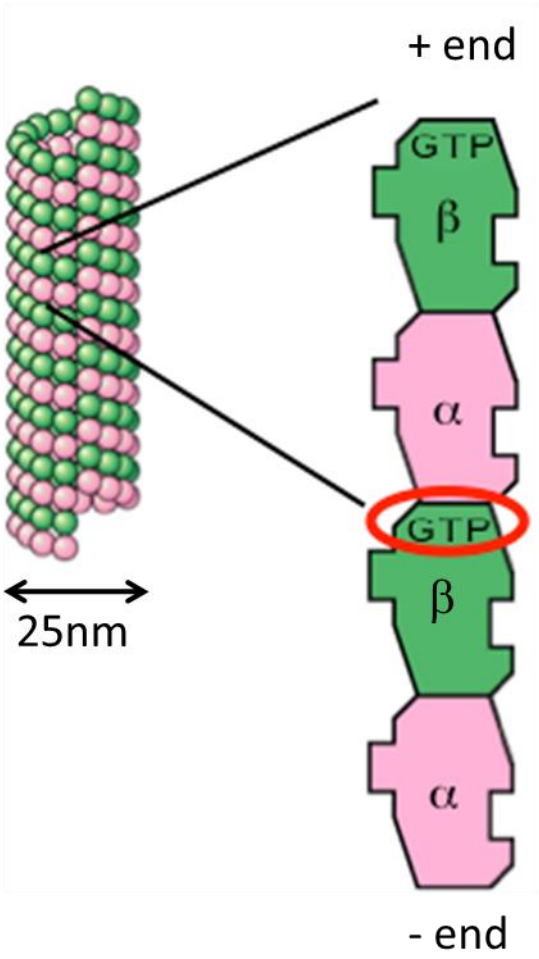

Figure 1.1: The αβ-tubulins assemble in a head-to-tail fashion to form the hollow cylindrical microtubule with distinct polarity. The red oval highlights the hydrolysable GTP site bound to the β-tubulin.

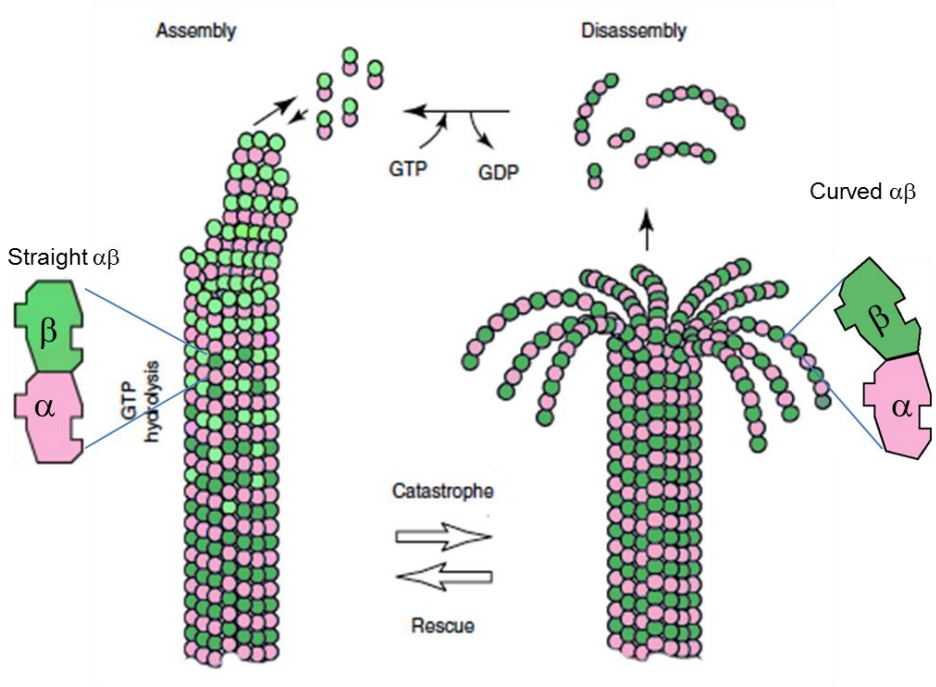

Figure 1.2: Growing and shirinking MTs have characteristic conformations at their plus ends.

During assembly sheet like polymer structures made out of non-straight αβ-tubulins are observed at the plus ends. GTP bound αβ-tubulin heterodimers assemble on the plus ends to form the GTP-cap (lighter green). Upon incorporation the αβ-tubulin on the top initiates the GTP hyrolysis of the one below it. During disassembly protofilaments made of only GDP αβ-tubulins (darker green) were observed to curve and peel off. The transition from growth (assembly) to shrinking (disassembly) is called a catastrophe event whereas the transition from shrinking to growth is called a rescue event.

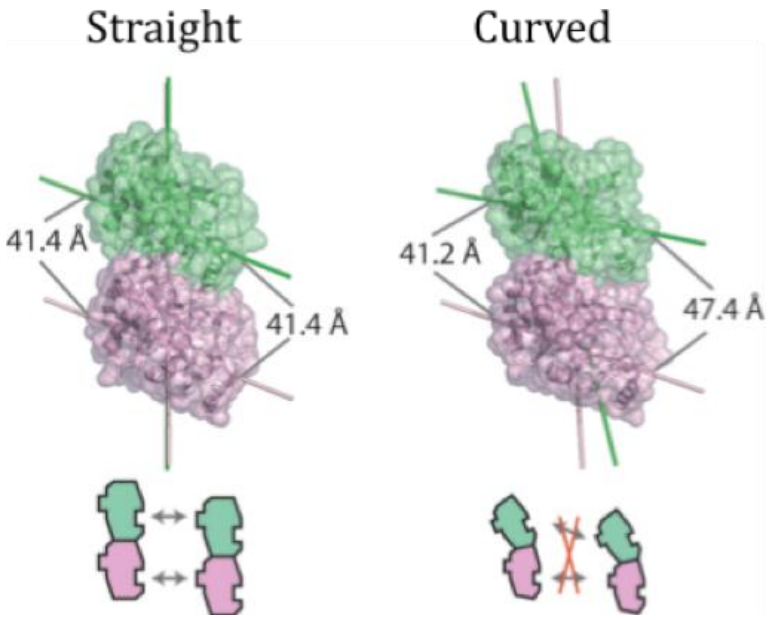

Figure 1.3: Two conformations of αβ-tubulin.

Longitudinal and lateral interaction surfaces are aligned in the straight (1JFF, left), but not in the curved (1SA0, right) conformation. In the curved conformation, the α- and β-tubulin protofilament and lateral interaction axes are skewed by 11° and 6°, respectively; these rearrangements separate equivalent laterally interacting atoms by up to 6 Å. This misalignment of interfaces presumably destabilizes lateral interactions between curved αβ-tubulins.

Regulation of microtubule dynamics

A comprehensive understanding of the structural and molecular mechanisms that generate and regulate dynamic instability remains elusive

In vivo, the dynamic behavior of microtubules is highly regulated by conserved regulatory proteins that bind to MT lattice or MT plus ends (5). Even though these conserved regulatory proteins (MAPs - Microtubule-associated proteins) have been studied extensively, the mechanisms of regulation are still poorly understood at a molecular level (6). The lack of structural information is partly why our understanding of how these regulatory proteins and drugs recognize and regulate αβ-tubulin is limited.

Proteins belonging to the Stu2p/XMAP215/Dis1 family interact with αβ-tubulins using their N-terminal TOG domains to promote MT elongation

Stu2p/XMAP215/Dis1 (Suppressor of Tub2 / Microtubule Associated Protein 215 kDa / Distorted Trichomes 1) proteins belong to a conserved family of proteins that are MT growth accelerators. They are conserved from yeast to humans and they have vital cellular roles in regulating MT dynamics during the formation of the mitotic spindle and the interphase (20, 21). These are elongated proteins that have conserved N-terminal TOG (Tumor overexpressed gene) domains that are αβ-tubulin binding modules (22). CLASP (Cytoplasmic linker-associated proteins) proteins, which are another conserved family of proteins, also have TOG domains and they are involved in MT rescue and MT catastrophe suppression (22-26).

Stu2p/XMAP215 proteins

Proteins from the Stu2p/XMAP215/Dis1 family are MT polymerases

The Stu2p/XMAP215/Dis1 family of proteins uses multiple TOG domains that function together to promote MT elongation (27). Stu2p, the Saccharomyces cerevisae member of this family, is essential to promote MT growth in yeast (28). Other family members include: Xenopus laevis XMAP215, Schizosaccharomyces pombe Alp14 (Altered polarity protein 14) and Dis1 (Distorted trichomes 1), Arabidopsis thaliana MOR1 (Microtubule organization 1), Caenorhabditis elegans Zyg9 (Zygote defective protein 9), Drosophila melanogaster MiniSpindles (MSPS) and human ch-TOG (Colonic and hepatic tumor over-expressed gene) (28-33).

Previous studies show that the members of Stu2p/XMAP215/Dis1 localize to MT plus ends, MT organizing centers, kinetochores and MT lattices. In vivo studies show loss of function of these proteins results in reduced MT growth rates, increased catastrophe frequencies and short interphase MTs (28, 29, 32, 34-36). Knockdown of these proteins was also shown to lead to spindle abnormalities and short astral MTs (32, 37, 38). They are also required for the regulation of kinetochore-MT attachment (29, 39). Stu2p, the yeast member of this protein family, was shown to be involved in the elongation of MTs from the kinetochore and enable the spindle-kinetochore attachment (40). XMAP215 was first identified in Xenopus extracts, where it was shown to promote MT assembly (41). Later, in vitro studies with XMAP215 showed that this protein binds to the growing MT plus ends where it acts to increase growth rates up to tenfold (24, 42). To do that, each XMAP215 localizes to the plus end of the MT, resides there moving

with the plus end as it grows, long enough to promote the addition of about 25 αβ-tubulin heterodimers to the growing end before it dissociates (24). Having multiple αβ-tubulin binding TOG domains, XMAP215 was initially thought to bind multiple αβ-tubulins at a time and load them to the growing MT plus end as preformed αβ-tubulin oligomers (43). However, other studies presented results suggesting that a single XMAP215 can bind only one αβ-tubulin heterodimer at a time (22, 24). It was also shown that XMAP215 and Stu2p could also catalyze the reverse reaction, the depolymerization of the MTs. On MTs that were stabilized with a non-hydrolysable GTP analog GMPCPP, in the presence of low concentrations of soluble αβ-tubulin these proteins acted as MT depolymerases (44, 45). Therefore, Stu2p/XMAP215/Dis1 family of proteins were suggested to act catalytically as processive MT polymerases, and they promote reversibly the addition of single αβ-tubulin heterodimers onto the growing MT plus end. However, the molecular mechanisms by which Stu2p/XMAP215/Dis1 family of proteins recognize αβ-tubulin heterodimers in solution, at the growing MT plus end, and as a part of the MT lattice to promote assembly remain unknown.

Other roles of the Stu2p/XMAP215/Dis1 family of proteins remain to be discovered

S. pombe has two proteins that belong in this family: Alp14 and Dis1 (27, 29). Alp14 was shown to promote αβ-tubulin-MT assembly at MT plus ends as Stu2p and XMAP215 (46), whereas Dis1 localizes at kinetochores binding to the Ndc80 complex and functions at spindles and kinetochores during chromosome segregation (47). Studies also show that Dis1 localizes along the MT lattice during interphase, and was suggested

to be involved in bundling MTs in the spindle and interphase arrays (48). S. cerevisae member Stu2p was shown to interact with the EB1 (End binding 1) and CLIP-170 (Cytoplasmic linker protein 170) orthologs Mal3 (Microtubule integrity protein 3) and Bik1p (nuclear fusion protein Bik1) (49). Many Stu2p/XMAP215/Dis1 family members were shown to be targeted to MTOCs (Microtubule organizing centers) by conserved transforming acidic coiled-coil (TACC) proteins to stabilize MTs during mitosis (49-53). There, complexes of XMAP215-TACC proteins function to increase the number and length of MTs. It is argued that to achieve that they promote the stabilization or anchoring of the MT minus ends (50, 53, 54).

TOG Domains

Conserved N-terminal TOG domains are αβ-tubulin binding modules

N-terminal TOG domains of Stu2p/XMAP215/Dis1 family exhibit a high degree of structural conservation. They are around 240 residue long repeats and CLASP family proteins also contain TOGL (TOGLike) domains that share weak sequence homology with the Stu2p/XMAP215/Dis1 family TOGs. The number of TOG domains varies in different organisms. For instance, yeast Stu2p/XMAP215/Dis1 proteins Alp14, Dis1, Stu2p have two TOG domains, C.elegans Zyg9 has three, and Xenopus XMAP215, human ch-TOG and Drosophila MSPS have five TOG domains (Figure 1.4.). CLASP family of proteins also contains a minimum of two conserved TOGL domains (25, 55). Even though the yeast Stu2p/XMAP215/Dis1 proteins only have two TOG domains, they exist as homodimers (22).

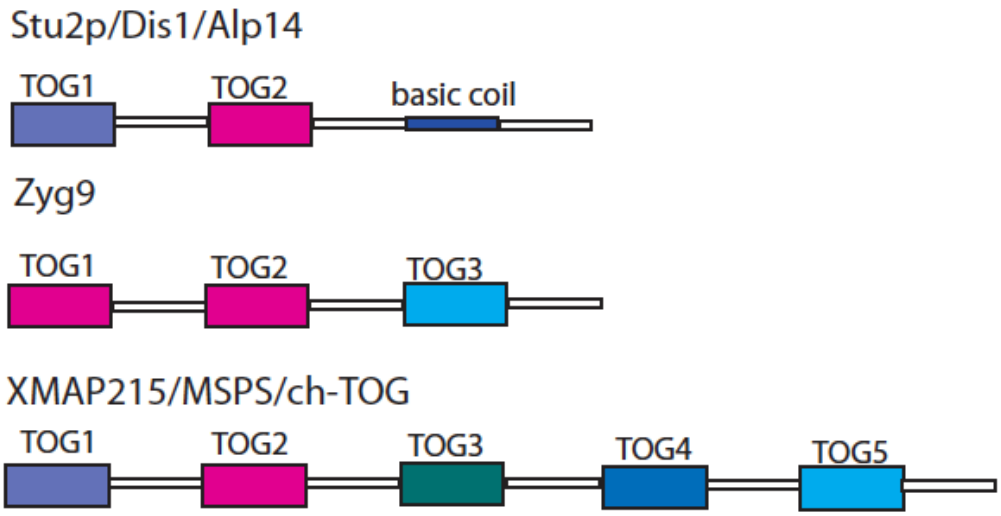

Figure 1.4: Domain organization of Stu2p/XMAP215/Dis1 family of proteins.

Yeast Alp14, Dis1, Stu2p have two TOG domains, C.elegans Zyg9 has three, and Xenopus XMAP215, human ch-TOG and Drosophila MSPS have five TOG domains. TOG domains are colored based on the conserved phylogenetic classes from the sequence alignment (56, 57).

The main function of these Stu2p/XMAP215/Dis1 family TOGs and CLASP TOGL domains is to bind to αβ-tubulin heterodimers (22, 23, 25, 58). The TOG and TOG like domains of XMAP215, Stu2p and Cls1p were shown to bind non-polymerized αβ-tubulin heterodimers in solution, however they did not bind the αβ-tubulin that are incorporated in MT polymer (24, 25). The implication is: the TOG domains recognize and differentiate features of non-polymerized αβ-tubulin from when it is incorporated into the MT lattice.

The S. cerevisiae Stu2p is a homodimer that contains two different TOG domains in each of its monomers. The stoichiometry of binding to a αβ-tubulin heterodimer was thought to be one Stu2p homodimer to one αβ-tubulin heterodimer in solution based on a gel filtration binding assay (22). Stu2p has a C-terminal coiled coil region that is responsible for its dimerization (Figure 1.4.). XMAP215, which is a monomer, on the other hand has five TOG domains, and the stoichiometry of binding to a αβ-tubulin heterodimer also was thought to be one XMAP215 per tubulin dimer (24).

Crystal structures of three individual TOG domains from yeast, Drosophila and C. elegans in combination with mutational analysis of surface residues on the TOG domains define the binding site for αβ-tubulin. These domains contain a conserved a-helical fold consisting of six HEAT (Huntington, elongation factor 2, phosphatase 2A, TOR PI-3 kinase) repeats (Figure 1.5. bottom) (23, 26). The sequence similarity among the TOG domains is around 6%. The conserved regions are either hydrophobic residues buried between neighboring α-helices to stabilize the overall globular structure of the domain or they are located on one edge of the TOG domain containing five short loops

(L1 – L5) that connect the HEAT repeats. These loops make up the most conserved surface of the TOG domains (Figure1.5.), and mutations of the conserved surface residues of these loops disrupt binding to the αβ-tubulin heterodimer in solution (26). This demonstrates that the surface composed of loops L1 –L5 of the TOG domains is the αβ-tubulin binding face of these domains. Using the PROMALS web server we performed a multiple sequence alignment of the αβ-tubulin interacting L1- L5 loops within the different TOG domains and showed that several residues in these are strictly conserved across all TOG classes (56, 57) (Figure 1.6.).

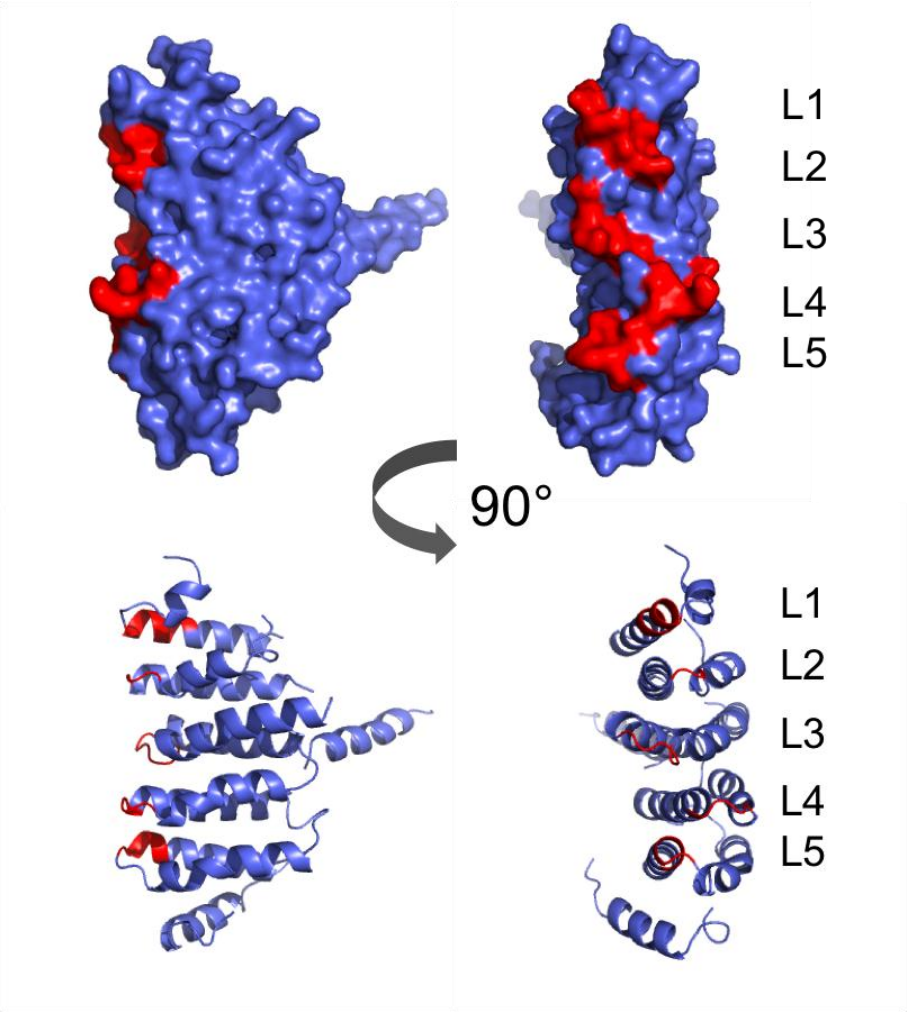

Figure 1.5: TOG domains contain a conserved α-helical fold consisting of six HEAT repeats. The sequence similarity among the TOG domains is only around 6%, however our sequence alignment results show that 12 out of the 15 conserved residues are located on the same edge of the TOG domains (56, 57). The conserved surfaces (highlighted in red) contain five short loops (L1 – L5) that are connecting the HEAT repeats and residues that are previously shown to be essential for tubulin binding are located in loops L1, L3 and L4.

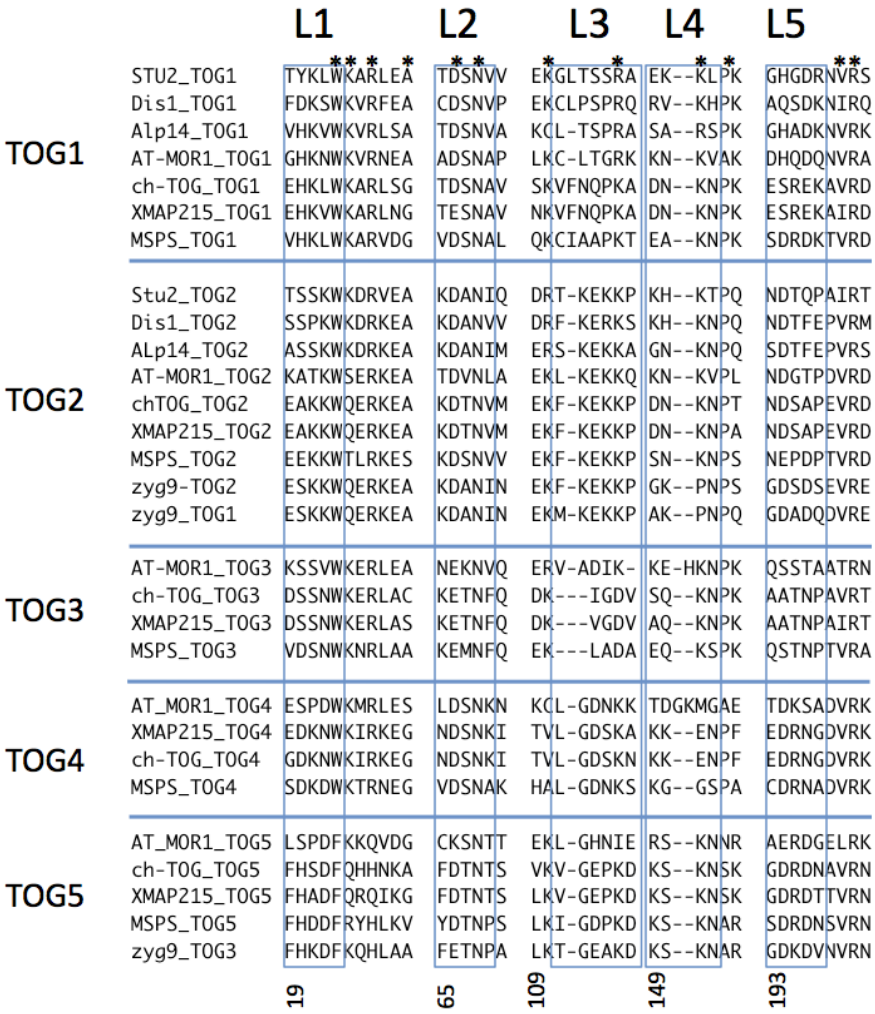

Figure 1.6: The sequence alignment of the conserved loop regions among TOG domains of different species.

The sequence alignment is divided into groups based on the conserved phylogenetic classes from the sequence alignment (56, 57). The residue numbers indicate the corresponding first TOG1 residue on that region and boxes are drawn around the residues of corresponding loop region. The conserved residues are marked with * signs.

TOG:tubulin interactions

Lack of structural information on TOG:αβ-tubulin complex makes studying TOG:αβ-tubulin interactions challenging

A recent study showed that the ability to bind αβ-tubulin heterodimers is crucial for XMAP215 function. Decrease in total αβ-tubulin binding affinity caused by loss of αβ-tubulin binding functions of individual TOG domains resulted in the decrease of XMAP215 polymerase activity (59). The loss of αβ-tubulin binding function was achieved by mutating conserved residues on the L1-L5 loops, and the inactivation of all TOG domains simultaneously abolished the MT polymerase activity completely. Among the total five TOG domains, simultaneous inactivation of TOG1 and TOG2 in binding αβ-tubulin was enough to achieve 75% loss of MT-polymerase function impairing its ability to increase growth rates. In other studies negatively stained electron microscope images show that in the absence of αβ-tubulin, Stu2p homodimer and XMAP215 are elongated molecules with TOG domains and connecting flexible linkers. When Stu2p/XMAP215:αβ-tubulin complexes form, Stu2p and XMAP215 proteins were observed to wrap around non-polymerized αβ-tubulin heterodimers with their TOG domains and form a globular complex (22, 24). Stu2p and XMAP215 contain different numbers of distinct TOG domains to do that, Stu2p: TOG1 and TOG2, XMAP215: TOG1 to TOG5. This suggests that all TOG domains interact with the αβ-tubulin. It is however not known which TOG domain binds to which tubulin (α-, β- tubulin or αβ-tubulin simultaneously), or if each TOG domain binds to a different face of the αβ-

tubulin. Stu2p was also shown to recognize and bind the plus end of the MTs (24) and for Stu2p the TOG1 domain was not necessary for this even if the TOG1 domain was essential to promote MT elongation. Stu2p also has a basic linker after the TOG domains, which has been shown to bind to the microtubule lattice (22, 28).

The lack of structural information about TOG:αβ-tubulin interactions limits our ability to understand how multiple TOG domains work together to bind to unpolymerized αβ-tubulin or to the plus end of the MT, recruit unpolymerized αβ-tubulin to the MT end, and translocate to follow the growing MT plus end. We still don't understand the molecular basis for the selective recognition of unpolymerized αβ-tubulin and the MT plus end by the different TOG domains, even if the basic biochemical properties of these proteins are beginning to be discovered. The molecular details of the TOG:αβ-tubulin interaction surfaces are also unknown along with whether binding to αβ-tubulin affects or are affected by the curvature and/or the nucleotide state of the αβ-tubulin. Studying TOG:αβ-tubulin interactions has been challenging because the structure of a TOG:αβ-tubulin complex has not been determined, and it has not been possible to map the tubulin side of the interaction surfaces using site-directed mutants of the animal αβ-tubulin.

Obstacles in studying MT regulation

A fundamental obstacle that prevents more rapid progress is the lack of a routine, robust source of recombinant αβ-tubulin

αβ-tubulin is almost exclusively isolated from animal brain (where αβ-tubulin is abundant) for in vitro experiments. The widespread reliance on brain αβ-tubulin is in part explained by the failure of heterologous expression of αβ-tubulin in bacteria, likely because bacteria lack a number of dedicated chaperones required for the folding and assembly of αβ-tubulin heterodimers. This represents a substantial barrier to the in vitro analysis of αβ-tubulin and the production of site directed mutants. This in turn makes new structural and mechanistic studies of microtubule regulation very difficult if not all together prevent them. For instance, the natural tendency of αβ-tubulin to polymerize has made it very difficult to obtain suitable crystals of αβ-tubulin for structure determination and the very few crystals of αβ-tubulin were obtained by either manipulating the solution conditions or in complex with drug molecules or regulator proteins (12-14, 60). Site directed mutagenesis of surface residues to map binding sites for regulatory proteins is also impossible to perform using animal brain αβ-tubulin.

Site-directed mutants of yeast αβ-tubulin were previously purified from endogenous loci

A few studies reported recombinant purification of wild type or mutant αβ-tubulins from budding or fission yeast (61-67). However, the method used had several limitations. For instance; the scope of expressible mutants has been limited since the αβ-

tubulin was expressed constitutively from the endogenous loci and required the mutant αβ-tubulins to be able to functionally replace wild-type αβ-tubulin. The final yields of purified protein are also relatively poor because constitutive overexpression of αβ-tubulin is lethal in yeast (65). Therefore, these methods could not take advantage of maximal overexpression.

These studies, however established the feasibility and potential of in vitro studies of yeast αβ-tubulins. The molecular information available from the structures of αβ-tubulin in combination with the ability to purify recombinant αβ-tubulin from yeast might allow the design of αβ-tubulin mutants to facilitate new structural, biochemical, and functional studies.

In this work, we first present robust methods for identifying and purifying mutant αβ-tubulins with blocked assembly interfaces. The mutants we developed represent unique reagents that allow us to utilize experimental approaches that were previously unavailable because of the difficulties arising from the tendency of αβ-tubulin heterodimers to self-assemble. We then show results from X-ray crystallography and biochemical experiments enabled by these reagents to understand TOG:αβ-tubulin interactions using TOG1 and TOG2 domains of Stu2p and, we propose mechanisms by which TOG domains recognize different forms (curvature) of the αβ-tubulin in various states of MT elongation.

REFERENCES

1. Walczak CE & Heald R (2008) Mechanisms of mitotic spindle assembly and function. *International review of cytology* 265:111-158.
2. Desai A, Deacon HW, Walczak CE, & Mitchison TJ (1997) A method that allows the assembly of kinetochore components onto chromosomes condensed in clarified Xenopus egg extracts. *Proceedings of the National Academy of Sciences of the United States of America* 94(23):12378-12383.
3. Walker RA, *et al.* (1988) Dynamic instability of individual microtubules analyzed by video light microscopy: rate constants and transition frequencies. *The Journal of cell biology* 107(4):1437-1448.
4. Jordan MA & Wilson L (2004) Microtubules as a target for anticancer drugs. *Nature reviews. Cancer* 4(4):253-265.
5. Akhmanova A & Steinmetz MO (2008) Tracking the ends: a dynamic protein network controls the fate of microtubule tips. *Nature reviews. Molecular cell biology* 9(4):309-322.
6. Howard J & Hyman AA (2009) Growth, fluctuation and switching at microtubule plus ends. *Nature reviews. Molecular cell biology* 10(8):569-574.
7. Downing KH & Nogales E (1998) Tubulin structure: insights into microtubule properties and functions. *Current opinion in structural biology* 8(6):785-791.
8. Arnal I, Karsenti E, & Hyman AA (2000) Structural transitions at microtubule ends correlate with their dynamic properties in Xenopus egg extracts. *The Journal of cell biology* 149(4):767-774.

9. Chretien D, Fuller SD, & Karsenti E (1995) Structure of growing microtubule ends: two-dimensional sheets close into tubes at variable rates. *The Journal of cell biology* 129(5):1311-1328.

10. Muller-Reichert T, Chretien D, Severin F, & Hyman AA (1998) Structural changes at microtubule ends accompanying GTP hydrolysis: information from a slowly hydrolyzable analogue of GTP, guanylyl (alpha,beta)methylenediphosphonate. *Proceedings of the National Academy of Sciences of the United States of America* 95(7):3661-3666.

11. Vitre B, *et al.* (2008) EB1 regulates microtubule dynamics and tubulin sheet closure in vitro. *Nature cell biology* 10(4):415-421.

12. Lowe J, Li H, Downing KH, & Nogales E (2001) Refined structure of alpha beta-tubulin at 3.5 A resolution. *Journal of molecular biology* 313(5):1045-1057.

13. Nogales E, Wolf SG, & Downing KH (1998) Structure of the alpha beta tubulin dimer by electron crystallography. *Nature* 391(6663):199-203.

14. Ravelli RB, *et al.* (2004) Insight into tubulin regulation from a complex with colchicine and a stathmin-like domain. *Nature* 428(6979):198-202.

15. Barbier P, *et al.* (2010) Stathmin and interfacial microtubule inhibitors recognize a naturally curved conformation of tubulin dimers. *The Journal of biological chemistry* 285(41):31672-31681.

16. Buey RM, Diaz JF, & Andreu JM (2006) The nucleotide switch of tubulin and microtubule assembly: a polymerization-driven structural change. *Biochemistry* 45(19):5933-5938.

17. Rice LM, Montabana EA, & Agard DA (2008) The lattice as allosteric effector: structural studies of alphabeta- and gamma-tubulin clarify the role of GTP in microtubule assembly. *Proceedings of the National Academy of Sciences of the United States of America* 105(14):5378-5383.

18. Wang HW & Nogales E (2005) Nucleotide-dependent bending flexibility of tubulin regulates microtubule assembly. *Nature* 435(7044):911-915.

19. Nogales E & Wang HW (2006) Structural mechanisms underlying nucleotide-dependent self-assembly of tubulin and its relatives. *Current opinion in structural biology* 16(2):221-229.

20. Gard DL, Becker BE, & Josh Romney S (2004) MAPping the eukaryotic tree of life: structure, function, and evolution of the MAP215/Dis1 family of microtubule-associated proteins. *International review of cytology* 239:179-272.

21. Bratman SV & Chang F (2008) Mechanisms for maintaining microtubule bundles. *Trends in cell biology* 18(12):580-586.

22. Al-Bassam J, van Breugel M, Harrison SC, & Hyman A (2006) Stu2p binds tubulin and undergoes an open-to-closed conformational change. *The Journal of cell biology* 172(7):1009-1022.

23. Slep KC & Vale RD (2007) Structural basis of microtubule plus end tracking by XMAP215, CLIP-170, and EB1. *Molecular cell* 27(6):976-991.

24. Brouhard GJ, *et al.* (2008) XMAP215 is a processive microtubule polymerase. *Cell* 132(1):79-88.

25. Al-Bassam J, *et al.* (2010) CLASP promotes microtubule rescue by recruiting tubulin dimers to the microtubule. *Developmental cell* 19(2):245-258.

26. Al-Bassam J, Larsen NA, Hyman AA, & Harrison SC (2007) Crystal structure of a TOG domain: conserved features of XMAP215/Dis1-family TOG domains and implications for tubulin binding. *Structure* 15(3):355-362.

27. Ohkura H, Garcia MA, & Toda T (2001) Dis1/TOG universal microtubule adaptors - one MAP for all? *Journal of cell science* 114(Pt 21):3805-3812.

28. Wang PJ & Huffaker TC (1997) Stu2p: A microtubule-binding protein that is an essential component of the yeast spindle pole body. *The Journal of cell biology* 139(5):1271-1280.

29. Garcia MA, Vardy L, Koonrugsa N, & Toda T (2001) Fission yeast ch-TOG/XMAP215 homologue Alp14 connects mitotic spindles with the kinetochore and is a component of the Mad2-dependent spindle checkpoint. *The EMBO journal* 20(13):3389-3401.

30. Whittington AT, *et al.* (2001) MOR1 is essential for organizing cortical microtubules in plants. *Nature* 411(6837):610-613.

31. Charrasse S, *et al.* (1998) The TOGp protein is a new human microtubule-associated protein homologous to the Xenopus XMAP215. *Journal of cell science* 111 (Pt 10):1371-1383.

32. Cullen CF, Deak P, Glover DM, & Ohkura H (1999) mini spindles: A gene encoding a conserved microtubule-associated protein required for the integrity of the mitotic spindle in Drosophila. *The Journal of cell biology* 146(5):1005-1018.

33. Rockmill B & Fogel S (1988) DIS1: a yeast gene required for proper meiotic chromosome disjunction. *Genetics* 119(2):261-272.

34. Tournebize R, *et al.* (2000) Control of microtubule dynamics by the antagonistic activities of XMAP215 and XKCM1 in Xenopus egg extracts. *Nature cell biology* 2(1):13-19.

35. Brittle AL & Ohkura H (2005) Mini spindles, the XMAP215 homologue, suppresses pausing of interphase microtubules in Drosophila. *The EMBO journal* 24(7):1387-1396.

36. Kawamura E & Wasteneys GO (2008) MOR1, the Arabidopsis thaliana homologue of Xenopus MAP215, promotes rapid growth and shrinkage, and suppresses the pausing of microtubules in vivo. *Journal of cell science* 121(Pt 24):4114-4123.

37. Gergely F, Draviam VM, & Raff JW (2003) The ch-TOG/XMAP215 protein is essential for spindle pole organization in human somatic cells. *Genes & development* 17(3):336-341.

38. Cassimeris L & Morabito J (2004) TOGp, the human homolog of XMAP215/Dis1, is required for centrosome integrity, spindle pole organization, and bipolar spindle assembly. *Molecular biology of the cell* 15(4):1580-1590.

39. Tanaka K, *et al.* (2005) Molecular mechanisms of kinetochore capture by spindle microtubules. *Nature* 434(7036):987-994.

40. Kitamura E, *et al.* (2010) Kinetochores generate microtubules with distal plus ends: their roles and limited lifetime in mitosis. *Developmental cell* 18(2):248-259.

41. Gard DL & Kirschner MW (1987) A microtubule-associated protein from Xenopus eggs that specifically promotes assembly at the plus-end. *The Journal of cell biology* 105(5):2203-2215.

42. Kinoshita K, Arnal I, Desai A, Drechsel DN, & Hyman AA (2001) Reconstitution of physiological microtubule dynamics using purified components. *Science* 294(5545):1340-1343.

43. Cassimeris L, Gard D, Tran PT, & Erickson HP (2001) XMAP215 is a long thin molecule that does not increase microtubule stiffness. *Journal of cell science* 114(Pt 16):3025-3033.

44. van Breugel M, Drechsel D, & Hyman A (2003) Stu2p, the budding yeast member of the conserved Dis1/XMAP215 family of microtubule-associated proteins is a plus end-binding microtubule destabilizer. *The Journal of cell biology* 161(2):359-369.

45. Shirasu-Hiza M, Coughlin P, & Mitchison T (2003) Identification of XMAP215 as a microtubule-destabilizing factor in Xenopus egg extract by biochemical purification. *The Journal of cell biology* 161(2):349-358.

46. Al-Bassam J, *et al.* (2012) Fission yeast Alp14 is a dose-dependent plus end-tracking microtubule polymerase. *Molecular biology of the cell* 23(15):2878-2890.

47. Hsu KS & Toda T (2011) Ndc80 internal loop interacts with Dis1/TOG to ensure proper kinetochore-spindle attachment in fission yeast. *Current biology : CB* 21(3):214-220.

48. Roque H, Ward JJ, Murrells L, Brunner D, & Antony C (2010) The fission yeast XMAP215 homolog Dis1p is involved in microtubule bundle organization. *PloS one* 5(12):e14201.

49. Chen XP, Yin H, & Huffaker TC (1998) The yeast spindle pole body component Spc72p interacts with Stu2p and is required for proper microtubule assembly. *The Journal of cell biology* 141(5):1169-1179.

50. Lee MJ, Gergely F, Jeffers K, Peak-Chew SY, & Raff JW (2001) Msps/XMAP215 interacts with the centrosomal protein D-TACC to regulate microtubule behaviour. *Nature cell biology* 3(7):643-649.

51. Cullen CF & Ohkura H (2001) Msps protein is localized to acentrosomal poles to ensure bipolarity of Drosophila meiotic spindles. *Nature cell biology* 3(7):637-642.

52. Sato M, Vardy L, Angel Garcia M, Koonrugsa N, & Toda T (2004) Interdependency of fission yeast Alp14/TOG and coiled coil protein Alp7 in microtubule localization and bipolar spindle formation. *Molecular biology of the cell* 15(4):1609-1622.

53. Kinoshita K, *et al.* (2005) Aurora A phosphorylation of TACC3/maskin is required for centrosome-dependent microtubule assembly in mitosis. *The Journal of cell biology* 170(7):1047-1055.

54. Bellanger JM & Gonczy P (2003) TAC-1 and ZYG-9 form a complex that promotes microtubule assembly in C. elegans embryos. *Current biology : CB* 13(17):1488-1498.

55. Slep KC (2010) Structural and mechanistic insights into microtubule end-binding proteins. *Current opinion in cell biology* 22(1):88-95.

56. Pei J & Grishin NV (2007) PROMALS: towards accurate multiple sequence alignments of distantly related proteins. *Bioinformatics* 23(7):802-808.

57. Pei J, Kim BH, Tang M, & Grishin NV (2007) PROMALS web server for accurate multiple protein sequence alignments. *Nucleic acids research* 35(Web Server issue):W649-652.

58. Ostrowski J, *et al.* (2007) Pharmacological and x-ray structural characterization of a novel selective androgen receptor modulator: potent hyperanabolic stimulation of skeletal muscle with hypostimulation of prostate in rats. *Endocrinology* 148(1):4-12.

59. Widlund PO, *et al.* (2011) XMAP215 polymerase activity is built by combining multiple tubulin-binding TOG domains and a basic lattice-binding region. *Proceedings of the National Academy of Sciences of the United States of America* 108(7):2741-2746.

60. Gigant B, *et al.* (2000) The 4 A X-ray structure of a tubulin:stathmin-like domain complex. *Cell* 102(6):809-816.

61. Barnes G, Louie KA, & Botstein D (1992) Yeast proteins associated with microtubules in vitro and in vivo. *Molecular biology of the cell* 3(1):29-47.

62. Davis A, Sage CR, Dougherty CA, & Farrell KW (1994) Microtubule dynamics modulated by guanosine triphosphate hydrolysis activity of beta-tubulin. *Science* 264(5160):839-842.

63. Davis A, Sage CR, Wilson L, & Farrell KW (1993) Purification and biochemical characterization of tubulin from the budding yeast Saccharomyces cerevisiae. *Biochemistry* 32(34):8823-8835.

64. Gupta ML, Jr., Bode CJ, Georg GI, & Himes RH (2003) Understanding tubulin-Taxol interactions: mutations that impart Taxol binding to yeast tubulin. *Proceedings of the National Academy of Sciences of the United States of America* 100(11):6394-6397.

65. Gupta ML, Jr., *et al.* (2002) beta-Tubulin C354 mutations that severely decrease microtubule dynamics do not prevent nuclear migration in yeast. *Molecular biology of the cell* 13(8):2919-2932.

66. Uchimura S, Oguchi Y, Hachikubo Y, Ishiwata S, & Muto E (2010) Key residues on microtubule responsible for activation of kinesin ATPase. *The EMBO journal* 29(7):1167-1175.

67. Uchimura S, *et al.* (2006) Identification of a strong binding site for kinesin on the microtubule using mutant analysis of tubulin. *The EMBO journal* 25(24):5932-5941.

68. Pecqueur L, *et.al.* (2012) A designed ankyrin repeat protein selected to bind tubulin caps the microtubule plus end. *Proceedings of the National Academy of Sciences of the United States of America* 109(30):12011-6.

69. Yajima H, *et.al.* (2012) Conformational changes in tubulin in GMPCPP and GDP-taxol microtubules observed by cryoelectron microscopy. *The Journal of cell biology* 198(3):315-22.

70. Maurer SP, *et.al.* (2012) EBs recognize a nucleotide-dependent structural cap at growing microtubule ends. *Cell* 149(2):371-82.

CHAPTER TWO

Design, Overexpression, and Purification of Polymerization-Blocked Yeast *αβ*-Tubulin Mutants

Abstract

Microtubule dynamics play essential roles in intracellular organization and cell division. They result from structural and biochemical properties of αβ-tubulin heterodimers and how these polymerizing subunits interact with themselves and with regulatory proteins. The lack of routine access to recombinant αβ -tubulin represents an obstacle to deeper insight into αβ–tubulin structure, biochemistry, and recognition by regulatory proteins. Indeed, the widespread reliance on animal brain αβ-tubulin means that very few in vitro studies have taken advantage of powerful and ordinarily routine techniques like site-directed mutagenesis. Here we report new methods for purifying wild-type or mutant yeast αβ -tubulin from inducibly overexpressing strains of Saccharomyces cerevisiae.

Inducible overexpression is an improvement over existing approaches that rely on constitutive expression: it provides higher yields while also allowing otherwise lethal mutants to be purified. We also designed and purified polymerization-blocked αβ -tubulin mutants. These **"**blocked**"** forms of αβ-tubulin give a dominant lethal phenotype when expressed in cells; they cannot form microtubules in vitro and when present in mixtures inhibit the polymerization of wild-type αβ-tubulin. The effects of blocking mutations are

very specific, because purified mutants exhibit normal hydrodynamic properties, bind GTP, and interact with a tubulin-binding domain. The ability to overexpress and purify wild-type αβ-tubulin, or mutants like the ones we report here, creates new opportunities for structural studies of αβ-tubulin and its complexes with regulatory proteins (See Chapter 3 for the structural studies of an αβ-tubulin:TOG1 complex), and for biochemical and functional studies of microtubule dynamics and its regulation.

Experimental procedures

Plasmids and strains

To obtain plasmids capable of overexpressing tubulins, we amplified via polymerase chain reaction genes encoding Tub1p (α-tubulin) and Tub2p (β-tubulin) for insertion into the inducible expression plasmids p426Gal1 and p424Gal1(1), respectively (these are 2 μm plasmids that can be strongly induced when galactose is used as a carbon source). For template DNA, we used open reading frames ordered from Open Biosystems. The primers used to amplify Tub1 were

5′-GGCGGCGGATCCAAAATGAGAGAAGTTATTAGTATT-3′ (forward) and

5 ′-CGGCGGCTCGAGTTAAAATTCCTCTTCCTCAGCGTA-3′ (reverse);

primers used to amplify Tub2 and append a C-terminal His6 tag were

5′-GGCGGCCCCGGGAAAATGAGAGAAATCATTCATATC-3′ (forward) and

5′-CGGCGGCTGCAGTTAGTGGTGGTGGTGGTGGTGTTCAAAATTCTCA

GTGATTGG-3′ (reverse). Underlined sequences highlight the restriction sites used for cloning: BamHI and XhoI for Tub1 and SmaI and PstI for Tub2. Mutant genes were prepared from these expression plasmids using QuikChange mutagenesis (Stratagene), following the manufacturer's instructions. Weakly inducible expression plasmids expressing wild-type or mutant tubulins were constructed by subcloning the appropriate coding region into p416GalS (for Tub1 constructs) or p415GalS (for Tub2 constructs) (1); these plasmids give substantially lower levels of maximal expression because they are maintained at close to single copy and they also carry a debilitated version of the Gal1 promoter. To obtain a plasmid capable of overexpressing the TOG1 domain

(residues1−317) from Stu2p, we amplified this sequence from an open reading frame (Open Biosystems) using primers

5′-GGGCCCCCATGGGCTCAGGAGAAGAAGAAGTA-3′ (forward, NcoI) and

5′-CGCGCGCTCGAGTTAGTGGTGGTGGTGGTGGTGACTGAAGGTGTCT ATTTGAAC-3′ (reverse, His6, XhoI) and cloned it into pET15b (Novagen). To obtain a plasmid capable of overexpressing the Schizosaccharomyces pombe Eb1 homologue Mal3, we amplified this gene from S. pombe cDNA (a generous gift from S. Braun, University of California, San Francisco, CA) using primers

5′-GGGCCCCATATGGGCAGCCATCATCATCATCATCACAGCATGTCTG AATCTCGGCAAGAGC-3′ (forward, NdeI) and

5′-GCGCGCCTCGAGTTAAAACGTGATATTCTCATCGTC-3′ (reverse, XhoI) and cloned it into pET29b (Novagen). For all cloning, Escherichia coli strain DH5α was the host for DNA manipulation. The integrity of expression constructs was verified by sequencing performed by the McDermott Sequencing Core at the University of Texas Southwestern Medical Center.

Protein expression and purification.

For strong overexpression of wild-type or mutant αβ-tubulin in yeast, the appropriate p426Gal1 and p424Gal1 plasmids were cotransformed into strain JEL1 (MAT**α** leu2 trp1 ura3−52 prb1−1122 pep4−3 **Δ**his3::PGAL10-GAL4) (2). Starting with small overnight cultures, we grew strains in 1 L of selective medium (CSM-Ura- Trp). This culture was then used to inoculate ~15 L of YPGL (2% peptone, 1% yeast extract, 3% glycerol, and 2% lactate) in a homemade fermentation device that consisted of an

autoclavable 20 L plastic carboy (Nalgene), a silicone barrel warmer (McMaster-Carr), and vigorous aeration to maintain cells in suspension. After approximately 24 h, galactose powder was added to 2%, and cells were induced for 3−5 h before being harvested. Cell pellets were frozen at −80 °C after being harvested. Using this basic protocol, we typically obtained ~100 g of cells (wet paste) from 15 L of culture. For protein purification, cell pellets were thawed and resuspended in lysis buffer [50 mM HEPES (pH 7.4), 500 mM NaCl, 10 mM MgSO4, and 30 mM imidazole] with 1 mM PMSF before being ruptured by three passes through a microfluidizer (M110-P, Microfluidics) at ~25000 psi. All purification steps were performed at 4 °C. The crude lysate was clarified by centrifugation (30 min at 17000g in an SS-34 rotor) before being loaded onto a 5 mL cartridge Ni-affinity column (Ni-NTA Superflow, Qiagen). After being extensively washed in lysis buffer and then low-salt buffer [25 mM HEPES (pH 7.4), 1 mM MgSO4, and 30 mM imidazole], protein was eluted with elution buffer [25 mM PIPES (pH 6.9), 1 mM MgSO4, and 250 mM imidazole]. Protein-containing fractions (identified using a Bradford assay) were pooled. Our estimate is that these pooled fractions are approximately one-third αβ-tubulin. At this point, the pooled eluate can by frozen after addition of glycerol to a final concentration of 20% or loaded directly onto a 2 mL Source-Q column (GE) and eluted with a 40 column volume NaCl gradient [buffer A being 25 mM PIPES (pH 6.9), 2 mM MgSO4, 1 mM EGTA, and 50 μM GTP; buffer B being buffer A plus 1 M NaCl]. The αβ-tubulin-containing fractions were pooled and dialyzed against buffer A before they were used. They can be frozen in liquid nitrogen and stored at −80 °C. The TOG1 domain from Stu2p (residues 1−317) and S.pombe Eb1 family member Mal3 were purified as described in refs (3), (4), and (5)

with minor modifications.

Phenotypic assay

For examining the effects of low-level expression of additional wild-type or mutant αβ-tubulin, the appropriate p416GalS and p415GalS plasmids were transformed into strain BY4742 (MATa his3Δ1 leu2Δ0 lys2Δ0 ura3Δ0) (6).We validated the assay by cloning "benchmark" mutants with known phenotype to serve as controls (see Results for details). Strains containing these benchmark mutants and/or candidate polymerization-blocked mutants were cultured in selective medium (CSM-URA-LEU for strains co-expressing Tub1 and wild-type or mutant Tub2, or CSM-URA for strains expressing only wild-type or mutant Tub1). Serial 10-fold dilutions of cultures were transferred to selective plates containing 2% glucose (non-inducing) or 2% galactose (inducing) using an inoculating manifold and imaged after being grown for 3−4 days at 30 °C. To identify a growth phenotype from the Tub1 mutants, it was necessary to add a variable amount of the microtubule stress agent benomyl to the plates (in the range of 5−15 μg/mL).

In vitro assays

Gel filtration experiments were performed by loading 200 μL of 5 μM protein onto a Superdex 200 10/ 300 column equilibrated in 25 mM Tris (pH 7.5), 200 mM NaCl, 1 mM MgCl2, and 1 mM EGTA. The bed volume of the column is 25 mL, and the void volume is 8.2 mL. GTP binding experiments were performed using a filter binding assay adapted from ref (7). Briefly, 0.5 μM αβ-tubulin samples were incubated in binding buffer [25 mM PIPES (pH 6.9), 1 mM EGTA, 2 mM MgCl2, 50 μg/mL BSA, 5 μM GTP,

and 100 μM ATP] containing [γ-^{32}P]GTP, applied to BA85 nitrocellulose filters, and rapidly washed with wash buffer [25 mM PIPES (pH 6.9), 2 mM MgCl2, and 1 mM EGTA]. Radioactivity was measured by scintillation counting. Experiments were performed in quadruplicate, and results were corrected for background by subtracting the counts measured from reaction mixtures that did not contain αβ-tubulin. Microtubule "spindown" experiments for assaying polymerization were performed by incubating protein in assembly buffer [2.5−10% glycerol, 100 mM PIPES (pH 6.9), 2 mM MgSO4, and 0.20 mM EGTA] for 30 min at 30 °C. For electrophoretic analysis, the contents of the assembly reaction mixtures were spun at 96000g at 30 °C for 30 min in a prewarmed TLA-100 rotor, the supernatant was carefully removed, and the pellet was resuspended in 1Å~ SDS buffer such that pellet and supernatant fractions had equal volumes. For fluorescence imaging, a portion of the assembly reaction mixture was cross-linked by 10-fold dilution into assembly buffer containing 1% glutaraldehyde. Cross-linking was quenched by 5-fold dilution into assembly buffer containing 20 mM Tris (pH 6.9), and 30 μL of these quenched, cross-linked reaction mixtures was then applied to the top of a glycerol cushion [20% glycerol in BRB80, BRB80 being 80 mM PIPES (pH 6.8), 1 mM MgCl2, and 1 mM EGTA] and spun through the cushion onto polylysine-coated coverslips. Coverslips were stained using FITC-DM1α (Sigma-Aldrich) for imaging by fluorescence. The experiments for determining the critical concentration for polymerization were performed similarly, with the following modifications: the incubation time was 45 min, and no cross-linking was performed. αβ-tubulin concentrations in the supernatant and pellet were quantified by the Bradford assay. Circular dichroism (CD) experiments were performed after protein had been exchanged

into 20 mM sodium phosphate, 5 mM MgSO4, and 0.1 mM GTP (pH 7.0). CD spectra were recorded at room temperature using an AVIV 62DS spectrometer. Data were collected with 1 nm spacing, using 3s averaging at each point. Three scans were averaged to yield the data shown. After a buffer scan had been subtracted, spectra were normalized to units of mean molar residue ellipticity (degrees square centimeter per decimole per residue) using protein concentrations determined by amino acid analysis (performed by the Keck Biotechnology Resource Laboratory at Yale University, New Haven, CT) according to the equation $[\theta(\lambda)] = \theta obs(\lambda)/ (10ncl)$, where $[\theta(\lambda)]$ is the mean residue molar ellipticity as a function of wavelength, n is the number of residues in the protein, c is the concentration of the protein (molar), l is the sample path length (centimeters), and $\theta obs(\lambda)$ is the observed ellipticity as a function of wavelength (nanometers).

Results

Purification of αβ -tubulin from overexpressing strains of yeast

We cloned Tub1 and Tub2 into inducible expression plasmids, co-transformed these plasmids into yeast, and induced expression in densely growing yeast cultures. Western blots clearly demonstrate inducible overexpression of both Tub1p and Tub2p (Figure 2.1. A) in strains carrying the tubulin overexpression plasmids we constructed. Using relatively simple two-step purification, we obtain multi milligram quantities of very pure Tub1p:Tub2p-H6 (~3−4 mg from 100 g of cells) (Figure 2.1. B). These yields are approximately 4-fold higher than those reported previously (8, 9), a modest gain that nevertheless has significant practical benefits because it reduces the cumbersome work associated with large culture volumes. For example, 100 g of cell paste can be obtained from as little as 1 L of culture using fed batch fermentation (data not shown). We performed several experiments to demonstrate that the purified yeast αβ-tubulin was functional. First, the tubulin is purified as a stoichiometric heterodimer (see the lightly loaded lane in Figure 2.1. B where distinct bands are visible for Tub1p and Tub2p) even though only Tub2p carries a His6 tag. Second, the purified αβ-tubulin readily forms MTs (Figure 2.2. A) that assemble with a critical concentration of ~1 μM as judged by linear extrapolation of pelleting material (Figure 2.2. B), consistent with prior observations (10). Third, the purified αβ-tubulin shows an elution profile virtually identical to that of animal αβ-tubulin on a gel filtration column (Figure 2.3. A) (both elute at 13.6 mL from a Superdex 200 10/300 column with a bed volume of 25 mL and a void volume of 8.2 mL), indicating that the yeast αβ-tubulin is free of aggregation defects and has the expected

hydrodynamic properties. Fourth, we confirmed two known interactions with regulatory proteins, showing that the purified αβ-tubulin forms a complex with the TOG1 domain from Stu2p (recapitulating results of refs (4) and (5) but using yeast αβ-tubulin) (Figure 2.3. B), and that it is stimulated to polymerize by the addition of the Eb1 family protein Mal3 (observing much more numerous, shorter microtubules in the presence of Mal3 recapitulates results of ref (3) showing that Mal3 stimulates MT assembly) (Figure 2.3. C). The Mal3- dependent stimulation of assembly can also be readily observed by sodium dodecyl sulfate−polyacrylamide gel electrophoresis (SDS−PAGE) analysis of spindowns (data not shown). Finally, we used a filter binding assay to demonstrate that at equal concentrations, the purified αβ-tubulin binds an amount of GTP similar to that bound by animal αβ -tubulin (Figure 2.4.). The observed binding is specific because it can be competed away with excess cold GTP, occurs in the presence of excess cold ATP, and depends on the concentration of αβ –tubulin present in the reaction mixtures. We also verified that the microtubule-stabilizing drug epothilone enhanced the polymerization of purified αβ -tubulin (as demonstrated in ref (11); Figure 2.5.). Together, these data indicate that the αβ –tubulin purified from overexpressing strains is functional.

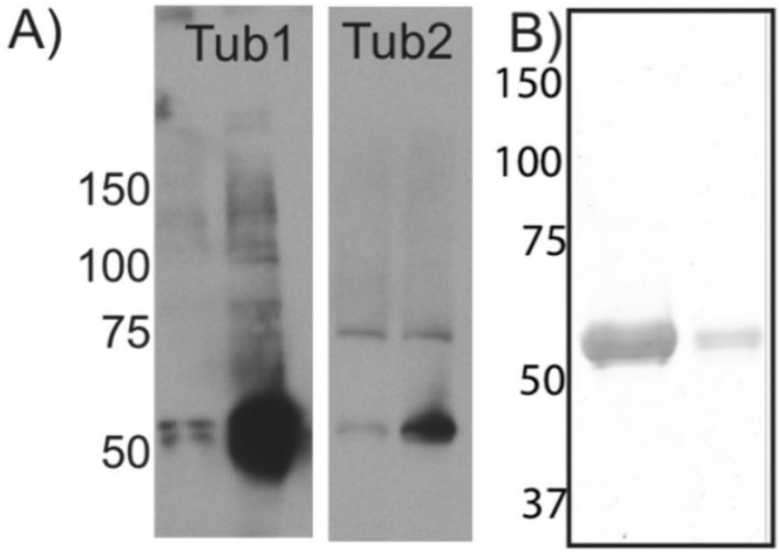

Figure 2.1: Overexpression and purification of yeast αβ-tubulin

A) Western blots before (left) and after (right) induction with galactose demonstrate significant overexpression of both Tub1p and Tub2p (loading was normalized by the A_{600} of the culture).

B) SDS−PAGE of the purified αβ-tubulin, with one heavily loaded (5.1 μg) lane to demonstrate purity and one lightly loaded (0.2 μg) lane to better resolve the closely spaced bands for Tub1p and Tub2p.

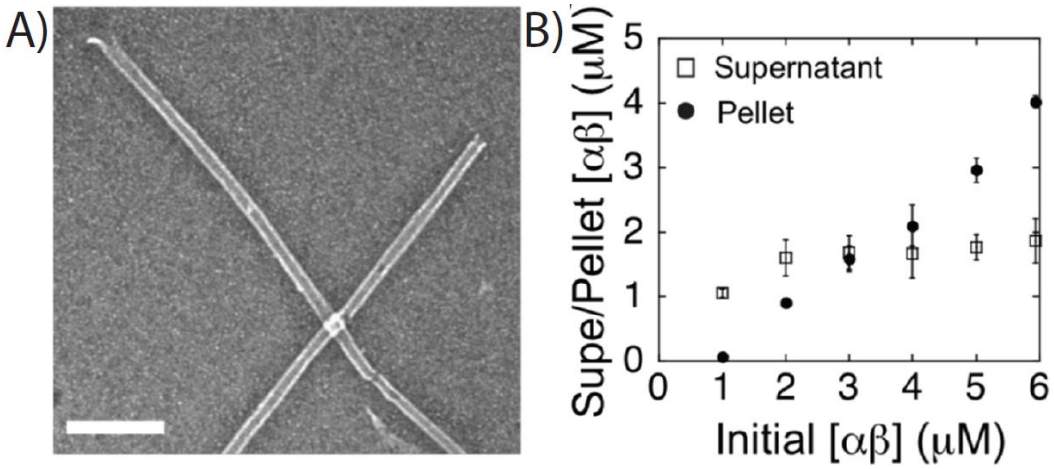

Figure 2.2: Assays for polymerization properties of yeast αβ-tubulin.

A) Negative stain electron micrograph demonstrating that the purified yeast αβ-tubulin forms MTs (bar is 200 nm) (right).

B) Protein concentrations in the supernatant (□) and pellet (●) fractions of microtubule assembly reaction mixtures plotted as a function of the initial αβ-tubulin concentration. Error bars indicate the standard deviation of three independent measurements. The critical concentration for assembly is 0.95 μM as measured by linear extrapolation of pelleted material to y = 0 and 1.75 μM as measured by the constant amount of material in the supernatant.

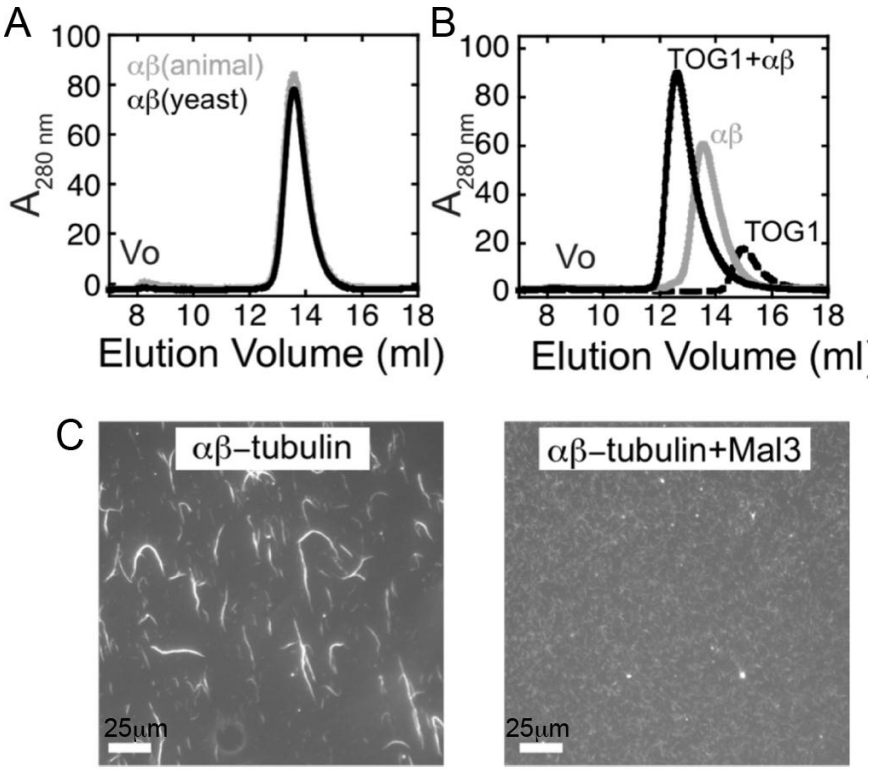

Figure 2.3: Purified yeast αβ-tubulin shows the expected hydrodynamic properties and interacts normally with two different αβ-tubulin binding proteins.

A) Comparative gel filtration chromatography showing that yeast (black) and animal brain (gray) αβ-tubulin elute at almost identical volumes (13.6 mL on a Superdex 200 10/300 column), consistent with the 100 kDa molecular mass of an αβ-tubulin heterodimer.

B) Gel filtration chromatography showing that the purified yeast αβ-tubulin (gray) forms a complex (black) with the TOG1 domain from Stu2p (black dashed).

C) Fluorescence micrographs demonstrating that the purified yeast αβ-tubulin is stimulated to form MTs by the addition of Eb1 family protein Mal3.

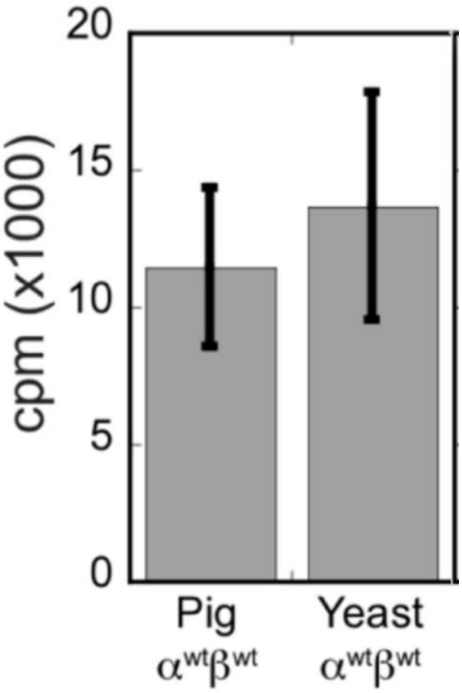

Figure 2.4: A filter binding assay demonstrates that at equal concentrations wild-type yeast or porcine αβ-tubulin bind comparable amounts of GTP.

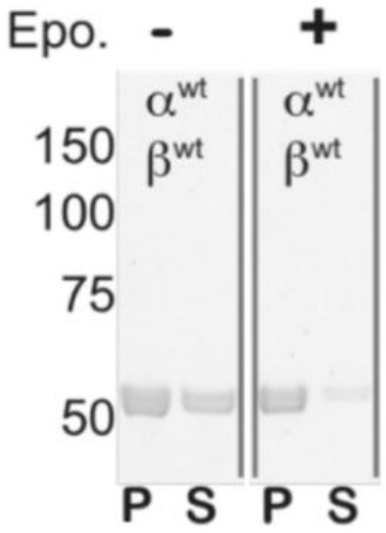

Figure 2.5: SDS−PAGE analysis of spindown experiments (P, pellet; S, supernatant) demonstrates that wild-type αβ-tubulin readily forms MTs. The polymerization is enhanced with the action of epothilone, a natural product that drives MT assembly stabilizing MTs.

A phenotypic assay for inducible dominant negative phenotypes

We hypothesized that mutants with a blocked polymerization interface would inhibit polymerization by reversibly capping protofilaments, and that they should therefore give a dominant-negative phenotype when expressed in yeast. If true, this would provide a convenient assay for rapidly ranking the order of potency of candidate mutants. To explore this possibility, we first developed and validated a plate assay (Figure 2.6.) to screen for an inducible dominant-negative phenotype using galactose inducible plasmids to express viable and dominant negative alleles of αβ -tubulin that had been previously identified by genetic screening (dominant lethal mutants include Tub1-E255A30 and Tub2-E327A,D328A,E329A, which was previously described as Tub2− 446 (12); benign mutants include Tub1p- R327A,D328A,R331A and Tub2p-E125A,D128A, previously described as Tub1− 83532 and Tub2− 422 (12) , respectively). We were able to avoid the toxicity associated with overexpression of wild-type αβ –tubulin (13) by taking advantage of expression plasmids that give very low maximal expression levels (1) (see Experimental Procedures). Tub2p-expressing plasmids were always balanced by a plasmid expressing wild-type Tub1 to avoid the toxicity of unbalanced Tub2p expression (13). Overexpression of Tub1p in yeast is not nearly as deleterious, so co-transforming a plasmid expressing Tub2 was not necessary. In this assay, inducing the expression of the known dominant-negative αβ -tubulin mutant (listed above) strongly inhibited cell growth, but inducing expression of wild-type or **"** neutral**"** alleles (listed above) was without significant consequence (Figure 2.6.).

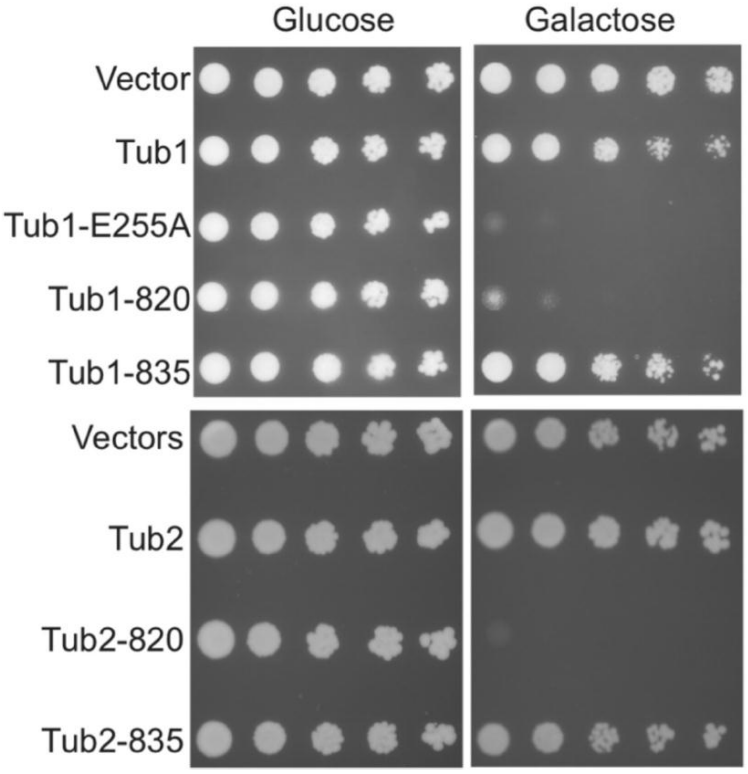

Figure 2.6: Phenotypic assay for an inducible dominant-negative growth defect validated using mutant α- or β-tubulin alleles of known phenotype. Strains expressing wild-type and/or previously characterized benign (Tub1−835 and Tub2−422) and dominant lethal (Tub1-E255A, Tub1−820, and Tub2−446) alleles (see Experimental Procedures) of Tub1 or Tub2 from galactose-inducible plasmids were plated onto glucose (noninducing) or galactose (inducing plates). Expressing known dominant lethal alleles identified in previous alanine scanning experiments (12, 14, 15) gives a strong inducible growth phenotype, but expressing wild-type or benign alleles does not.

Design and phenotypic characterization of polymerization-blocking mutants

The tendency of αβ-tubulin to polymerize represents a significant obstacle to structural and biochemical studies. A key feature of our overexpression strategy is that it should expand the scope of **"**purifiable**"** mutants by eliminating the requirement that the mutants support viability. In what follows, we explore this in more detail by demonstrating that it is possible to overexpress and purify site-directed and dominant lethal mutant forms of αβ -tubulin that cannot polymerize because the mutations **"**blocked**"** a polymerization interface. A similar approach has been used successfully to create a nonpolymerizable actin mutant (16) that has led to multiple new structures of actin (17-19). To the best of our knowledge, no analogous tubulin mutants exist. For practical reasons, we initially targeted the longitudinal interface: it is thought to be significantly stronger than the lateral interface, and it has been defined in atomic detail (20-23). Guided by the structure of αβ-tubulin, (20, 24) we introduced several sets of mutations on the plus (Tub2p) or minus (Tub1p) end surfaces of the heterodimer that we predicted would interfere with longitudinal interactions without otherwise compromising the structural integrity of the protein (Figure 2.7.). We chose residues to mutate by manually identifying interfacial side chains with substantial solvent exposure in the isolated αβ –tubulin heterodimer but that become buried by longitudinal association. We introduced disruptive mutations by altering the charge and/or size of the chosen residues. We introduced a number of mutations on either the plus or minus end of αβ -tubulin (Figure 2.7., Table 2.1., and data not shown). We then used our phenotypic plate assay to screen candidate blocked mutants for their ability to produce an inducible dominant-negative growth phenotype. Inducing the expression of the candidate-blocked β-tubulin

(Tub2p) mutants gave very strong growth inhibition (Figure 2.8.). This result is consistent with the idea that the mutants were poisoning normal microtubule behavior by interfering with subunit addition at the plus end of microtubules. Initially, we were surprised to note that inducing expression of all candidate-blocked α-tubulin (Tub1p) mutants failed to produce significant growth defects (data not shown). This is in marked contrast to the strong dominant lethal phenotype of Tub1p-E255A and Tub1p-820 (Figure 2.8.) and to the results obtained with candidate-blocked Tub2 mutants (Figure 2.8.). We reasoned that because plus end growth is the dominant mode of MT growth in yeast (25), a heterodimer blocked on its minus end might effectively be **"**invisible**"** to the growing polymer. This could explain the apparent lack of growth phenotype, because the primary effect of expressing such a mutant at low levels would essentially be an only slight **"** dilution**"** of the amount of functional αβ -tubulin. We hypothesized that the effects of such a mutant might become more readily apparent under conditions of microtubule stress. Rescreening of the mutants in the presence of increasing concentrations of a microtubule stress agent, benomyl (a MT destabilizing drug), revealed substantial dominant-negative growth phenotypes for several of our designed minus end mutants (Figure 2.8. and Table 2.1). These results are consistent with (but do not unambiguously establish) a blocking effect of the plus end and minus end mutations. Ongoing work in our laboratory is examining how expression of these plus and minus end-blocked mutant αβ -tubulins affects the microtubule cytoskeleton in vivo (not shown).

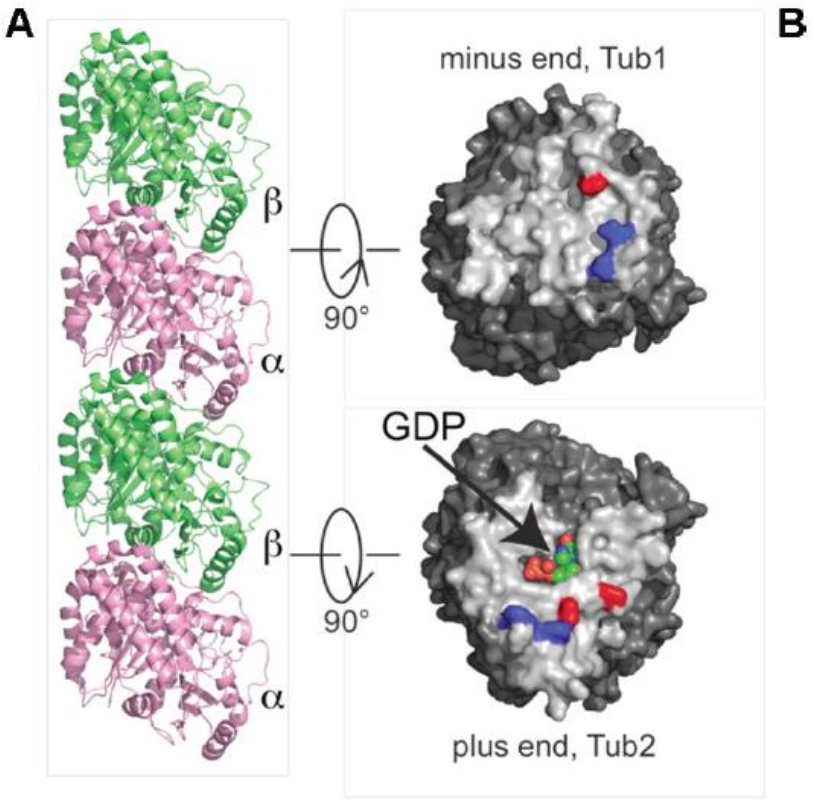

Figure 2.7: Design of mutations to block each of two polymerization interfaces of αβ-tubulin.

A) Representation of the longitudinal association between two αβ-tubulin (α, pink; β, green) as revealed in the crystal structure of the "straight" conformation of αβ-tubulin (20)

B) Surface views of the plus (bottom) and minus (top) end of the interacting αβ-tubulin heterodimers. The surface area buried by the association is depicted in a lighter color, and the nucleotide bound to β-tubulin is represented as spheres. The locations of candidate blocking mutations on the longitudinal interface of Tub1 and Tub2 are colored blue or red, and the amino acid changes are listed in Table 2.1.

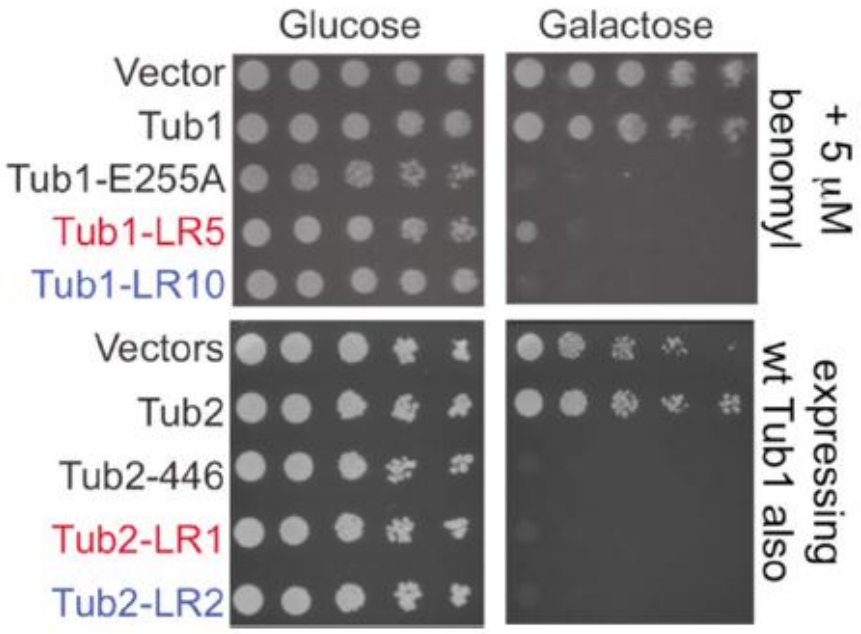

Figure 2.8: Phenotypic characterization of mutations to block each of two polymerization interfaces of αβ-tubulin.

A) Expressing the blocked mutants in yeast produces a strong dominant-negative phenotype, whereas expressing wild-type tubulins does not. Tub2−446 and Tub1-E255A are known dominant lethal alleles that were used as positive controls (see Figure 2.6.). For the Tub1 experiment only, the plates contain 5 μg/mL benomyl; for the Tub2 experiments, all strains (except empty vectors) also inducibly express wild-type Tub1 to avoid the deleterious effects of unbalanced Tub2 expression. Mutant labels colored in red and blue matches the color coding in Figure 2.7.

Tub1 LR5	T349E
Tub1 LR10	T326Q,Q330W
Tub2 LR1	T175R,V179R
Tub2 LR2	F394A,W397E

*Polymerization-blocked mutants on the minus end (Tub1) and plus end (Tub2) of yeast αβ-tubulin.

Table 2.1: Interface-Blocking Mutations on Tub1p (α -tubulin) and Tub2p (β -tubulin)*

Purification and in vitro characterization of αβ-tubulin mutants blocked on the plus or minus end

To directly probe the polymerization behavior of candidate blocked mutants outside the cell, and to rule out the possibility that the mutant-induced growth defect resulted from folding or other defects unrelated to polymerization, we overexpressed and purified a number of mutants for in vitro studies. We prepared strains carrying the mutant genes on strong galactose inducible expression plasmids (see Experimental Procedures), and we grew and induced these strains as described above for wild-type αβ-tubulin. Using the same purification protocol, we purified milligram amounts of candidate polymerization blocked mutants. The mutants we chose to pursue in vitro all gave strong inducible growth defects in the phenotypic assay, so their purification demonstrates that it is possible to purify biochemically relevant quantities of otherwise lethal αβ–tubulin mutants (see refs (26, 27) for recent examples of purifying lethal mutations, albeit at substantially lower yields). In what follows, we will focus on more detailed in vitro characterization of two strongly blocked mutants, one on each longitudinal surface of the heterodimer. We analyzed the polymerization behavior of the mutants using a bulk assay for microtubule assembly. αβ-tubulins were incubated under microtubule assembly conditions, and polymerized and unpolymerized αβ-tubulins were separated by centrifugation. The extent of polymerization was assessed by Coomassie gel analysis of the supernatant and pellet and verified by microscopic examination of the polymerization reactions. These experiments revealed that the blocked mutants are severely compromised for self-assembly. Under conditions where wild-type αβ-tubulin readily forms microtubules, the plus and minus end-blocked mutants do not (Figure 2.9. and data

not shown). Even when challenged with epothilone, a natural product that drives polymerization by stabilizing microtubules, the mutants fail to polymerize (Figure 2.9.). This resistance to epothilone-induced polymerization cannot be trivially explained by a defect in epothilone binding, because the sites of mutation are distant from the epothilone-binding site (which is near a lateral interface (28)). We also examined how variable doses of plus end or minus end-blocked mutants affected the polymerization of wild-type tubulin when present in a mixture. At stoichiometries of 1:1 and lower, the presence of either blocked mutant potently inhibited the ability of wild-type tubulin to form microtubules (Figure 2.10.). Thus, even under conditions where the concentration of wild-type αβ-tubulin present would ordinarily be sufficient to form abundant microtubules, the presence of a blocked mutant is strongly inhibitory. Presumably, this **"** in vitro dominant-negative**"** behavior results because the mutants use their **"**normal**"** polymerization interfaces to bind to microtubule initiation intermediates and/or to elongating microtubules, and this binding poisons growth because the blocked interface interferes with further subunit addition. In the bulk assays, we observe significant inhibition of assembly down to mutant:wild-type stoichiometries as low as 1:6 [**~**17% (Figure 2.10.)].

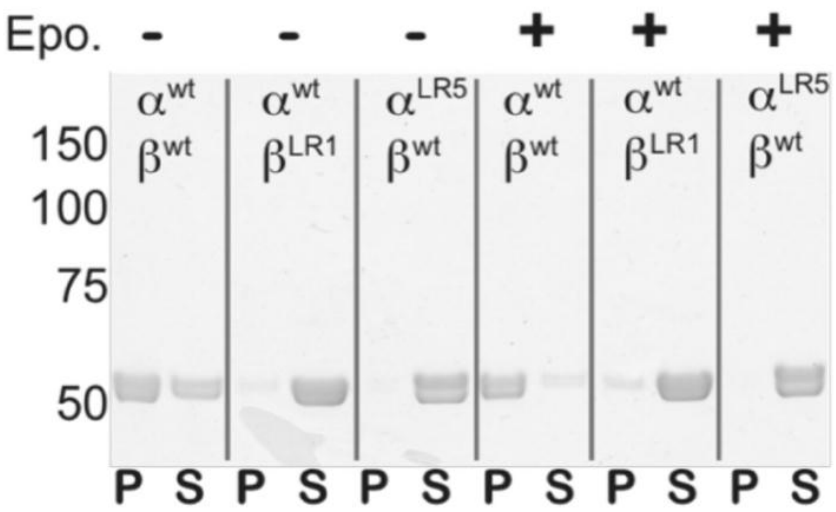

Figure 2.9: Purified αβ-tubulin mutants have a severe polymerization defect

SDS−PAGE analysis of spindown experiments (P, pellet; S, supernatant) demonstrates that tubulins with blocking mutations on the plus (Tub2) or minus (Tub1) end of the heterodimer do not self-assemble under conditions where wild-type αβ-tubulin readily forms MTs. The polymerization defect is severe, because the mutants resist the action of epothilone, a natural product that drives MT assembly because it stabilizes MTs.

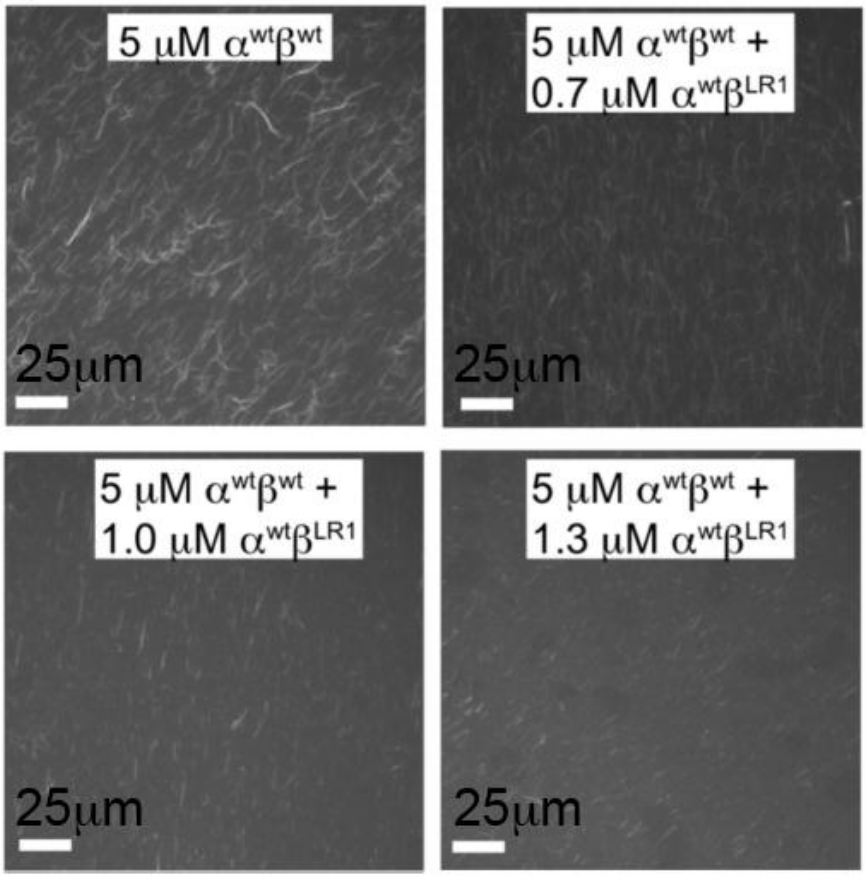

Figure 2.10: Purified αβ-tubulin mutants have a severe polymerization defect

Fluorescence micrographs of MT assembly reaction mixtures containing identical concentrations (5 μM) of wild-type αβ-tubulin but with variable amounts of the mutant heterodimer containing the blocked Tub2-LR1 (top left, no mutant; top right, 10% blocked mutant; bottom left, 15% blocked mutant; bottom right, 20% blocked mutant) show that the blocked mutant interferes with the assembly of wild-type αβ-tubulin at stoichiometries as low as ~1:7. Presumably, this inhibition occurs because the mutant binds to and poisons the growth of microtubules and/or microtubule assembly intermediates.

Biochemical characterization indicates that the mutations do not compromise the folding and polymerization-independent properties of the heterodimers. Indeed, like the wild-type protein, they are purified as heterodimers that migrate normally on gel filtration (Figure 2.11.). They also retain the ability to bind the TOG1 domain from Stu2p in a gel filtration assay. We were unable to test interactions with Mal3, as we did for wild-type αβ -tubulin, because these interactions require MT formation. Finally, the mutants remain competent to bind GTP as determined by a filter binding assay (Figure 2.12). Also, consistent with the indirect assays for structural integrity described above, wild-type and plus end-blocked mutants give very similar circular dichroism spectra (Figure 2.13). Together, these observations suggest that the biochemical consequences of mutations introduced on the polymerization interfaces are local, without significant consequences for the biochemical properties of distant sites.

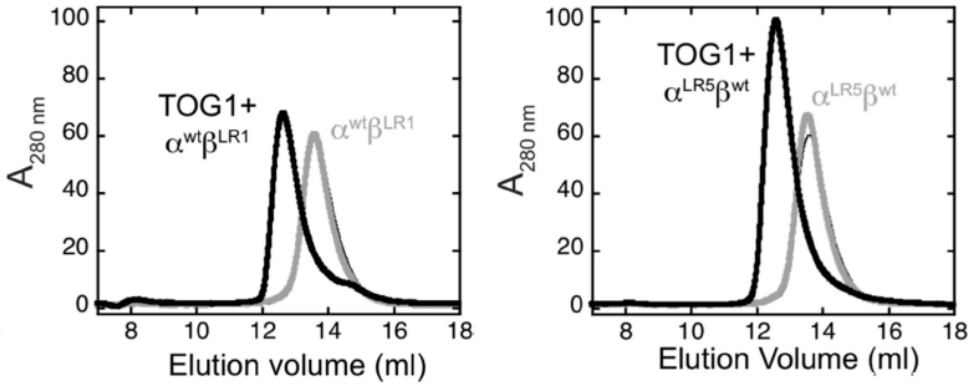

Figure 2.11: Mutants with blocking mutations on the plus end (left) or on the minus end (right) migrate normally on gel filtration (gray curves; the thin black curve shows the elution profile of wild-type αβ-tubulin for reference) and remain competent to interact with the TOG1 domain from Stu2p (black curves).

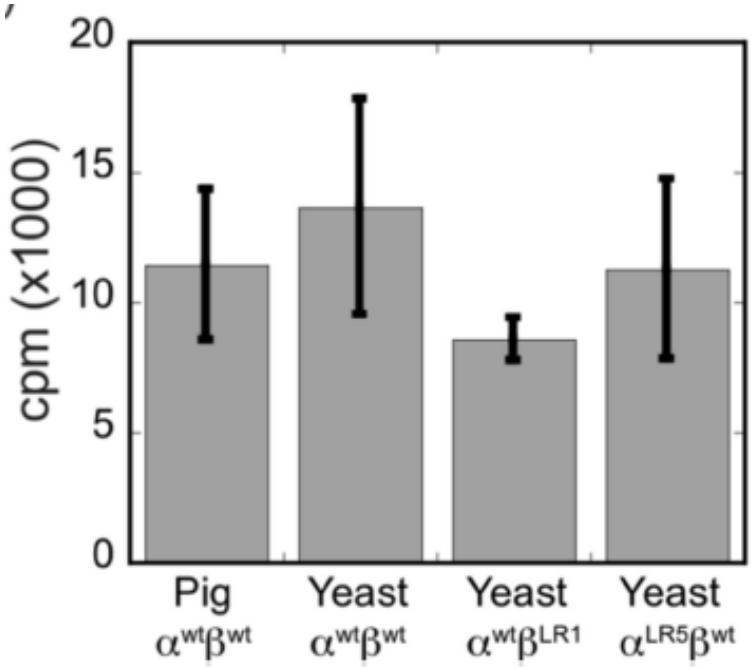

Figure 2.12: A filter binding assay demonstrates that at equal concentrations, blocked mutants of Tub1 or Tub2 bind comparable amounts of GTP like wild-type yeast or porcine αβ-tubulin does.

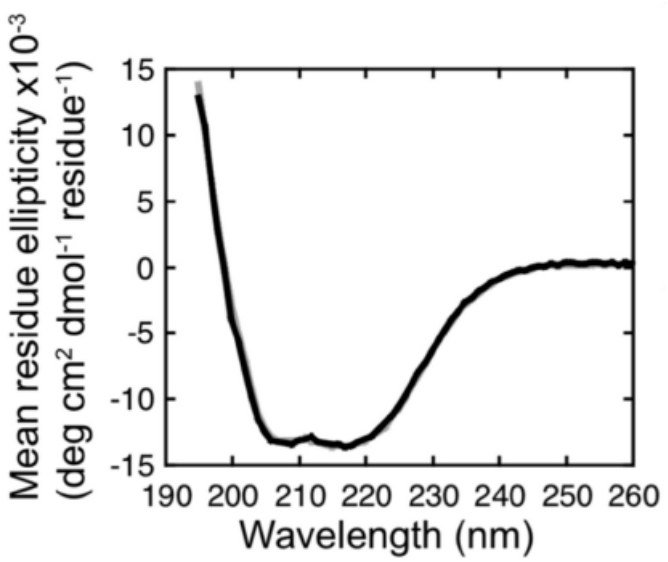

Figure 2.13: Circular dichroism spectra for the wild type (gray) and the plus end-blocked mutant (black) are very similar.

Discussion

The near exclusive use of animal brain αβ-tubulin represents a significant obstacle to in vitro studies of αβ -tubulin structure and biochemistry. One reason for this is the fact that αβ-tubulin purified from animal brains is a mixture of multiple α- and β-tubulin isotypes. This isotypic heterogeneity complicates mechanistic analysis: the different isotypes can have different biochemical properties, but experimental observations represent population-weighted averages. Interpreting measurements taken in the presence of heterogeneity with a single set of parameters that ignores these differences may not always be appropriate. Furthermore, and for obvious reasons, animal brain αβ–tubulin cannot be subjected to powerful and ordinarily routine techniques like site-directed mutagenesis. As a result, only a small handful of studies (8, 9, 26, 27, 29, 30) have attempted to use surface mutagenesis of αβ-tubulin to modulate the interactions of αβ-tubulin with itself and/or to map or modulate the interactions of αβ-tubulin with regulatory factors. To address these and other limitations, we sought to develop a new source of recombinant αβ -tubulin that would be amenable to site-directed mutagenesis.

We first described techniques that allow affinity-tagged wildtype yeast αβ -tubulin to be purified from inducibly overexpressing strains of yeast. We chose yeast as an expression host because stringent requirements for eukaryote-specific chaperones have so far prevented the expression of functional αβ -tubulin in bacteria, and methods for purifying fungal αβ-tubulins from yeast already existed (3, 8, 10, 27, 31). Yeast and animal αβ-tubulin form microtubules with different dynamic properties, so systematically studying the polymerization dynamics of this non-animal αβ-tubulin should provide new

mechanistic insight into the biochemical determinants of microtubule dynamics. However, because the constitutive overexpression of αβ -tubulin is lethal in yeast (13), obtaining fungal αβ -tubulins in sufficient quantities using already existing methods was cumbersome and challenging. By avoiding the limitations associated with constitutive expression from the genomic loci, inducible overexpression increased yields by at least 4-fold over the best yields previously reported (9). The purified αβ -tubulin passes multiple tests for function: it polymerizes with a critical concentration consistent with prior studies (10), binds GTP, and interacts with the two regulatory proteins that we tested. The milligram-scale yields we obtain remain admittedly low compared to what can be achieved with animal brains (~50 mg up to grams depending on the number of brains used), but as discussed below, we believe that this disadvantage is significantly outweighed by the potential benefits that will accompany routine access to site-directed αβ–tubulin mutants.

To establish that inducible overexpression of αβ-tubulin in yeast represented a general strategy for purifying wild-type or mutant αβ-tubulin, we wanted to purify a mutant that could not support viability using the same protocol developed to purify wild-type αβ-tubulin. Depending on the mutant, this expression and purification would be difficult if not impossible using the preexisting methods for purifying fungal αβ-tubulin, because constitutive expression of a nonviable αβ-tubulin mutant would be lethal.

Prior genetic studies have identified a number of lethal mutant αβ-tubulin alleles in yeast, but purifying one of them for the kind of proof-of-principle experiments described here did not seem optimal: because the mechanistic effect of the mutation-induced changes for many of these alleles has not yet been determined, showing that the

in vitro behavior of the mutant was consistent with its in vivo phenotype would not have been straightforward.

Instead of using a preexisting allele, and also because we have an interest in facilitating new structural studies of αβ -tubulin, we instead chose to design and purify the first polymerization blocked lethal alleles of αβ -tubulin as a way to demonstrate the robustness of our expression and purification strategy. The tendency to polymerize makes αβ -tubulin notoriously difficult to crystallize. The very few structures of αβ -tubulin that are available (a conformation compatible with microtubule structure was determined using electron crystallography (20, 23), and a conformation incompatible with microtubule structure was determined by X-ray crystallography of a complex with a microtubule depolymerizing factor (24)) have framed our understanding in vital ways. However, despite intense effort, fundamental structural questions about αβ-tubulin conformation and about how microtubule-associated proteins recognize αβ-tubulin remain unanswered. New structures of αβ -tubulin will be required to resolve these and other long-standing issues. Inspired by an analogous approach that produced non-polymerizable actin mutants (16), we took advantage of the existing structures of αβ-tubulin to design **"**polymerization-blocking**"** mutations on longitudinal self-association interfaces. Our approach targeted solvent-exposed sites on the longitudinal polymerization interfaces that become substantially buried by self-assembly contacts. We then introduced mutations that we anticipated would be very disruptive to polymerization, typically replacing small, uncharged side chains (e.g., α -tubulin T349 or β -tubulin V179) with large, charged ones (e.g., α -tubulin T349E or β -tubulin V179R). Our approach was not intended to be exhaustive, and it is likely that other sites and/or

substitutions can also produce polymerization blocked αβ-tubulins. However, because these first designs met our criteria (dominant lethal phenotype, inability to polymerize in vitro, and inhibitory activity against the polymerization of wildtype αβ-tubulin) for a severe polymerization block, we have begun to focus on the design and purification of other classes of mutants.

In summary, the results reported here represent a significant technical advance that overcomes several longstanding problems that had been associated with the widespread reliance on endogenous brain αβ-tubulin and/or purification of recombinant αβ-tubulin from sources constitutively expressing it. The blocked mutants we developed appear to behave as exquisitely specific competitive inhibitors of polymerization, and it therefore seems likely that using them in functional assays will provide new insights into the mechanisms underlying microtubule polymerization dynamics. On the structural front, we have already used the plus end-blocked mutant described here to determine a new structure of αβ -tubulin bound to a regulatory protein (Chapter 3) and we anticipate that more structures will be forthcoming. More generally, because site-directed αβ – tubulin mutants can now be purified much more routinely, it should now be possible to purify any number of αβ -tubulin mutants identified in prior genetic screens, and by studying their behavior in vitro, we should gain deeper mechanistic insight into the biochemical changes underlying the mutant phenotype. Our preliminary experiments also suggest that it will be possible to purify yet other classes of mutants, including, for example, those incorporating peptide tags for site-specific fluorescent labeling or with any number of other engineered modifications designed to facilitate new measurements or probe specific molecular features or interactions. These results establish robust

methods for identifying and purifying mutant αβ -tubulins, including mutants that would otherwise be lethal. The mutants with blocked assembly interfaces that we developed represent unique reagents that open new experimental approaches and revitalize old ones.

In the following chapter I describe the use of the plus end polymerization blocked αβ-tubulin that we presented in this chapter to study the molecular mechanisms of αβ-tubulin-TOG interactions. We use it to co-crystallize a TOG:αβ-tubulin complex and biophysically characterize the mechanisms of recognition. For instance we use our polymerization blocked αβ-tubulin mutant in assays such as analytical ultracentrifugation (AUC) to study αβ-tubulin –TOG domain binding where, formation of αβ-tubulin dimers and trimers during the course of the experiment could give rise to difficulties in the analysis of the sedimentation data.

REFERENCES

1. Mumberg D, Muller R, & Funk M (1994) Regulatable promoters of Saccharomyces cerevisiae: comparison of transcriptional activity and their use for heterologous expression. *Nucleic acids research* 22(25):5767-5768.
2. Lindsley JE & Wang JC (1993) On the coupling between ATP usage and DNA transport by yeast DNA topoisomerase II. *The Journal of biological chemistry* 268(11):8096-8104.
3. des Georges A, *et al.* (2008) Mal3, the Schizosaccharomyces pombe homolog of EB1, changes the microtubule lattice. *Nature structural & molecular biology* 15(10):1102-1108.
4. Al-Bassam J, van Breugel M, Harrison SC, & Hyman A (2006) Stu2p binds tubulin and undergoes an open-to-closed conformational change. *The Journal of cell biology* 172(7):1009-1022.
5. Slep KC & Vale RD (2007) Structural basis of microtubule plus end tracking by XMAP215, CLIP-170, and EB1. *Molecular cell* 27(6):976-991.
6. Brachmann CB, *et al.* (1998) Designer deletion strains derived from Saccharomyces cerevisiae S288C: a useful set of strains and plasmids for PCR-mediated gene disruption and other applications. *Yeast* 14(2):115-132.
7. Brandt DR & Ross EM (1986) Catecholamine-stimulated GTPase cycle. Multiple sites of regulation by beta-adrenergic receptor and Mg2+ studied in reconstituted receptor-Gs vesicles. *The Journal of biological chemistry* 261(4):1656-1664.

8. Gupta ML, Jr., *et al.* (2002) beta-Tubulin C354 mutations that severely decrease microtubule dynamics do not prevent nuclear migration in yeast. *Molecular biology of the cell* 13(8):2919-2932.

9. Gupta ML, Jr., Bode CJ, Georg GI, & Himes RH (2003) Understanding tubulin-Taxol interactions: mutations that impart Taxol binding to yeast tubulin. *Proceedings of the National Academy of Sciences of the United States of America* 100(11):6394-6397.

10. Davis A, Sage CR, Wilson L, & Farrell KW (1993) Purification and biochemical characterization of tubulin from the budding yeast Saccharomyces cerevisiae. *Biochemistry* 32(34):8823-8835.

11. Bode CJ, *et al.* (2002) Epothilone and paclitaxel: unexpected differences in promoting the assembly and stabilization of yeast microtubules. *Biochemistry* 41(12):3870-3874.

12. Reijo RA, Cooper EM, Beagle GJ, & Huffaker TC (1994) Systematic mutational analysis of the yeast beta-tubulin gene. *Molecular biology of the cell* 5(1):29-43.

13. Burke D, Gasdaska P, & Hartwell L (1989) Dominant effects of tubulin overexpression in Saccharomyces cerevisiae. *Molecular and cellular biology* 9(3):1049-1059.

14. Anders KR & Botstein D (2001) Dominant-lethal alpha-tubulin mutants defective in microtubule depolymerization in yeast. *Molecular biology of the cell* 12(12):3973-3986.

15. Richards KL, *et al.* (2000) Structure-function relationships in yeast tubulins. *Molecular biology of the cell* 11(5):1887-1903.

16. Joel PB, Fagnant PM, & Trybus KM (2004) Expression of a nonpolymerizable actin mutant in Sf9 cells. *Biochemistry* 43(36):11554-11559.

17. Ducka AM, *et al.* (2010) Structures of actin-bound Wiskott-Aldrich syndrome protein homology 2 (WH2) domains of Spire and the implication for filament nucleation. *Proceedings of the National Academy of Sciences of the United States of America* 107(26):11757-11762.

18. Nair UB, *et al.* (2008) Crystal structures of monomeric actin bound to cytochalasin D. *Journal of molecular biology* 384(4):848-864.

19. Rould MA, Wan Q, Joel PB, Lowey S, & Trybus KM (2006) Crystal structures of expressed non-polymerizable monomeric actin in the ADP and ATP states. *The Journal of biological chemistry* 281(42):31909-31919.

20. Lowe J, Li H, Downing KH, & Nogales E (2001) Refined structure of alpha beta-tubulin at 3.5 A resolution. *Journal of molecular biology* 313(5):1045-1057.

21. Li H, DeRosier DJ, Nicholson WV, Nogales E, & Downing KH (2002) Microtubule structure at 8 A resolution. *Structure* 10(10):1317-1328.

22. Nogales E, Whittaker M, Milligan RA, & Downing KH (1999) High-resolution model of the microtubule. *Cell* 96(1):79-88.

23. Nogales E, Wolf SG, & Downing KH (1998) Structure of the alpha beta tubulin dimer by electron crystallography. *Nature* 391(6663):199-203.

24. Ravelli RB, *et al.* (2004) Insight into tubulin regulation from a complex with colchicine and a stathmin-like domain. *Nature* 428(6979):198-202.

25. Maddox PS, Bloom KS, & Salmon ED (2000) The polarity and dynamics of microtubule assembly in the budding yeast Saccharomyces cerevisiae. *Nature cell biology* 2(1):36-41.

26. Uchimura S, Oguchi Y, Hachikubo Y, Ishiwata S, & Muto E (2010) Key residues on microtubule responsible for activation of kinesin ATPase. *The EMBO journal* 29(7):1167-1175.

27. Uchimura S, *et al.* (2006) Identification of a strong binding site for kinesin on the microtubule using mutant analysis of tubulin. *The EMBO journal* 25(24):5932-5941.

28. Nettles JH, *et al.* (2004) The binding mode of epothilone A on alpha,beta-tubulin by electron crystallography. *Science* 305(5685):866-869.

29. Davis A, Sage CR, Dougherty CA, & Farrell KW (1994) Microtubule dynamics modulated by guanosine triphosphate hydrolysis activity of beta-tubulin. *Science* 264(5160):839-842.

30. Dougherty CA, Sage CR, Davis A, & Farrell KW (2001) Mutation in the beta-tubulin signature motif suppresses microtubule GTPase activity and dynamics, and slows mitosis. *Biochemistry* 40(51):15725-15732.

31. Barnes G, Louie KA, & Botstein D (1992) Yeast proteins associated with microtubules in vitro and in vivo. *Molecular biology of the cell* 3(1):29-47.

CHAPTER THREE

A TOG:αβ-tubulin Complex Structure Reveals Conformation-Based Mechanisms for a Microtubule Polymerase

Abstract

Stu2p/XMAP215/Dis1 family proteins are evolutionarily conserved regulatory factors that use αβ-tubulin-interacting TOG (tumor overexpressed gene) domains to catalyze fast microtubule growth. Catalysis requires that these polymerases discriminate between unpolymerized and polymerized forms of αβ-tubulin, but how they do so has remained unclear. We report the structure of the TOG1 domain from Stu2p bound to yeast αβ-tubulin. TOG1 binds αβ-tubulin in a way that excludes equivalent binding of a second TOG domain. Furthermore, TOG1 preferentially binds a "curved" conformation of αβ-tubulin that cannot be incorporated into microtubules, contacting α- and β-tubulin surfaces that do not participate in microtubule assembly. Conformation-selective interactions with αβ-tubulin explain how TOG-containing polymerases discriminate between unpolymerized and polymerized forms of αβ-tubulin, and how they selectively recognize the growing end of the microtubule.

Experimental Procedures

Protein expression and purification

Wild-type or mutant yeast αβ-tubulin was purified from inducibly overexpressing strains of S. cerevisiae using Ni-affinity and anion exchange chromatography as described previously in chapter 2 of this study (1). Stu2p TOG1 domain constructs (1-317 or 1-272) were overexpressed in E. coli and purified by Ni-affinity and gel filtration chromatography. All mutants were prepared using QuikChange (Stratagene) mutagenesis with primers designed according to the manufacturer's instructions. The integrity of all expression constructs was confirmed by DNA sequencing.

Crystallization and data collection

For crystallization, pure polymerization blocked yeast αβ-tubulin (β:T175R,V179R) and TOG1 domain were mixed at equimolar stoichiometry and concentrated to ~3.5 mg/ml using Amicon Ultra concentrators with a 30 kDa cutoff. The final buffer composition was 25 mM PIPES pH 6.9, 2 mM MgSO4, 1 mM EGTA, ~300 mM NaCl, 1mM GTP. Sparse-matrix crystallization screening (typically mixing protein with precipitants at 1:1 and 2:1 protein:reservoir ratios, using 200 nl of reservoir solution) was performed using a Phoenix DT Drop Setter (Rigaku); the results were not very sensitive to the salt concentration present in the protein solution. Small, needle-like crystals were obtained in multiple PEG-containing conditions from initial screens using a TOG1 (1-317) construct. These lead crystals proved difficult to optimize, but larger crystals were obtained using a truncated construct (residues 1-272). All optimization and

scale-up experiments were performed using crystallization robotics due to variable crystal quality and the difficulty of preparing large amounts of the TOG1:αβ-tubulin complex. The crystal reported here was grown in a 600 nl sitting drop (400 nl TOG1:αβ-tubulin complex in 25 mM PIPES pH 6.9, 2 mM MgSO4, 1 mM EGTA, 200 mM NaCl, 1 mM GTP + 200 nl of reservoir solution: 20% (v/v) PEG 400, 0.1 M MES pH 5.9) equilibrated against reservoir solution, harvested directly from the drop, and dipped into cryoprotectant (20% PEG400, 40% glycerol, 200 mM NaCl, 0.1 M MES pH 5.9) prior to freezing in liquid nitrogen.

Diffraction data were collected at 19 ID beamline at Argonne National Laboratory at APS via remote data collection and the data was processed using HKL3000 (2). Crystals adopt space group P21 with approximately 57% solvent and one complex in the asymmetric unit. The diffraction was anisotropic (minimum Bragg spacings 3.44 Å, 2.88 Å, and 2.65 Å in the weakest, intermediate, and strongest diffracting directions). We used 2.88 Å as the high-resolution cut-off to avoid excessive loss of completeness.

Space group	$P2_1$
Unit cell parameters [Å,°]	89.12, 98.03, 91.36, b=100.3
Wavelength [Å]	0.9794
Resolution range [Å]	50.00-2.88 [3.54-3.44] (2.95-2.88)
Unique reflections	33,974 [1,745] (1,301)
Multiplicity of observations	4.0 [4.2] (3.2)
Data completeness [%] (geometric)	97.2 [100](76.6)*
Data completeness [%] (informative)	74.3 [88.7](22.6)**
R_{merge} [%]	12.4 [31.8] (96.7)
$\langle I \rangle / \langle \sigma I \rangle$	10.2 [4.4] (0.9)
Wilson B-value [$Å^2$]	46.7
Anisotropy [$Å^2$] relative to the best direction (010)	
ΔB in (100) direction (a), ΔB in (001) direction (c)	+32, +42
Anisotropic $\langle I \rangle / \langle \sigma(I) \rangle$	(3.54-3.44) 8.9 / 12.3 /2.3
(resolution shell) directions a / b / c	(2.95-2.88) 2.0 / 3.9 / 0.4
Approximate anisotropic resolution limits in the directions a / b / c [Å]	2.88 / 2.88*** / 3.44

Table 3.1: Diffraction data statistics

Numbers in squared brackets represent the cumulative statistics for the high-resolution shell in the weakest diffracting direction. The high resolution limit was selected as the resolution beneath which the anisotropic $\langle I \rangle / \langle \sigma(I) \rangle$ was less than 2.0. Numbers in parentheses represent the cumulative statistics for the highest resolution shell used.

*: The data collection geometry was such that all reflections to 2.88 Å resolution passed through diffraction conditions multiple times. Diffraction data used in refinement are 75% complete to 3.44 Å. The falloff in geometric completeness at higher resolution is the result of the diffraction anisotropy. Accordingly, although some diffraction data extending to 2.88 Å resolution were used in refinement, the effective resolution of the structure we describe is lower.

**: The informative completeness is based on the data actually used in refinement after

converting intensities to amplitudes. The relatively weak diffraction measureable from our crystals means that the informative completeness is significantly lower than the geometric completeness, especially for the higher resolution data.

***: As judged by the anisotropic $\langle I \rangle / \langle \sigma(I) \rangle$, the crystal diffracted to a minimum Bragg spacing of 2.65 Å in this direction. Given the weak overall diffraction and low completeness at higher resolutions due to the anisotropy, we chose to not include this small amount of higher resolution data as part of the refinement.

Refinement and model building

All crystallographic calculations after diffraction data processing were performed using Phenix (3). Phases were obtained by molecular replacement, using search models designed to minimize the effects of model bias. Curved conformation (4) (pdb code 1SA0) models for α- and β-tubulin gave significantly better results than did straight conformation in terms of the log likelihood gain achieved through the placement of the subunit (5) (pdb code 1JFF) models. Two different TOG domain structures (TOG2 domain from Stu2p (6), pdb code 2QK1 and TOG3 domain from Zyg9 (7), pdb code 2OF3) gave essentially equivalent results. Two forms of each search model were prepared: a poly-alanine one, and a 'sculpted' one that retained sidechains at conserved positions in poly-alanine background. GTP and GDP were stripped from the models prior to searching in order to obtain unbiased electron density for any bound nucleotides. Three separate maps were computed for the initial model building, one for each chain (for example, for the initial building of α-tubulin, we performed molecular replacement using a poly-ALA α-tubulin search model and sculpted models for the other two proteins). Model building was performed in Coot (8). Disordered regions were removed, and new sidechains were manually placed into each chain where the electron density indicated that was appropriate. The three rebuilt chains were then combined into a single model and subjected to additional cycles of refinement and rebuilding. GTP molecules were modeled early in the process because the electron density clearly indicated that both α- and β-tubulin contained a GTP molecule in their nucleotide-binding site. Because the data were relatively weak and anisotropic, the model was refined conservatively as appropriate for a moderate resolution structure. In the early stages we included secondary

structure restraints to help maintain good backbone geometry. These restraints were abandoned in later stages of refinement because they ceased to provide significant improvement as judged by parallel refinements. Owing to the moderate resolution, we sought to minimize the number of adjustable parameters, using torsion-angle simulated annealing and a combination of TLS with a single grouped B-factor for each residue. We also periodically ran tests to optimize the relative weighting of the X-ray and chemical restraints, consistently observing that optimal results (low R_{free} and low R_{free}-R_{work}) were obtained when the covalent geometry was tightly restrained to ideal values. For example, allowing the geometry to relax by choosing a weight such that bond and angle deviations in the refined model are 0.01 Å and 1.3° results in R_{free} decreasing by 0.3% while R_{work} decreases by substantially more, 2.5%. The tighter geometry therefore helps avoid over-fitting. Furthermore, although the completeness of our data decreases at higher resolution, a model refined against these data shows better geometry (fewer Ramachandran and sidechain outliers, and fewer clashes) than models refined without these incomplete but higher resolution data.

Model (residues)	Chain A: 1-280, 285-439 Chain B: 1-35, 39-174, 178-277, 283-432 Chain C: 11-40, 51-87, 91-213, 225-246, 254-272 2 GTP, 2 Mg
R_{work} (R_{free})	0.207 (0.268)
Maximum likelihood estimated coordinate error [Å]	0.38
Bond rms deviation [Å]	0.003
Angle rms deviation [°]	0.697
Residues in most favored ϕ/ψ regions [%]	92.1
Residues in disallowed ϕ/ψ regions [%]	1.5
Rotamer outliers [%]	6.7
B-factor (all, macromolecule, ligands)	64.4, 64.5, 46.3
Molprobity clashscore	17.86

R_{free} was calculated from a test set comprising 4% of the diffraction data about 1000 reflections).

Table 3.2: Model and refinement statistics

R_{free} was calculated from a test set comprising 4% of the diffraction data (about 1000 reflections).

*The B-factors of ligands are comparable to the B-factors of nearby protein residues. Ligands have lower average B-factors than the protein because regions of the structure distant from the GTP-binding sites have more elevated B-factors.

Rescue and spindle length assays

We used a rescue assay similar to the one reported in (9). We obtained CUY1147 (10), a yeast strain that allows conditional depletion of Stu2p in the presence of Cu2+, and pWP70 (11), a CEN plasmid expressing HA-tagged Stu2p from its own promoter, as generous gifts from T. Huffaker (Cornell U.). To use pWP70 (and derivatives) in CUY1147, we first disrupted the LEU2 gene with a marker coding for G418 resistance to create the CUY1147* strain. Site-directed mutants in Stu2p were prepared using QuikChange mutagenesis with pWP70 as the template. For the rescue assay, CUY1147* transformed with pWP70 (wildtype control), various mutants), or p415Gal1 (an empty expression plasmid that confers the ability to grow on media lacking Leucine). Strains were grown overnight in CSM-Leu media, normalized to A_{600} = 1, plated at serial tenfold dilutions onto CSM-Leu plates containing various additives (control: DMSO; Stu2p depletion: 500 μM CuS04 and various amounts of benomyl – 0, 5, 10, and 20 μg/ml), and imaged after three or seven days for growth at 30 °C or room temperature, respectively. A growth phenotype was observable at both growth temperatures. Room temperature plates containing 20μg/ml benomyl are shown in (Figure 3.6.)

For the spindle length measurements, CUY1147* transformed with pWP70 (wildtype Stu2p rescue) or with pWP70-Stu2p(R200A) (TOG1:αβ-tubulin interaction disrupting mutant) strains were grown overnight, diluted to 0.3 A_{600} and cultured in the presence of 500 μM CuSO4 to initiate depletion of endogenous Stu2p. After 2 hours, we added hydroxyurea (0.1 M final concentration) to synchronize the cells by arresting them in early S phase. Arrest was confirmed by immunofluorescence and DIC imaging (not shown). After 3 hours of arrest, we released cells by washing them twice before

resuspending them in fresh media containing 500 μM CuSO4. Cells were fixed immediately (to verify arrest) and one hour after release (to image spindle length) by a one hour treatment with 4% formaldehyde at room temperature. After washing twice with PBS to remove formaldehyde, cells were resuspended in 40 mM potassium phosphate pH 6.5, 0.5 mM MgCl2 , 1.2 M sorbitol before permeabilization with zymolyase 100T for 30 minutes at 30 °C. After washing to remove zymolyase, cells were stained with a FITC conjugated anti-α-tubulin antibody (DM1α, Sigma-Aldrich) in a dark humid chamber at room temperature for 90 minutes before preparing slides using DAPI-containing mounting media.

Analysis of tubulin conformation, bending angle, and the TOG1 binding epitopes

Analogously to prior studies (12-14), different tubulin monomer conformations were compared after pairwise superposition in Pymol (15) using the structurally conserved N-terminal domain (residues 1:180). Root mean square Cα coordinate differences were computed for selected secondary structural elements using the rms_cur command. The H6-H7 and intermediate domain β-strands are defined in Table 3.3. The intra-heterodimer bending angle was determined by analyzing the transformation required to superimpose the α-tubulin chain onto the β-tubulin chain using the Cα positions of the rigid N-terminal domain (similar results are obtained from superposition's using all Cα positions). The hypothetical model of TOG1 associated with straight αβ-tubulin (pdb code: 1JFF) was prepared by first superimposing straight αβ-tubulin onto yeast αβ-tubulin using the Cα positions in the rigid N-terminal domain of α-tubulin (residues in this domain are directly contacted by the TOG1 domain), and

subsequently deleting the model for yeast αβ-tubulin. To identify the αβ-tubulin surfaces involved in lateral microtubule contacts, we used proximity-based selections in Pymol after superimposing the α- and β-tubulin monomers of the TOG1:αβ-tubulin complex onto the central protofilament of an atomic model of the microtubule.

	α and β-tubulin (1JFF/1SA0)	α-tubulin (yeast)	β-tubulin (yeast)	γ-tubulin (1Z5V)
H6-H7	206:244	207:245	206:244	207:245
β-sheet	268:274 314:321 351:357 373:380	269:275 315:322 352:358 374:381	266:272 312:319 349:355 363:370	269:275 319:326 356:362 373:380

Table 3.3: Residue ranges used for comparing the relative arrangement of tubulin subdomains.

Gel filtration and microtubule nucleation and co-sedimentation experiments

Gel filtration experiments were performed by loading 200 µl of 5 µM protein onto a Superdex 200 10/300 column equilibrated in 25 mM Tris pH 7.5, 100 mM NaCl, 1 mM MgCl2, 1 mM EGTA. To record the kinetics of microtubule assembly with and without added TOG domain, we used an Agilent 8453 spectrophotometer to follow the timecourse at A350 nm after reactions were warmed to initiate assembly by directly pipetting cold reactions into a pre-warmed cuvette. All assays contained 15 µM animal brain αβ-tubulin (25% of the reaction mix, in BRB80 containing 1 mM GTP, 1 mM DTT, and 25% glycerol; BRB80 is 80 mM PIPES pH 6.8, 1 mM MgCl2, 1 mM EGTA) and 3 µM TOG1, 3 µM TOG2, or buffer (10% of the reaction mix in the gel filtration buffer described above). The assay buffer was 50 mM MES pH 6.6, 5 mM MgSO4, 1 mM EGTA, 3.4 M glycerol.

We also used microtubule 'spindown' experiments as an alternate way to assay microtubule assembly. These were performed by yeast αβ-tubulin with or without TOG domains in assembly buffer (100 mM PIPES pH 6.9, 2 mM MgSO4, 2 mM EGTA, 10% Glycerol; protein concentration 3.5-5 µM) for 30 minutes at 30 °C. A portion of the assembly reaction was cross-linked by diluting 10-fold into assembly buffer containing 1% glutaraldehyde. Cross-linking was quenched after 3 minutes by 5-fold dilution into assembly buffer containing 20 mM Tris pH 6.9. 30 µl of these quenched, cross-linked reactions were applied to the top of a glycerol cushion (20% glycerol in BRB80) and spun through the cushion onto poly-lysine coated coverslips. Coverslips were stained using FITC-DM1α (Sigma-Aldrich) for imaging by fluorescence.

Microtubule co-sedimentation experiments were preformed similarly using 3 µM αβ-

tubulin and with TOG1 or TOG2 added after an initial period of microtubule formation. Epothilone B (Sigma-Aldrich) was included for additional microtubule stabilization. No cross-linking was performed and, after incubation with TOG1, microtubules were harvested by centrifugation at 50,000 xg at 30 °C for 30 minutes in a pre-warmed TLA-100 rotor. Supernatant was carefully removed, and the pellet was resuspended in 1X SDS buffer such that pellet and supernatant fractions were of equal volume. The fractions were subsequently analyzed by gel-electrophoresis. Control experiments (not shown) reproduced the microtubule sedimentation previously demonstrated for an unrelated protein, Mal3(16).

Fluorescence anisotropy

To obtain fluorescently-labeled TOG1 or TOG2 domains, we used PCR to append a sequence coding for WDCCPGCCK between the C-terminal His6 tag and the stop codon in our expression construct. After expressing and purifying the resulting proteins (as described above), we labeled them with a bis-arsenical fluorescein dye (Lumio green, Invitrogen) at room temperature for 80 minutes in the dark. The labeled proteins were then re-purified by gel filtration on a Superdex 200 10/300 column in order to remove unreacted dye. Polymerization-competent yeast tubulin was purified as described above (in 50 μM GTP or GDP) and dialyzed into 25 mM TRIS pH 7.5, 1 mM EGTA, 1 mM MgCl2, 100 mM NaCl and 50 μM (GTP or GDP). Anisotropy measurements were made with an Alpha−scan spectrofluorimeter (Photon Technology International, Santa Clara, California), using 20 nM labeled TOG2 mixed with various concentrations of αβ-tubulin. The dye was excited with polarized light at 507 nm.

Emitted light was detected at 527 nm through both horizontal and vertical polarizers. Measurements were made at 5-s intervals for 180 s, and the average anisotropy was calculated using PTI Felix software. Dissociation-equilibrium constants (K_d) were calculated by fitting the equation:

$$r = r_f + (r_b - r_f)\left(\frac{(K_d + [\alpha\beta] + [TOG2]) - \sqrt{(K_d + [\alpha\beta] + [TOG2])^2 - 4[\alpha\beta][TOG2]}}{2[TOG2]}\right)$$

to the ligand-concentration dependence of the anisotropy. Here r_f is the anisotropy value of free Lumio–TOG2, r_b is the anisotropy of Lumio–TOG2 bound to αβ-tubulin, [TOG2] is the concentration of Lumio-TOG2, and [αβ] is the concentration of αβ-tubulin (ligand).

Analytical ultracentrifugation

Samples for analytical ultracentrifugation (TOG1, TOG2, TOG1-TOG2, and polymerization-blocked αβ-tubulin) were purified and dialyzed as described above but with the GTP concentration reduced to 20 μM in order to avoid excessive absorbance coming from the nucleotide. Final buffer conditions were 25 mM Tris pH 7.5, 1 mM MgCl2, 1 mM EGTA, 100 mM NaCl, 20 μM GTP. Concentrations for the samples shown in Figure 3.5. are: TOG1, 5.26 μM; αβ-tubulin: 1.2 μM; mix: 8.76 μM TOG1 and 1.45 μM αβ-tubulin; TOG2: 2.25 μM; αβ-tubulin: 0.6 μM; mix: 11.28 μM TOG2 and 0.79 μM αβ-tubulin. Concentrations for the samples shown in Figure 3.17. are: αβ-tubulin: 1.2 μM; TOG1-TOG2: 3.7 μM; low TOG1-TOG2 mix: 0.46 μM TOG1-TOG2 and 1.5 μM αβ-tubulin; high TOG1-TOG2 mix: 10.8 μM TOG1-TOG2 and 1.5 μM αβ-tubulin. Samples were mixed and incubated at 4 °C for at least one hour prior to the

experiment. All analytical ultracentrifugation experiments were carried out in an Optima XL-I centrifuge using an An50-Ti rotor (Beckman–Coulter). Approximately 390 μl of each sample were placed in charcoal-filled, dual-sector Epon centerpieces. Sedimentation (rotor speed: 50,000 rpm) was monitored using absorbance optics, and centrifugation was conducted at 20° C after the centrifugation rotor and cells had equilibrated at that temperature for at least 2.5 hours. Data were analyzed using SEDFIT and SEDPHAT (available at http://www.analyticalultracentrifugation.com) (17, 18). Protein partial specific volumes, buffer viscosities, and buffer densities were calculated using SEDNTERP (19). The molar mass obtained from the Svedberg equation for all species analyzed is listed in Table 3.4.

Species	Observed molar mass (g/mol)	Theoretical molar mass (g/mol)
TOG1	39,600	36,685
TOG2	33,000	28,780
TOG1-TOG2	66,000	64,624
αβ-tubulin	113,000	102,686
TOG1:αβ-tubulin	140,000	139,371
TOG2:αβ-tubulin	123,000	131,466
TOG1-TOG2:(αβ-tubulin)	160,000	167,310
TOG1-TOG2:$(\alpha\beta\text{-tubulin})_2$	N/A*	269,996

Table 3.4: Molar masses obtained by analytical ultracentrifugation.

Molar masses were obtained from the Svedberg equation using the refined values of the sedimentation coefficient (s) and the diffusion coefficient (D, obtained as a function of s and the refined frictional ratio (fr)).

*The frictional ratio of this species refined to an uncharacteristically low value (~1.2). Given the high frs of the constituents (1.45 for αβ-tubulin and 1.55 for TOG1-TOG2), it is likely that this "species" actually represents a rapidly reacting "reaction boundary," which may result in depressed refined frs in a c(s) analysis (20).

Results

To establish the structural basis of TOG:tubulin recognition, we determined the crystal structure of the TOG1 domain from Stu2p bound to αβ-tubulin (Figure 3.1.). We used a polymerization-blocked mutant of yeast αβ-tubulin to obtain crystals (1). The structure was determined by molecular replacement from crystals that diffracted anisotropically to 2.88 Å (minimum Bragg spacing of 3.44 Å in the weakly diffracting direction, overall completeness of 74.6%) **(**Tables 3.1 and 3.2). The structure contains guanosine triphosphate (GTP) at the exchangeable nucleotide-binding site of αβ-tubulin (Figure 3.1. inset). TOG1 forms a flat, layered structure similar to that observed for other TOGs (Figure 3.1. and Figure 3.2.) (6, 7). Almost the entire narrow, evolutionarily conserved face of TOG1 (6, 7) interacts with αβ-tubulin (Figure 3.1. and Figure 3.2.), burying ~1600 Å2 of surface area, 58% of which is attributable to the partial interface with β-tubulin.

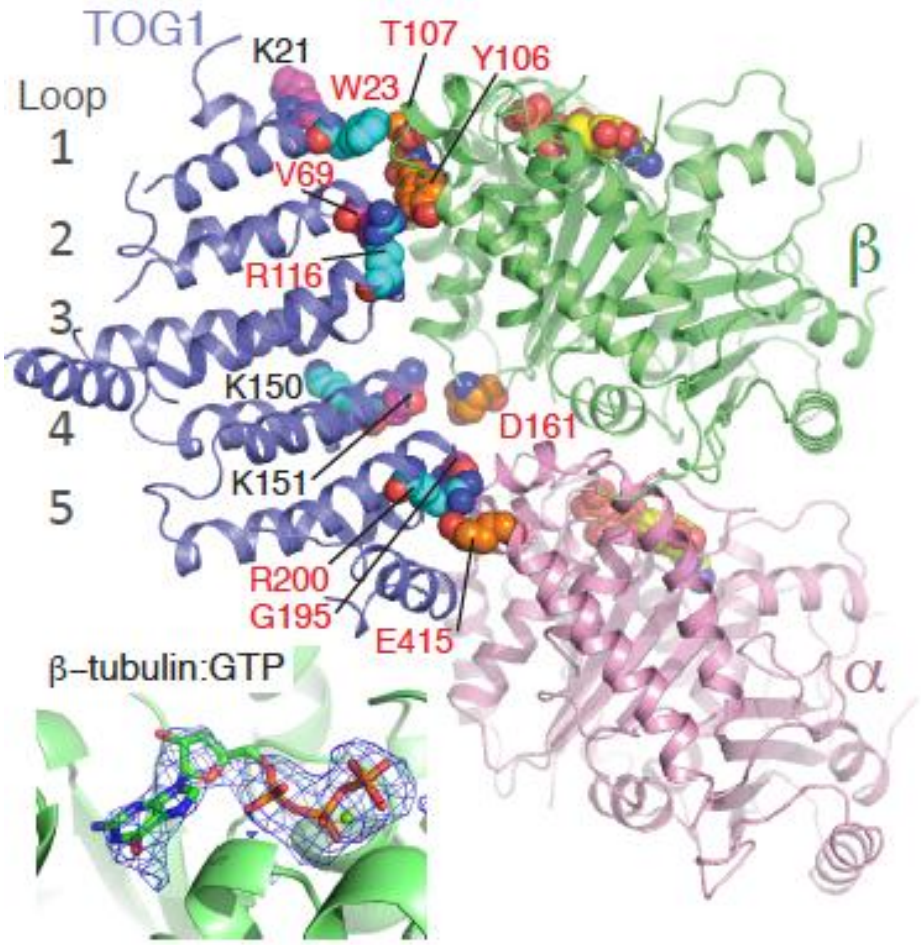

Figure 3.1: Structure of a TOG1:αβ-tubulin complex, revealing noteworthy contacts with α- and β-tubulin.

Cartoon representation of the complex (pink, α-tubulin; green, β-tubulin; blue, TOG1). Contacts probed by mutagenesis are represented as sphere, as are GTPs. Y, Tyr; G, Gly. Mutations of the residues highlighted with red label disrupt the TOG1:tubulin binding.

(Inset) mF0-DFc omit electron density map contoured at 3.5σ and computed from a model without nucleotides: β-tubulin is bound to GTP.

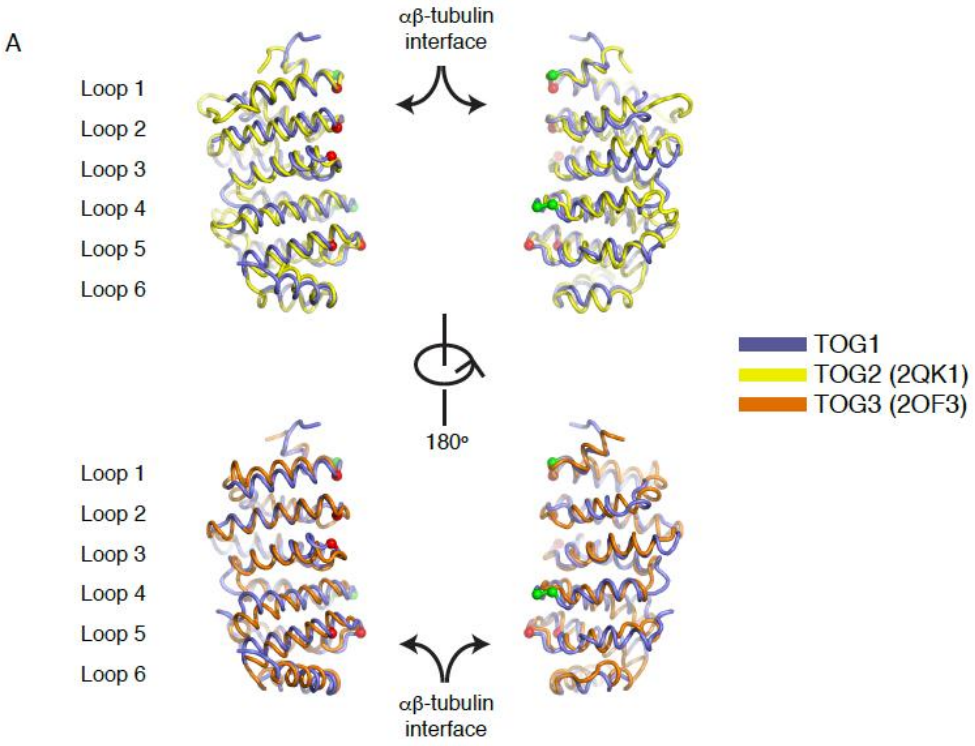

B

	Loop 1	Loop 2
	- *	*
Stu2p TOG1	17 RLTYKL**WK**A 25	66 DS**NVV**AQ 72
Stu2p TOG2	335 RITSSKWKD 343	383 DANIQAV 391
Zyg9 TOG3	655 QLFHKDFKQ 663	699 ETNPAAL 707

	Loop 3	Loop 4
	*	--
Stu2p TOG1	112 L**T**SS**R**ATT 119	149 EK**KLP**KLI 156
Stu2p TOG2	424 TKEKKPSV 431	467 KHKTPQIR 474
Zyg9 TOG3	742 TGEAKDNM 749	778 KSKNARQR 785

	Loop 5	Loop 6
	* *	
Stu2p TOG1	192 **AGHGDR**NV**R**S 201	228 KL**K**P**IQ**VK**D** 236
Stu2p TOG2	511 VNDTQPAIRT 520	544 HLDNLKRKK 552
Zyg9 TOG3	817 VGDKDVNVRN 826	849 RMADKDKSL 857

Figure 3.2: Comparative analysis of TOG domain sequence and structure

A) Structures of the TOG2 domain from Stu2p (pdb code 2QK1, yellow) and the TOG3 domain from Zyg9 (pdb code 2OF3, orange) were superimposed on the TOG1 structure

using the ‘super’ command in PyMol. ‘Front’ and ‘back’ views are shown, and the αβ-tubulin-interacting region faces the center. Locations where TOG1 mutations disrupted αβ-tubulin binding are indicated with red spheres at the Cα position. Locations where TOG1 mutations did not disrupt αβ-tubulin binding are indicated with green spheres at the Cα position. In our hands, individual K150A or K151A mutations did not disrupt αβ-tubulin binding, in contrast to a prior study in which the K150A, K151A double mutant did. We do not have an explanation for this apparent discrepancy, but our result is consistent with the D161A β-tubulin mutant that interacts normally with TOG1. Perhaps some other difference between yeast αβ-tubulin (used by us) and animal αβ-tubulin (used in the prior studies) is responsible for differing sensitivity in this region of TOG1. The three different TOG domains share a common structure that apparently tolerates variability in the detailed packing of some α-helical elements (TOG2: Loop 2, left panel and Loop 3, right panel; TOG3: Loop 2, right panel and Loop 5, left panel). The αβ-tubulin binding elements (center facing) are also structurally conserved but with some variability in positioning relative to each other. Loops on the opposite face are highly variable.

B) Structure-based multiple sequence alignment of the TOG1, TOG2, and TOG3 domains. Sequences are shown only in the vicinity of the αβ-tubulin contacting residues. Sites of disruptive or non-disruptive mutagenesis are indicated with a red * or green -, respectively. Residues of TOG1 with any atom within 5.5 Å of αβ-tubulin are indicated in bold. Probably only a subset of these residues (which show relatively strong sequence conservation) contributes substantially to αβ-tubulin binding.

The asymmetric mode of TOG1 binding apparently excludes analogous binding of TOG2 to the same heterodimer. This finding is unexpected because it was assumed that multiple TOGs could simultaneously engage a single αβ-tubulin heterodimer (7, 9, 21).

We used site-directed mutagenesis and a gel filtration binding assay to probe the importance of TOG1:αβ-tubulin contacts (Figure 3.3.) (6, 7). TOG1:αβ-tubulin interactions were affected by mutations on α- or β-tubulin–contacting loops of TOG1 or on contacted surfaces of α- or β-tubulin [e.g., W23A (Trp23→Ala23) or R200A (R, Arg) on TOG1, T107E (T, Thr; E, Glu) on β-tubulin, E415A on α-tubulin] (Figure 3.1. and Figure 3.3.). The importance of TOG1:W23 confirms findings from earlier studiesv(6, 7). The salt bridge between TOG1:R200 and α-tubulin:E415 (Figure 3.4.) that is required for robust TOG1: αβ-tubulin interactions (Figure 3.3.) rationalizes the strong evolutionary conservation of R200 in TOG domains (7). Analytical ultracentrifugation revealed that TOG1 and TOG2 each bind αβ-tubulin efficiently at low micromolar concentrations (Figure 3.5.). Thus, TOG1:αβ-tubulin interactions detected in solution require simultaneous engagement with both α- and β-tubulin as observed in the crystal, and TOG2 can interact with unpolymerized αβ-tubulin.

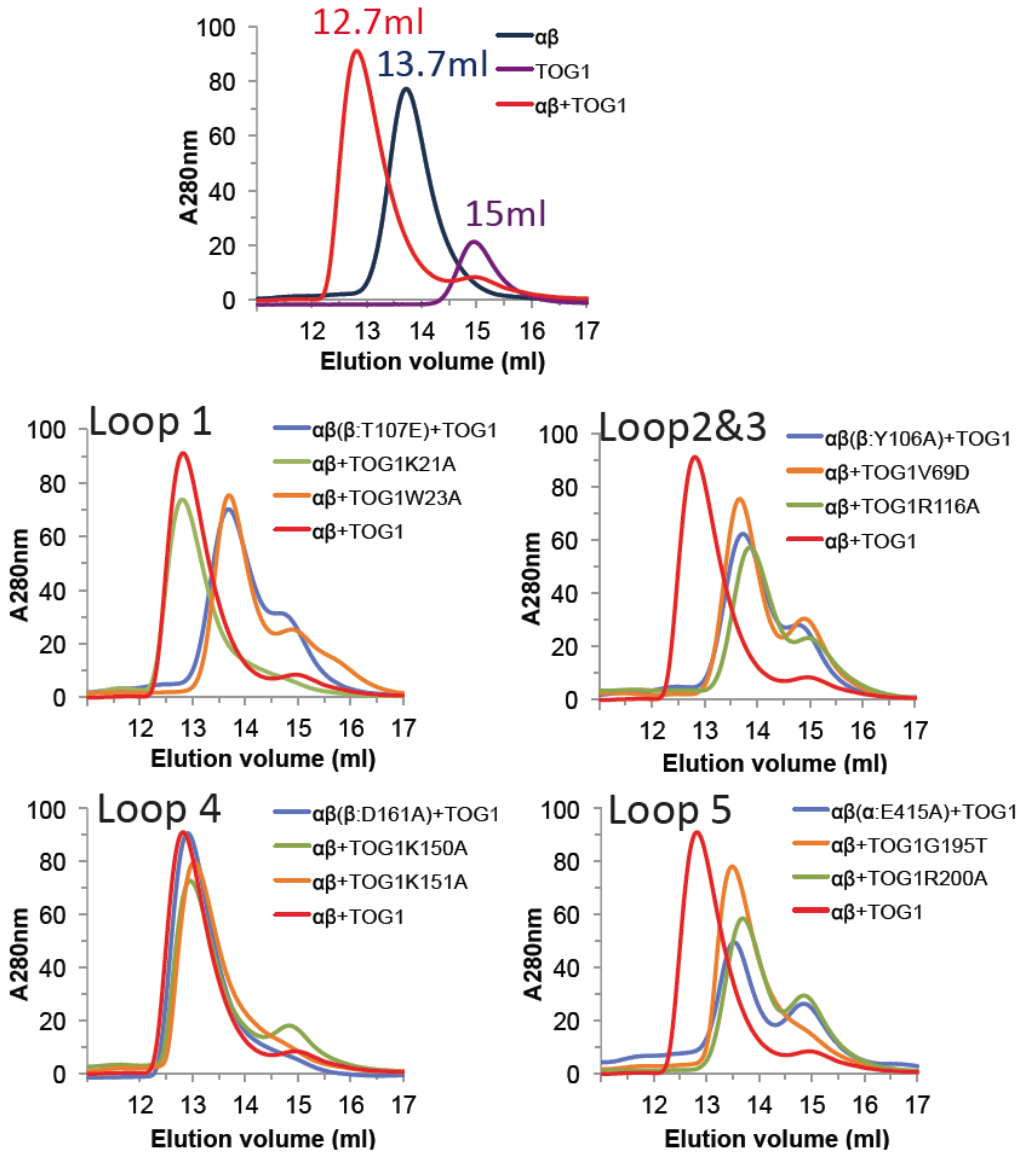

Figure 3.3: Size-exclusion chromatography assay for TOG1:αβ-tubulin interactions. TOG1: αβ-tubulin binding assay using interface mutants on loop 1-5. Size-exclusion chromatography assays were performed using individual proteins at 5 μM concentration.

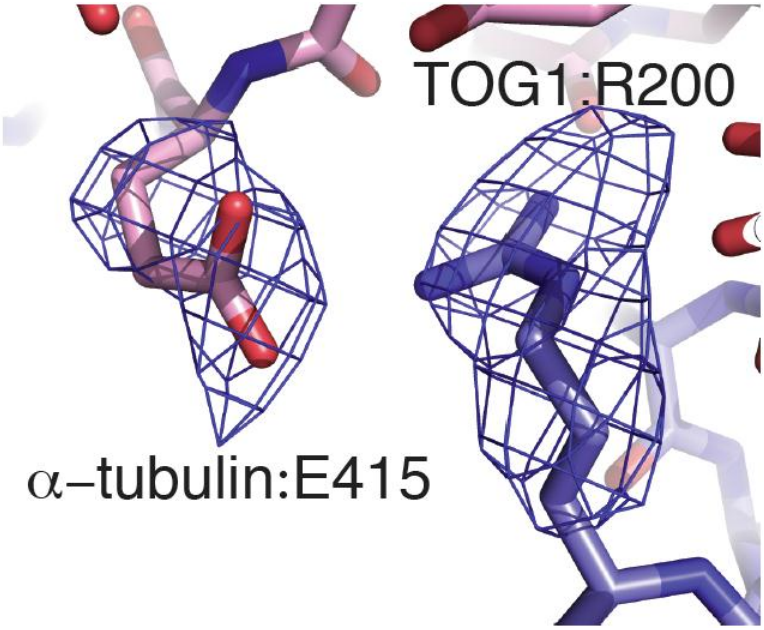

Figure 3.4: The R200:E415 salt bridge.

Annealed omit density for TOG1:R200 and α-tubulin:E415 contoured at 3σ. The model was subjected to torsion-angle dynamics-based simulated annealing refinement after deleting sidechain atoms for both residues. The resulting Fo-Fc map is shown here.

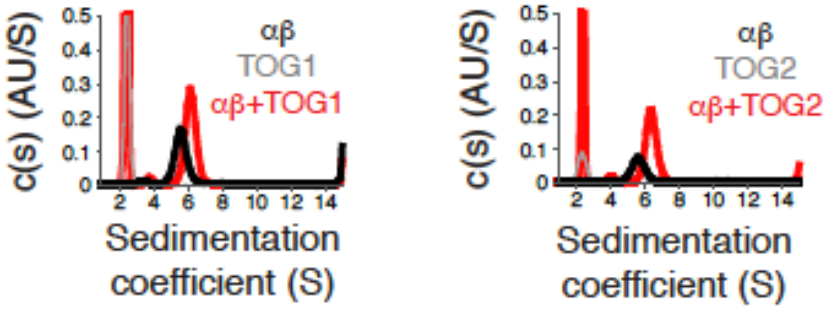

Figure 3.5: Analytical ultracentrifugation assays for TOG αβ-tubulin binding

TOG1 (left) and TOG2 (right) (gray) each form a 1:1 complex (red) with αβ-tubulin (black), as detected by analytical ultracentrifugation (Table 3.4.). Curves are shown from s = 1 S to eliminate a slowly sedimenting contaminant in the TOG2 run. c(s), signal population as a function of s; AU, absorbance units.

We used conditional depletion of Stu2p (10) and a rescue assay to investigate how mutations on the tubulin-interacting surfaces of TOG1 or TOG2 affect Stu2p function in vivo. Wild-type Stu2p and Stu2p with a TOG1 mutation (K21A; K, Lys) that did not interfere with αβ-tubulin binding completely rescued the growth defect arising from the depletion of endogenous Stu2p. In contrast, Stu2p with mutations in TOG1 [W23A, V69D (V, Val; D, Asp), or R200A] that affect αβ-tubulin binding was compromised for rescue (Figure 3.6. A). Mutations on the presumptive αβ-tubulin–interacting surface of TOG2 (W341A and R519A) affected rescue similarly to their TOG1 equivalent (W23A and R200A) (Figure 3.6. A). The R200A mutant of Stu2p displayed a defect in mitotic spindle elongation (Figure 3.6. B), similar to the complete removal of the TOG1 domain (9).

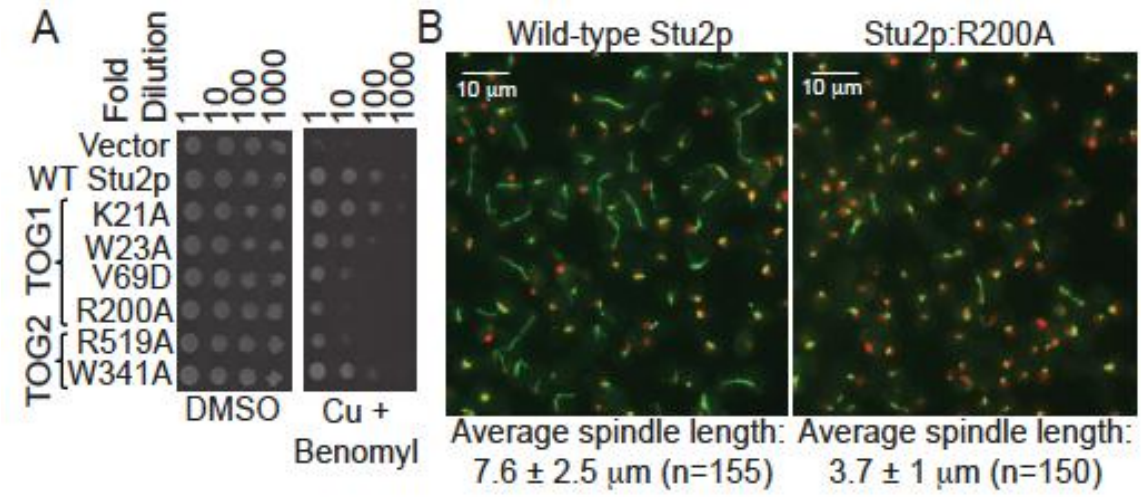

Figure 3.6: Disruptive point mutations on the tubulin-binding interfaces of TOG1 or TOG2 affect Stu2p function in vivo.

A) Yeast carrying plasmid-based rescue constructs of Stu2p were plated at serial dilutions on media containing dimethyl sulfoxide (DMSO) (control) or 500 mM CuSO4 (to deplete endogenous Stu2p) plus 20 mg/ml benomyl (to cause microtubule stress). TOG1 or TOG2 impaired for αβ-tubulin interactions only partially compensate for the depletion of endogenous Stu2p.

B) Fluorescence images at 1 hour after release from hydroxyurea arrest (green, αβ-tubulin; red, DNA) of yeast depleted of endogenous Stu2p and rescued with wild-type (left) or R200A (right) Stu2p. Spindle elongation is compromised when TOG1:αβ-tubulin interactions are impaired (R200A). n, number of spindles measured.

The conformations of α- and β-tubulin in the TOG1 complex are remarkably similar to each other (Figure 3.7., Figure 3.9.), to the curved α– and β-tubulin monomer conformations previously described (4), and to γ-tubulin (Figure 3.8., Figure 3.9.) (14). A 13° rotation is required to superimpose the α- and β-tubulin chains in the TOG1 complex. This quaternary arrangement also closely resembles that of a curved heterodimer (12° rotation) (4), which is characteristically distinct from the straight heterodimer (~1° rotation) (Figure 3.10.) (5). Instead, this curved conformation could represent a conserved ground state of αβ–tubulin.

Together, these observations add further support to a model in which the role of GTP is to promote assembly by tuning the strength of polymerization contacts (13) and/or by decreasing the free-energy difference between straight and curved conformations (22).

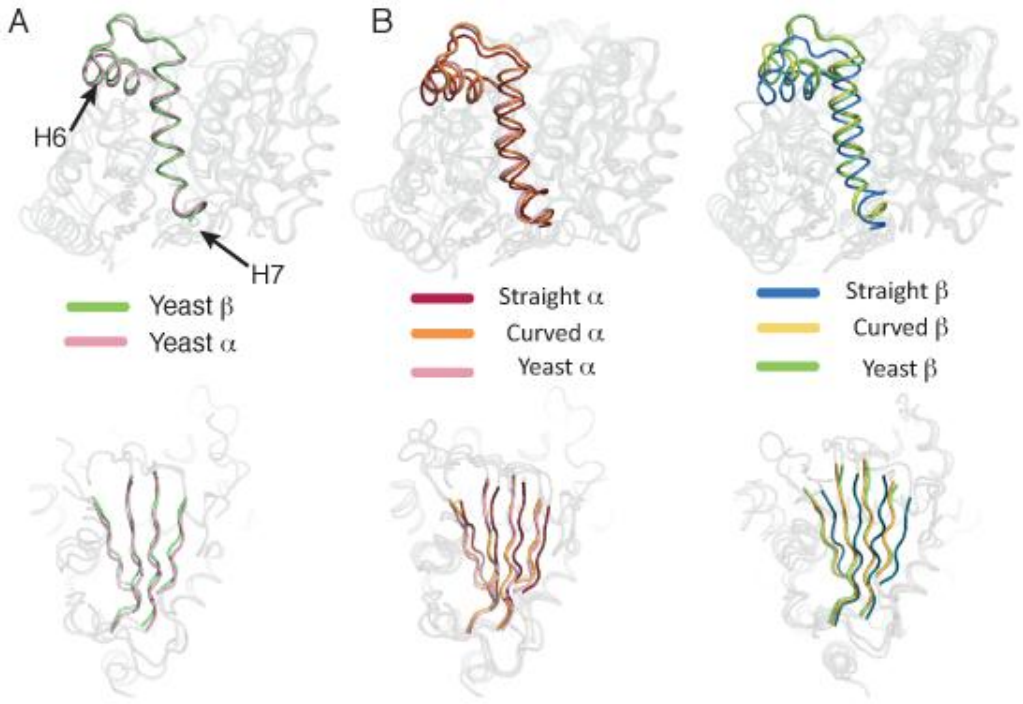

Figure 3.7: αβ-tubulin–GTP adopts a curved conformation.

A) Superposition of yeast α- (pink) and β-tubulin (green) shows similar positioning of the H6-H7 segment and intermediate domain β-sheet (represented with darker colors). The view is heavily clipped for clarity, and two helices have been omitted so as not to obscure the view of the β-strands.

B) Superposition of yeast α- and β-tubulin onto curved (α, orange; β, yellow) and straight (α, maroon; β, dark blue) structures shows the H6-H7 segments and intermediate domain β-sheet of yeast tubulins arranged as in earlier curved structures.

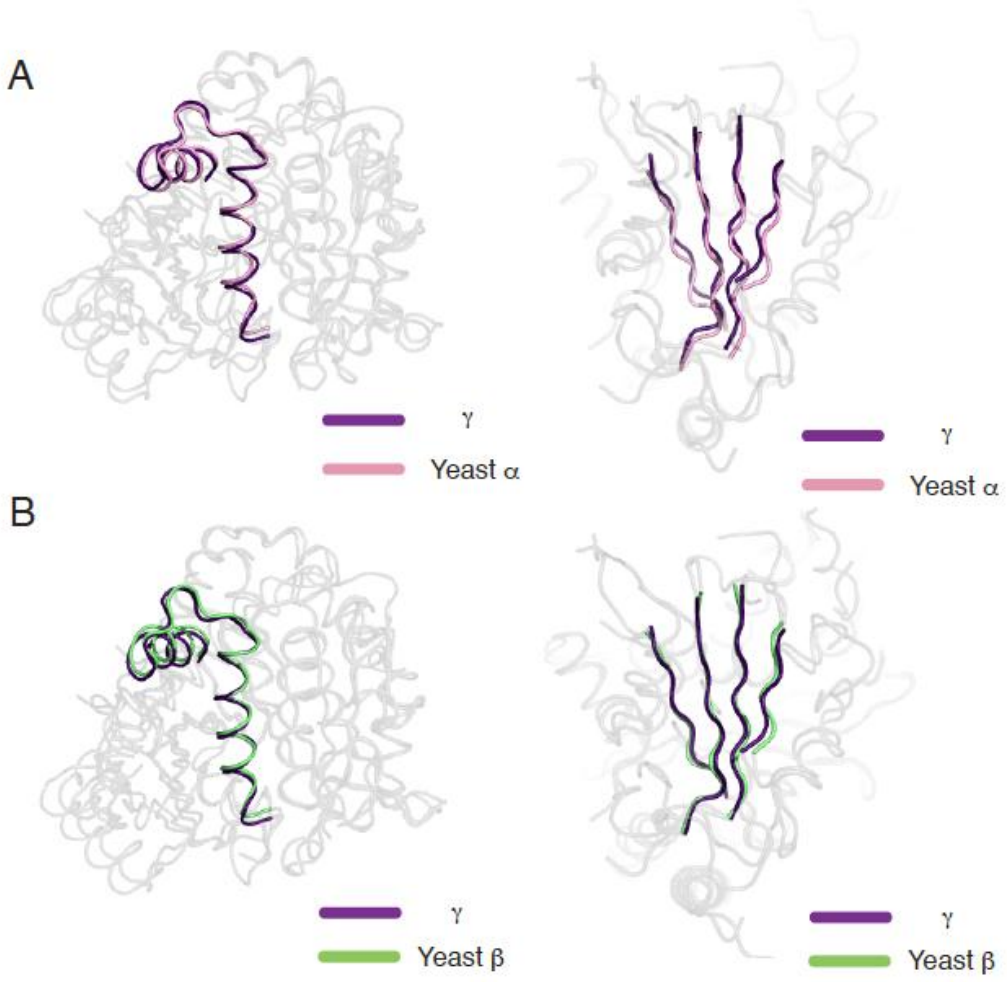

Figure 3.8: Structural comparison between αβ-tubulin-GTP and γ-tubulin-GTP

A) Superposition of yeast α-tubulin (pink) onto γ-tubulin:GTP reveals that the arrangement of helices H6-H7 (left panel, dark elements) and of the intermediate domain β-sheet (right panel, dark elements) in the two structures are very similar.

B) Superposition of yeast β-tubulin (lime) onto to the γ-tubulin:GTP reveals that the arrangement of helices H6-H7 (left panel, dark elements) and of the intermediate domain β-sheet (right panel, dark elements) in the two structures are very similar.

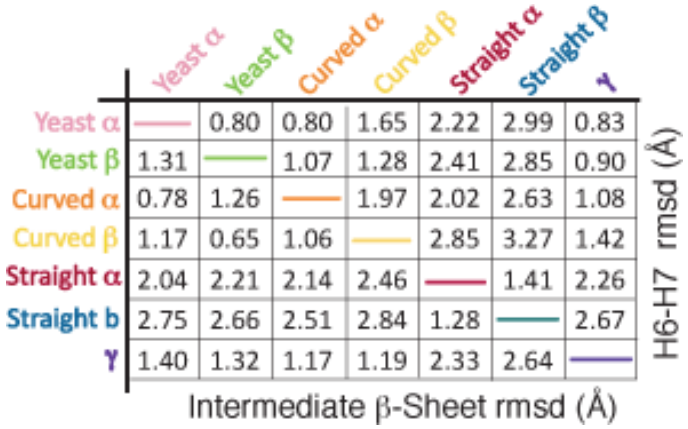

Figure 3.9: Pairwise Cα root mean square coordinate deviations (rmsd) between yeast α- and β tubulin and earlier structures, computed for the subdomains indicated (Table 3.3.)

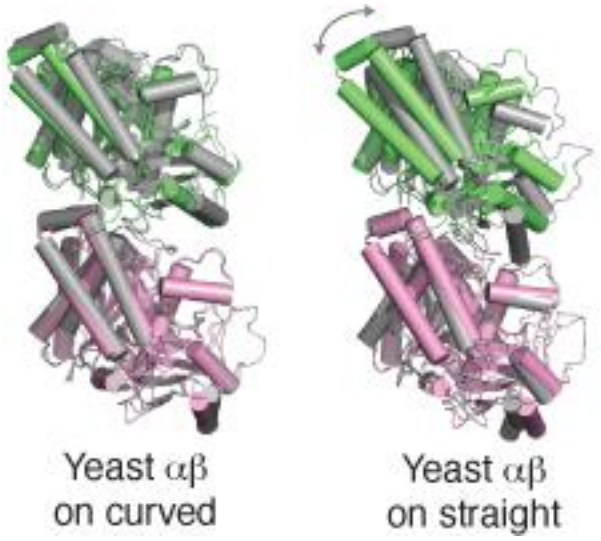

Figure 3.10: The quaternary structure of yeast αβ-tubulin (pink and green) resembles that of the curved form (gray, left) and differs from the straight form (gray, right).

The regions of curved αβ-tubulin that engage TOG1 move relative to each other in the transition to the straight conformation (Figure 3.11.). Thus, TOG1: αβ-tubulin interactions might be sensitive to αβ-tubulin quaternary structure, with a preference for curved αβ-tubulin. If TOG1 binds preferentially to curved αβ-tubulin, it should inhibit in vitro microtubule formation by stabilizing a microtubule incompatible conformation of αβ-tubulin. We used microtubule-assembly reactions to test this counterintuitive prediction, and we observed strong inhibition when TOG1 was present (Figure 3.12.), consistent with earlier observations (6). We did not observe inhibition for TOG1 mutants (e.g., W23A or R200A) (Figure 3.13.) that affect αβ-tubulin binding. TOG1 does not bind appreciably to straight αβ-tubulin in preformed microtubules (Figure 3.14.), despite the apparent accessibility of the TOG1- interacting epitopes on the outside of the microtubule (Figure 3.15.). Thus, TOG1 binds preferentially to curved αβ-tubulin. We obtained similar results for TOG2, indicating that it also binds preferentially to an αβ-tubulin conformation that cannot exist in the body of the microtubule.

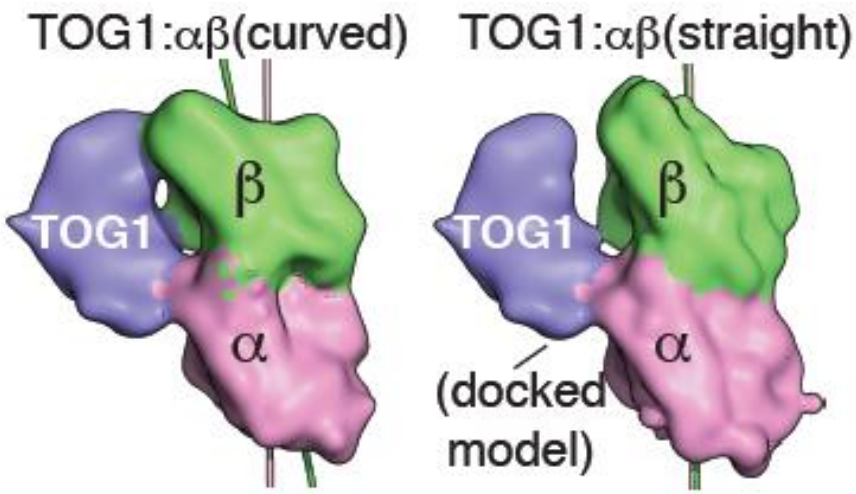

Figure 3.11: The structure of the TOG1:αβ-tubulin complex (left) and a docked model with straight αβ-tubulin (right) illustrates how TOG1-contacting epitopes on α- and β-tubulin move relative to each other in the two conformations.

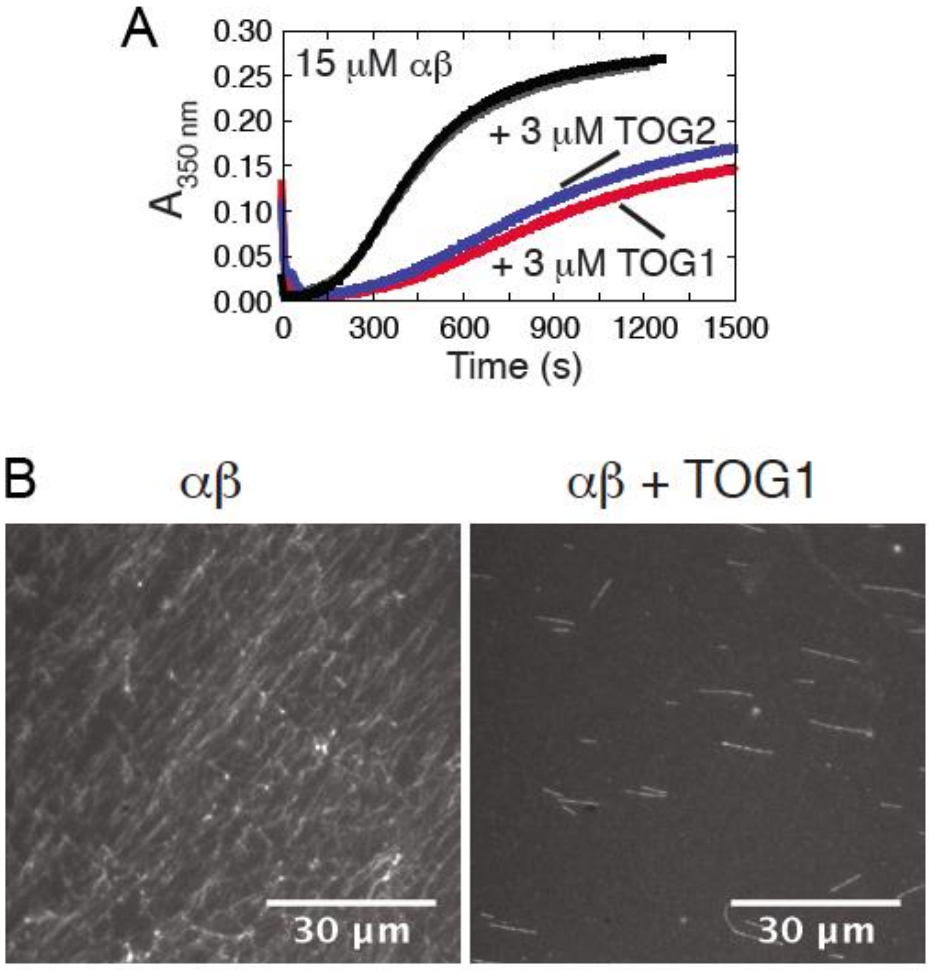

Figure 3.12: Isolated TOG1 and TOG2 inhibits microtubule assembly

A) Microtubule-assembly reactions (15 μM animal αβ-tubulin) containing 3 μM TOG1 (red) or TOG2 (blue) are inhibited relative to control reactions (black and gray) that received only buffer.

B) In vitro microtubule assembly assays examined by immunofluorescence reveal that stoichiometric addition of the TOG1 domain inhibits microtubule assembly. Similar results were obtained using TOG2 (not shown).

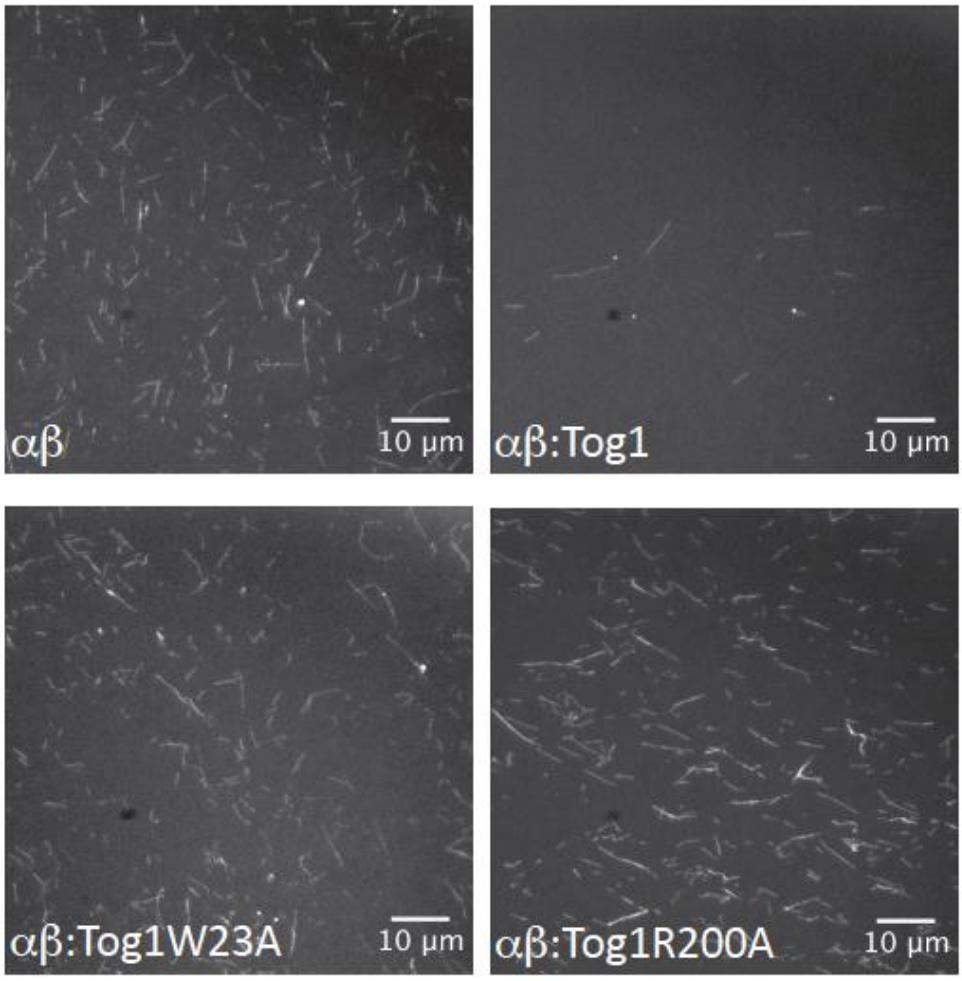

Figure 3.13: Mutations that disrupt TOG1:αβ-tubulin interactions interfere with TOG1-dependent inhibition of microtubule assembly.

Top row: addition of stoichiometric TOG1 domain to microtubule assembly reactions (3.5 μM yeast αβ-tubulin). Bottom row: TOG1 mutants (W23A and R200A) that interact poorly with αβ-tubulin show significantly reduced inhibitory activity when added to microtubule assembly reactions.

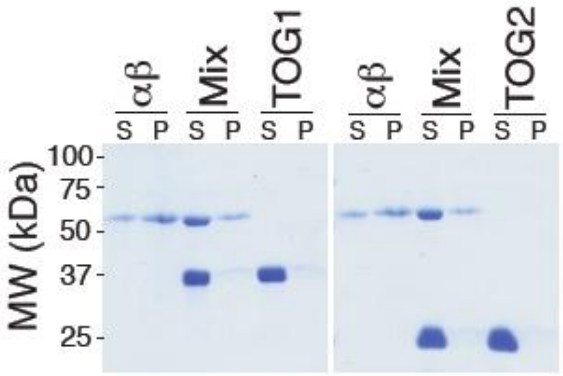

Figure 3.14: Microtubule co-sedimentation assay

The assay shows that TOG1 and TOG2 do not appreciably bind microtubules, even though the TOG-interacting epitopes are accessible on the outside of the microtubule (Figure 3.15.). MW, molecular weight; S, supernatant; P, pellet.

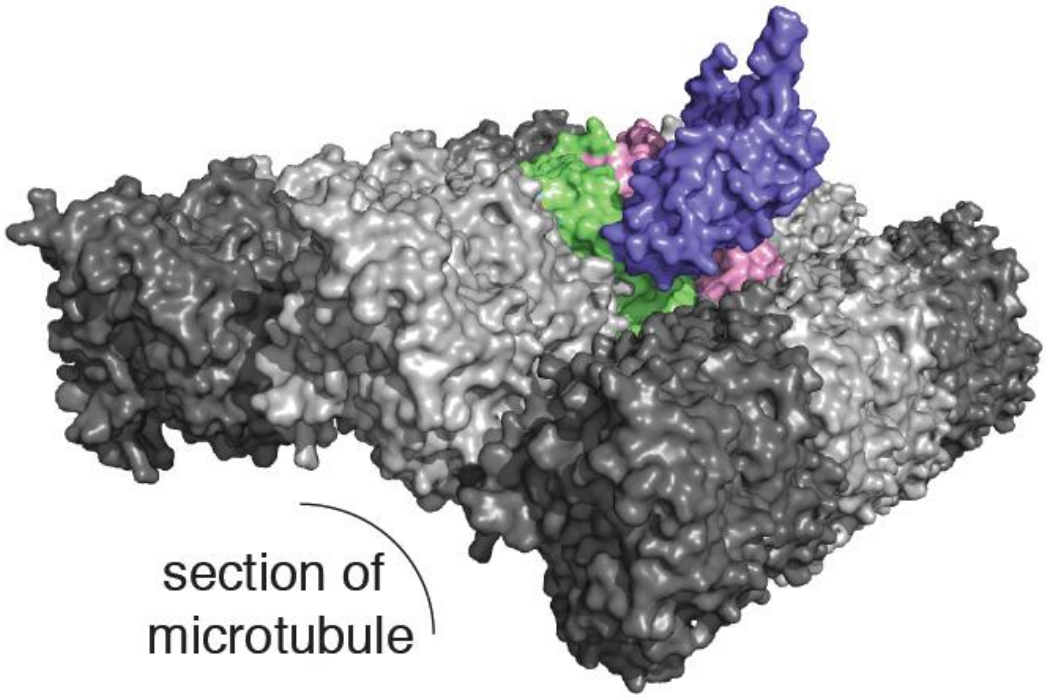

Fig. 3.15: The TOG1 interaction footprint relative to microtubule assembly contacts

To ask if the TOG1:αβ-tubulin interaction might occlude microtubule polymerization contact, we docked the TOG1:αβ-tubulin complex (colored) into a model of the microtubule (grey). The resulting model is artificial, because our data indicate that TOG1 binds very weakly, if at all, to the microtubule lattice. However, this docking experiment is most direct way to visualize how TOG1 binding would relate to the rest of the microtubule. No steric clashes between the TOG1 domain (slate) and the neighboring protofilament resulted. Thus, the TOG1-interacting epitopes are apparently accessible on the outer surface of the microtubule. This supports the conformation-selective model for TOG1:αβ-tubulin interactions: TOG1 does not bind microtubules because in microtubules αβ-tubulin adopts the straight conformation.

TOG2 binds to GTP- or guanosine diphosphate– bound αβ-tubulin with approximately equal affinity (200 to 300 nM) (Figure 3.16.), supporting a model in which the curvature of unpolymerized αβ-tubulin does not change appreciably as a function of the bound nucleotide. For the "hand-off" to the microtubule to be efficient, the affinity of αβ-tubulin:microtubule interactions must at least be comparable to that of TOG:αβ-tubulin interactions.

We used analytical ultracentrifugation to demonstrate that TOG1-TOG2 and αβ-tubulin interact in a manner that is most consistent with a fast interchange between 1:1 and 1:2 TOG1-TOG2: αβ-tubulin complexes (Figure 3.17., red trace). The observation of a TOG1-TOG2:(αβ-tubulin)2 complex is surprising, because earlier studies (9, 21) suggested that multiple TOG domains could simultaneously engage the same αβ-tubulin. Some of these earlier studies were conducted using a gel-filtration binding assay similar to the one we used, so it is possible that complexes with multiple αβ-tubulins were overlooked [we initially overlooked TOG2:αβ-tubulin interactions for the same reason (Figure 3.18.)]. Our data also show that the complex formed depends on the relative stoichiometry of TOG domains to αβ-tubulin.

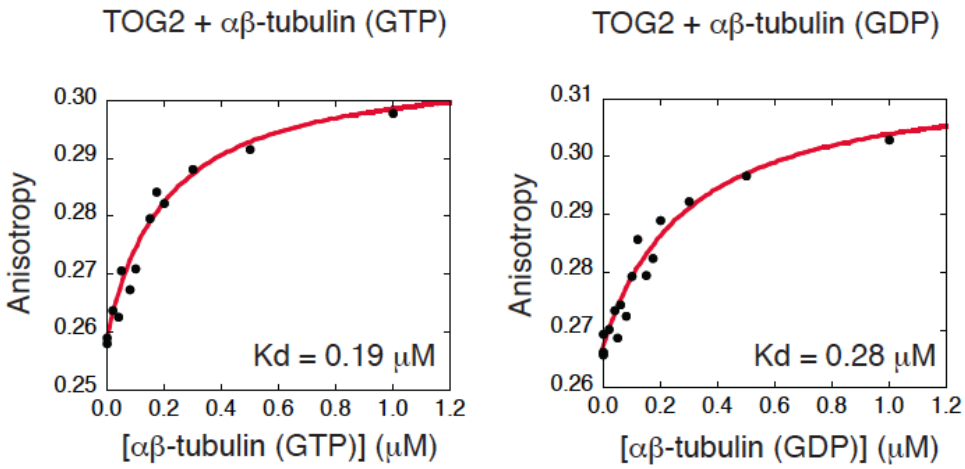

Figure 3.16: TOG2 binds comparably to GTP- and GDP-bound yeast αβ-tubulin

20 nM fluorescently labeled TOG2 was titrated with the indicated amounts of GTP- (left) or GDP-bound (right) αβ-tubulin (black circles). One experiment is shown. Dissociation equilibrium constants (Kd) were calculated by fitting a single-site binding model (see supplemental methods) to the ligand-concentration dependence of the anisotropy (red curves). The nucleotide state of αβ-tubulin has little, if any, effect on TOG2 binding.

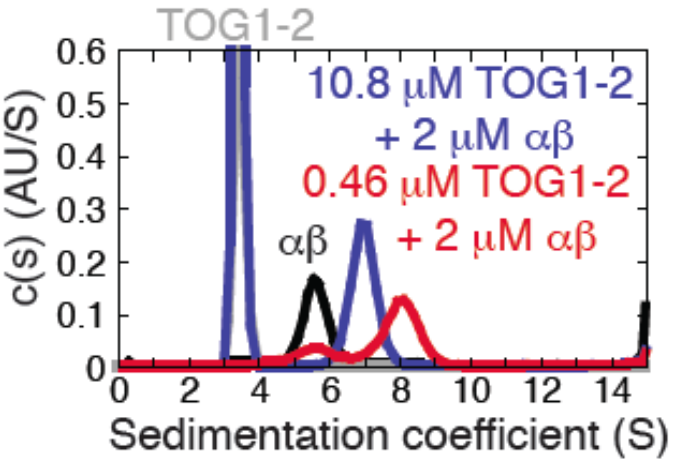

Figure 3.17: TOG1-TOG2 can engage αβ-tubulin with 1:2 TOG1-TOG2:αβ-tubulin stoichiometry

Size distributions showing that substoichiometric concentrations of TOG1-TOG2 mixed with αβ-tubulin (red) behave as a complex that sediments faster than αβ-tubulin alone (black) and the TOG1-TOG2:(αβ)1complex that results when TOGs are in molar excess over αβ-tubulin (blue).

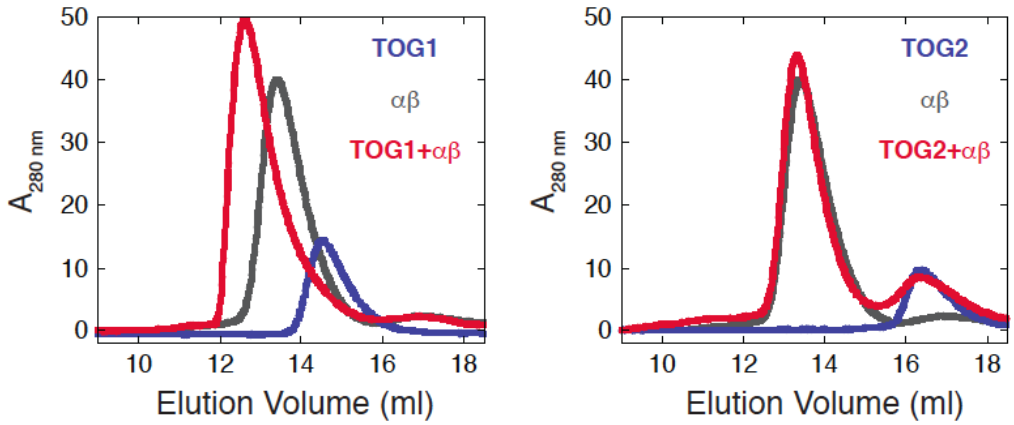

Figure 3.18: Size-exclusion chromatography assay for TOG1 (left panel) or TOG2 (right panel) binding to αβ-tubulin TOG1 and TOG2 domains apparently interact differently with αβ-tubulin in a gel filtration binding assay. Assays were performed using individual proteins at 5 μM concentration.

Discussion

We hypothesize that the structure we determined provides a model for substrate recognition in which TOG1 [which is dispensable for plus-end binding (9)] of microtubule-bound Stu2p would capture unpolymerized subunits and/or stabilize a collision complex through its relatively strong interactions with naturally curved αβ-tubulin (Figure 3.19.). Selective microtubule-end association is presumably the combined effect of a basic region in Stu2p providing microtubule lattice affinity (9) and TOG2 preferentially recognizing an end-specific conformation of αβ-tubulin. We speculate based on the polarity of TOG:αβ-tubulin engagement that the ordering of TOGs and the basic region dictates plus-end specificity. For TOG2 and the C-terminal basic domain to jointly mediate plus-end recognition, they must be able to engage the microtubule in a way that allows TOG2 to bind non straight αβ-tubulins at the very end and the basic region to simultaneously contact surfaces deeper in the polymer. This can only occur at the plus end. The conformational straightening in αβ-tubulin that accompanies lattice incorporation will result in lower-affinity TOG1 interactions (Figure 3.19.). In this hand-off mechanism, polymer incorporation and release of TOG1 for a subsequent round of capture would be intrinsically coupled by virtue of the conformational preferences of TOG1. Hand-off will become efficient only when TOG1 is tethered to free αβ-tubulin binding sites at the end of the microtubule; this explains the requirement for at least two TOGs (23), as well as why isolated TOG1 or TOG2 inhibits microtubule assembly despite functioning to promote assembly when part of Stu2p.

Collectively, our observations indicate that Stu2p/XMAP215 family proteins use conformation selective TOG:αβ-tubulin interactions to discriminate between unpolymerized and polymerized forms of αβ-tubulin. By extension, this result suggests that assembly dependent conformational change in αβ-tubulin plays an important role in dictating microtubule polymerization dynamics.

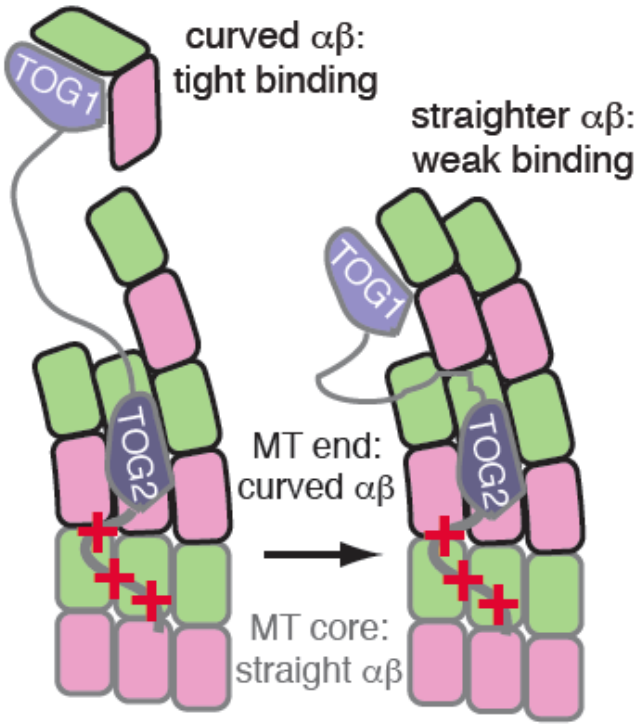

Figure 3.19: Minimal cartoon model illustrating how conformation-selective TOG:αβ-tubulin interactions contribute to function. "+++" denotes a basic region that provides microtubule affinity. TOG1 can efficiently capture unpolymerized αβ-tubulin in its naturally curved state (left), but binds less tightly to straight/straighter conformations of αβ-tubulin in the microtubule (right). TOG2 may also recognize a non-straight conformation of αβ-tubulin at the plus end of the MT.

REFERENCES

1. Johnson V, Ayaz P, Huddleston P, & Rice LM (2011) Design, overexpression, and purification of polymerization-blocked yeast alphabeta-tubulin mutants. *Biochemistry* 50(40):8636-8644.
2. Minor W, Cymborowski M, Otwinowski Z, & Chruszcz M (2006) HKL-3000: the integration of data reduction and structure solution--from diffraction images to an initial model in minutes. *Acta crystallographica. Section D, Biological crystallography* 62(Pt 8):859-866.
3. Adams PD, *et al.* (2010) PHENIX: a comprehensive Python-based system for macromolecular structure solution. *Acta crystallographica. Section D, Biological crystallography* 66(Pt 2):213-221.
4. Ravelli RB, *et al.* (2004) Insight into tubulin regulation from a complex with colchicine and a stathmin-like domain. *Nature* 428(6979):198-202.
5. Lowe J, Li H, Downing KH, & Nogales E (2001) Refined structure of alpha beta-tubulin at 3.5 A resolution. *Journal of molecular biology* 313(5):1045-1057.
6. Slep KC & Vale RD (2007) Structural basis of microtubule plus end tracking by XMAP215, CLIP-170, and EB1. *Molecular cell* 27(6):976-991.
7. Al-Bassam J, Larsen NA, Hyman AA, & Harrison SC (2007) Crystal structure of a TOG domain: conserved features of XMAP215/Dis1-family TOG domains and implications for tubulin binding. *Structure* 15(3):355-362.

8. Emsley P, Lohkamp B, Scott WG, & Cowtan K (2010) Features and development of Coot. *Acta crystallographica. Section D, Biological crystallography* 66(Pt 4):486-501.

9. Al-Bassam J, van Breugel M, Harrison SC, & Hyman A (2006) Stu2p binds tubulin and undergoes an open-to-closed conformational change. *The Journal of cell biology* 172(7):1009-1022.

10. Kosco KA*, et al.* (2001) Control of microtubule dynamics by Stu2p is essential for spindle orientation and metaphase chromosome alignment in yeast. *Molecular biology of the cell* 12(9):2870-2880.

11. Wang PJ & Huffaker TC (1997) Stu2p: A microtubule-binding protein that is an essential component of the yeast spindle pole body. *The Journal of cell biology* 139(5):1271-1280.

12. Aldaz H, Rice LM, Stearns T, & Agard DA (2005) Insights into microtubule nucleation from the crystal structure of human gamma-tubulin. *Nature* 435(7041):523-527.

13. Rice LM, Montabana EA, & Agard DA (2008) The lattice as allosteric effector: structural studies of alphabeta- and gamma-tubulin clarify the role of GTP in microtubule assembly. *Proceedings of the National Academy of Sciences of the United States of America* 105(14):5378-5383.

14. Nogales E & Wang HW (2006) Structural mechanisms underlying nucleotide-dependent self-assembly of tubulin and its relatives. *Current opinion in structural biology* 16(2):221-229.

15. DeLano WL & Lam JW (2005) PyMOL: A communications tool for computational models. *Abstr Pap Am Chem S* 230:U1371-U1372.

16. des Georges A*, et al.* (2008) Mal3, the Schizosaccharomyces pombe homolog of EB1, changes the microtubule lattice. *Nature structural & molecular biology* 15(10):1102-1108.

17. Schuck P (2000) Size-distribution analysis of macromolecules by sedimentation velocity ultracentrifugation and lamm equation modeling. *Biophysical journal* 78(3):1606-1619.

18. Schuck P, Perugini MA, Gonzales NR, Howlett GJ, & Schubert D (2002) Size-distribution analysis of proteins by analytical ultracentrifugation: strategies and application to model systems. *Biophysical journal* 82(2):1096-1111.

19. T. M. Laue BDS, R. M. Ridgeway, S. L. Pelletier (1992) *Analytical Ultracentrifugation in Biochemistry and Polymer Science* (The Royal Society of Chemistry, Cambridge).

20. Dam J & Schuck P (2005) Sedimentation velocity analysis of heterogeneous protein-protein interactions: sedimentation coefficient distributions c(s) and asymptotic boundary profiles from Gilbert-Jenkins theory. *Biophysical journal* 89(1):651-666.

21. Brouhard GJ*, et al.* (2008) XMAP215 is a processive microtubule polymerase. *Cell* 132(1):79-88.

22. Buey RM, Diaz JF, & Andreu JM (2006) The nucleotide switch of tubulin and microtubule assembly: a polymerization-driven structural change. *Biochemistry* 45(19):5933-5938.

23. Widlund PO*, et al.* (2011) XMAP215 polymerase activity is built by combining multiple tubulin-binding TOG domains and a basic lattice-binding region. *Proceedings of the National Academy of Sciences of the United States of America* 108(7):2741-2746.

CHAPTER FOUR

CONCLUSIONS AND FUTURE DIRECTIONS

Summary of this work

In summary, we presented robust methods for identifying and purifying mutant αβ-tubulins, including mutants that would otherwise be lethal when constitutively expressed. The mutants with blocked assembly interfaces that we developed represent unique reagents that would allow us to utilize experimental approaches that were previously disregarded because of the difficulties arising from the self-assembly tendency of αβ-tubulin heterodimers. These blocked mutants we developed appear to behave as specific competitive inhibitors of polymerization, and using them in functional assays would allow us study mechanisms underlying microtubule polymerization dynamics and mechanisms of interactions with regulatory proteins.

We used the plus end polymerization blocked αβ-tubulin to solve the crystal structure of the TOG1 domain of Stu2p in complex with yeast αβ-tubulin. Our structure and further biophysical characterizations of the complex provided a model for how TOG-containing polymerases discriminate between unpolymerized and polymerized forms of αβ-tubulin and how they selectively recognize the growing end of the microtubule. We made four observations that have implications for the mechanisms by which Stu2p/XMAP215 proteins promote microtubule assembly: (i) TOG1 makes substantial contacts with both α- and β-tubulin, binding in a way that apparently excludes equivalent

binding of a TOG2 domain to the same heterodimer, and a TOG1-TOG2 construct can bind to αβ-tubulin with 1:2 stoichiometry (ii) the TOG1-interacting surfaces on αβ-tubulin are distinct from those involved in microtubule assembly contacts, (iii) the conformation of GTP-bound αβ-tubulin is curved in the TOG1 complex, TOG2 binds to GTP- or GDP–bound αβ-tubulin with approximately equal affinity, and (iv) the TOG1 and the TOG2 domains from Stu2p can preferentially bind to a curved form of αβ-tubulin.

These observations reveal that conformation-selective TOG:αβ-tubulin interactions provide a mechanism to explain how Stu2p/XMAP215 family proteins discriminate between unpolymerized and polymerized forms of αβ-tubulin and how they capture free subunits and hand them off to the MT. We hypothesize that TOG1 of microtubule-bound Stu2p would capture unpolymerized αβ-tubulin in solution through its relatively strong interactions with naturally curved αβ-tubulin (Figure 3.19.). Microtubule-end association is presumably carried out by the combined effect of a basic region in Stu2p providing microtubule lattice affinity and TOG2 preferentially recognizing an end-specific conformation of αβ-tubulin. Then, the allosteric effects of lattice incorporation results in the straightening of the αβ-tubulin, thus lower-affinity αβ-tubulin:TOG1 interactions for the release of TOG1 for a subsequent round of capture.

New questions

Our new understanding of the TOG:αβ-tubulin interactions lead to new questions on MT plus end recognition and on assembly promotion by Stu2p/XMAP215 family of proteins. For instance, what conformation is TOG2 recognizing at the MT plus end, is it a different end-specific conformation of αβ-tubulin or is it a curved conformation similar to what TOG1 recognizes? Furthermore, our results showed that a construct of TOG1-TOG2 could engage 2 αβ-tubulins (Figure 3.17), is that interaction cooperative? If the interactions are in fact cooperative, are the αβ-tubulin interactions longitudinal or lateral? Does the length of the linker connecting TOG1 and TOG2 have an effect on cooperativity or some other function of Stu2p? We also demonstrated that the two TOG domains are biochemically similar in their interaction with αβ-tubulin. For example, they both preferentially bind to a curved conformation of αβ-tubulin with similar affinities (Figure 3.12. 3.13. 3.14. 3.16), and in vivo rescue assays and spindle length assays showed that mutating equivalent residues of TOGs on the αβ-tubulin binding surface resulted in similar phenotypes (Figure 3.6.). i.e. mutating R200 that we know to be essential for binding results in a severe growth phenotype as well as mutating R519 the TOG2 equivalent. This suggests that both TOGs bind to αβ-tubulin using the same surface. So, why are there two different types of them?

Plans and preliminary results

Crystallization of TOG1-TOG2:($\alpha\beta$-tubulin)$_2$ complex

We previously showed that both TOGs in the TOG1-TOG2:($\alpha\beta$-tubulin)$_2$ complex can engage their own $\alpha\beta$-tubulin (Figure 3.17.). Solving a structure of this complex could allow us to answer several of the questions we presented above, however our efforts to crystallize the $\alpha\beta$-tubulin:TOG1-TOG2 complex were not successful so far. One of the main problems had arisen from the proteolysis of the TOG1-TOG2 construct in the crystallization screens and resulted in crystals only containing $\alpha\beta$-tubulin bound to a single TOG domain (data not shown). To overcome this, future crystallization trials will be performed in the presence of protease inhibitors. We also think that the 70-residue long flexible disordered linker connecting the TOG1 and the TOG2 domains might be disruptive for crystal formation. Therefore, we will pursue our crystallization trials using TOG1-TOG2 constructs with shorter linkers (Figure 4.3.).

Are TOG1-TOG2:($\alpha\beta$-tubulin)$_2$ interactions cooperative?

It is likely that in a TOG1-TOG2:($\alpha\beta$-tubulin)$_2$ complex tubulin:tubulin interactions would make this complex form cooperatively. This actually could represent a mechanism for promoting MT assembly. It is worth pointing out that our in vitro binding experiments described previously made use of a plus end polymerization blocked mutant of $\alpha\beta$-tubulin that we designed to prevent MT self-assembly during the AUC runs (Figure 3.17.). It is possible that the polymerization blocking mutation could interfere

with the tubulin:tubulin interactions in the TOG1-TOG2:(αβ-tubulin)$_2$ complex and in return interfere with the formation of the complex with which we aim to study cooperativity (Figure 4.2.).

Working at 230nm in our AUC experiments will allow us to work at low protein concentrations

αβ-tubulins self-assemble in a concentration dependent manner, therefore working at lower αβ-tubulin concentrations could prevent simultaneous formation of αβ-tubulin:αβ-tubulin dimers. However, decreasing the αβ-tubulin concentrations in our AUC experiments would result in difficulties of detecting the proteins at 280nm. Therefore we proposed to use 230nm for protein detection to ensure the usage of lower protein concentrations in our AUC experiments. To test the reliability of usage of 230nm for protein detection we ran samples of αβ-tubulin (1.3μM), TOG1(3μM) and TOG1-TOG2 (1.8 μM) in the AUC (Figure 4.1.). In this test run at 230nm the corresponding noise levels were calculated to be 0.007 AU. This result suggests that we can work with protein concentrations of 0.1μM or even lower and still achieve sufficient signal. With this experimental setup we are going to be able to not only work at lower αβ-tubulin concentrations to prevent simultaneous self-assembly but we also will consume significantly less amount of protein in the experiments.

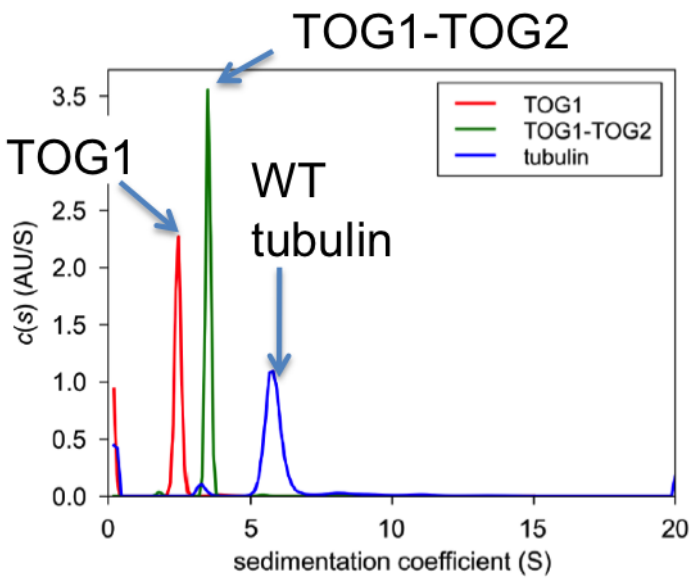

Figure 4.1: AUC runs of TOG1, TOG1-TOG2 and WT αβ-tubulin using 230nm for protein detection.

We will conduct TOG1-TOG2:αβ-tubulin titration experiments to study cooperativity

To study the cooperativity of the TOG1-TOG2:$(\alpha\beta\text{-tubulin})_2$ complex we will conduct titration experiments using AUC. Designing the titration experiment is challenging since introducing excess TOG domain results in the dissociation of the 1:2 complex (Figure 3.17.), therefore we aim to collect most of the titration points in a substochiometric mixture concentration region where the complex is most sensitive to cooperativity keeping the αβ-tubulin concentration constant at 0.3μM (around TOG binding Kd). Our initial AUC experiments showed that this region probably is within a factor of 2 to 3 of equimolar (Figure 3.17. and data not shown). Once the AUC titration assay is conducted a model of cooperativity will be fit to the sedimentation data.

The AUC assay could also be used to determine whether αβ-tubulins in the TOG1-TOG2:$(\alpha\beta\text{-tubulin})_2$ complex interact longitudinally or not. In the AUC the kinetics, the apparent affinity and the cooperativity of the complex should differ when polymerization blocked αβ-tubulin is used instead of wild type if the tubulins interact longitudinally (Figure 4.2.).

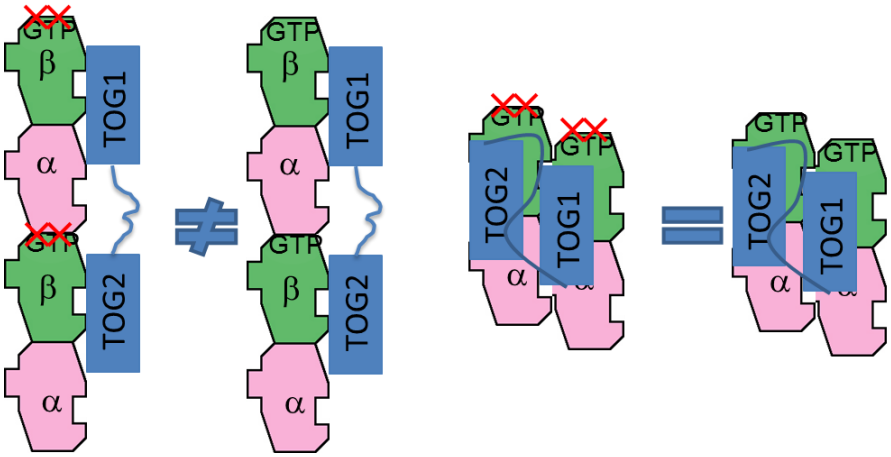

Figure 4.2: In AUC the kinetics/apparent affinity/cooperativity of the complex should look different when used polymerization blocked αβ-tubulin if tubulin:tubulin interactions are longitudinal.

Does length of the unstructured linker connecting TOG1 and TOG2 matter for binding αβ-tubulin?

The AUC cooperativity assay could also be used to determine whether changes in the linker length affect cooperativity, or not. To design the TOG1-TOG2 mutants with a shorter linker we analyzed the linker connecting TOG1 and TOG2 domains with multiple sequence alignment (1, 2) (Figure 4.3.). The sequence alignment did not show any significant conserved sequences. It is also notable that the length of this linker varies among species, for instance Xmap215 has a 43-residue linker, Zyg9 has 52 and Stu2p has 70. However, a predicted α-helical secondary structure is highlighted in all of the sequences we used for the multiple sequence alignment (3). This α-helical region is also visible in our structure (Figure 3.1.). While designing our shorter linker mutants we tried to avoid the removal of this helical region in our Δ14 Δ22 Δ32 deletion constructs, but in the Δ40 Δ50 Δ60 constructs this region is removed as well (Figure 4.3.).

We are also working creating constructs with longer linkers; however we do not yet have any TOG1-TOG2 constructs with longer connecting linkers.

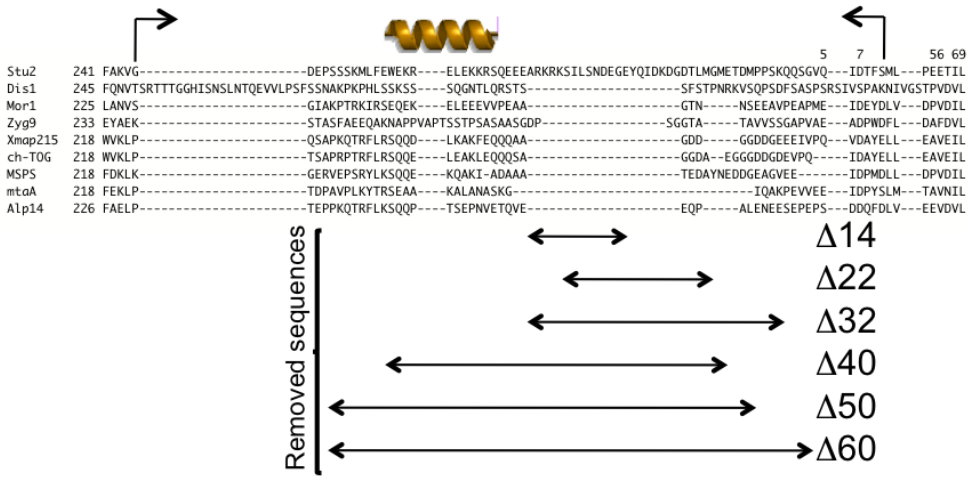

Figure 4.3: Multiple sequence alignment of the linker connecting TOG1 and TOG2

The sequence allignment shown no significant sequence conservation in the linker region. Arrows indicate the sequence corresponding to the linker and the predicted α–helical secondary structure is marked. The removed sequences to create the shorter linker mutants of TOG1-TOG2 is marked with two-headed arrows.

Shortening the linker connecting TOG1 and TOG2 impairs growth in the yeast rescue assays

Yeast (4) was transformed with the rescue plasmids (5) containing the wild type and mutant Stu2p coding sequences and spotted on inducing ($CoSO_4$) and non-inducing plates. The Stu2p coding sequence also contains an additional deletion mutation (ΔCC) at the dimerizing region to prevent homodimer formation so that cross-communication of the TOG domains of the different arms could be avoided. Copper causes the depletion of the endogenous Stu2p and the only copy of the protein should be the mutated form that is introduced via the plasmids.

Only the ΔCC Δ14 mutant rescued as well as the plasmid coding for the wild type Stu2p did and rest showed defective growth phenotypes where, ΔCC Δ60 mutant showed the most severe growth defect among all (Figure 4.4.). Shortening the linker between TOG1 and TOG2 in fact disrupted the Stu2p function in vivo. This observation could be further analyzed by looking at how shortening the linker affects the spindle lengths in yeast in vivo or the MT polymerase function in vitro.

From a practical point of view this assay also suggests candidates to use in crystallization trials to solve a structure of the TOG1-TOG2:αβ-tubulin complex as mentioned earlier in this chapter. Δ14 and Δ22 mutants of TOG1-TOG2 construct should be the most promising candidates to this end.

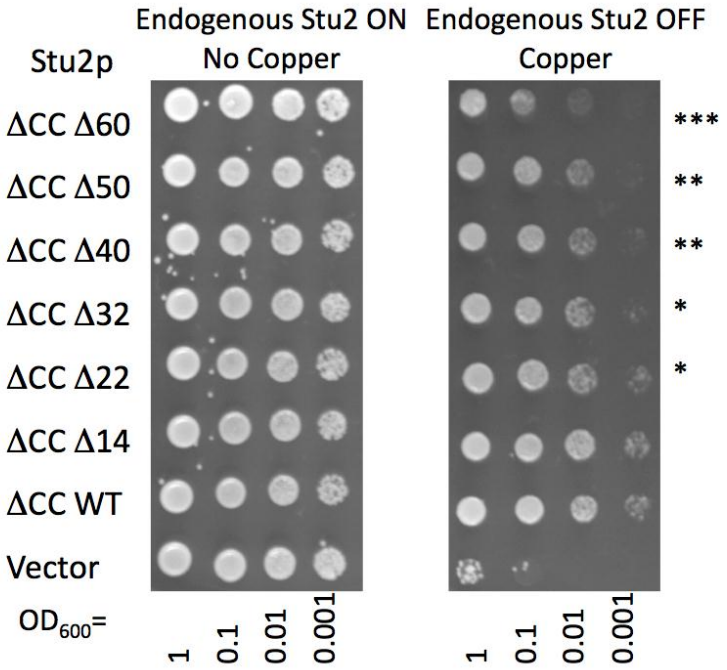

Figure 4.4: In vivo rescue assay to screen the shorter linker Stu2p mutants.

Left panel shows the control plate where the endogenous Stu2p is present to ensure uniform loading. In the right plate the endogenous Stu2p is depleted and shorter linker mutants of Stu2p is screened for rescue. Stars indicate the severity of the growth defect phenotype.

Does Stu2p/XMAP215 family of proteins require different TOG domains to function?

We have previously shown that TOG1 and TOG2 domains of Stu2p are biochemically very similar to each other in their interactions with αβ-tubulin (Chapter 3). They both preferentially bind to the curved MT incompatible form of αβ-tubulin with similar affinities. The in vivo rescue assay showed that mutating equivalent residues of TOGs on the αβ-tubulin-binding surface resulted in similar growth defect phenotypes. i.e. R200 that is shown to be essential for αβ-tubulin binding resulted in a severe growth phenotype as well as the R519 the TOG2 equivalent. This suggested that both TOGs bind to αβ-tubulin using the same surface. However, using size exclusion chromatography binding assays we were able to observe the TOG1:αβ-tubulin complex but we could not observe the TOG2:αβ-tubulin complex. This result suggests that the binding kinetics of the complexes is probably different. But the question is: does it matter? So, we planned to make several domain swap mutants and test them for function to start answering this question (Figure 4.5.).

These mutations could be introduced to full length Stu2p as well as the shorter constructs. αβ-tubulin binding properties of domain swap constructs including only the TOG1-TOG2 region could be studies using AUC binding assays. This should allow us to study the effects on cooperativity, the kinetics and apparent affinity of the αβ-tubulin complex formation. Then, domain swap mutants of longer and full length Stu2p could be used in functional assays such as the in vivo rescue assay and yeast spindle length assays as well as the in vitro MT assembly assays to study MT polymerase function.

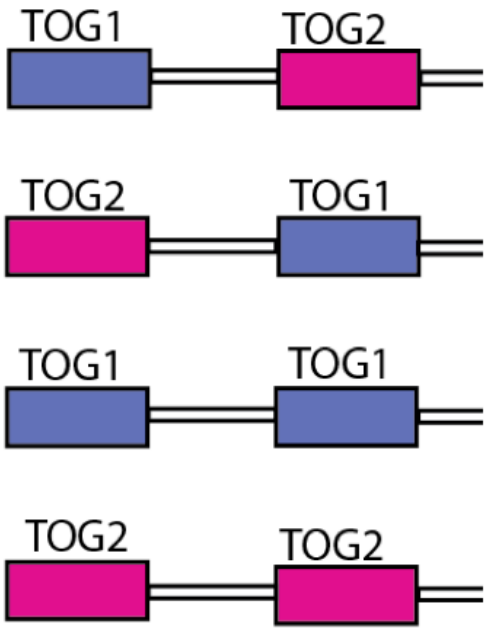

Figure 4.5: The domain swap constructs will allow us to study whether two distinct TOG domains are necessary or not.

The figure only shows the TOG1-TOG2 region of the Stu2p, however these mutations could be introduced to full length protein as well as the shorter constructs to study in vivo or in vitro effects of the domain swap.

Concluding remarks

In this work we first introduce the polymerization blocked mutants of αβ-tubulins that we developed as unique tools for biochemical studies of αβ-tubulins to avoid the difficulties that has arisen from the self-assembly tendency of tubulins. Then we use our plus end polymerization blocked αβ-tubulin to study αβ-tubulin TOG domain interaction and we propose a mechanism to explain how Stu2p/XMAP215 family protein discriminate between unpolymerized and polymerized forms of αβ-tubulin and how they capture free subunits and hand them off to the growing end of the MT. Our results lead to a new understanding of the TOG:αβ-tubulin interactions that in return raised new questions on MT plus end recognition and on assembly promotion by Stu2p/XMAP215 family of proteins. We proposed in vitro and in vivo biochemical experiments to answer these questions and we supported our plans with preliminary results.

The completed work presented in this dissertation was mainly focused on explaining TOG:αβ-tubulin interactions and answering the new questions presented should then allow us to explain how these TOG domains work together to achieve the polymerization function of Stu2p.

REFERENCES

1. Pei J & Grishin NV (2007) PROMALS: towards accurate multiple sequence alignments of distantly related proteins. *Bioinformatics* 23(7):802-808.
2. Pei J, Kim BH, Tang M, & Grishin NV (2007) PROMALS web server for accurate multiple protein sequence alignments. *Nucleic acids research* 35(Web Server issue):W649-652.
3. Jones DT (1999) Protein secondary structure prediction based on position-specific scoring matrices. *Journal of molecular biology* 292(2):195-202.
4. Kosco KA, *et al.* (2001) Control of microtubule dynamics by Stu2p is essential for spindle orientation and metaphase chromosome alignment in yeast. *Molecular biology of the cell* 12(9):2870-2880.
5. Wang PJ & Huffaker TC (1997) Stu2p: A microtubule-binding protein that is an essential component of the yeast spindle pole body. *The Journal of cell biology* 139(5):1271-1280.

NOTES ON CONTRIBUTIONS

Among the results presented at chapter 3 Dr. Vinu Johnson prepared the negative stain electron micrograph from wild type yeast αβ-tubulin. He worked on the design and cloning of the plus end blocked αβ-tubulin mutants and he and I did the comparative gel filtration chromatography experiments using animal, yeast αβ-tubulin and the plus end blocked mutant of yeast αβ-tubulin (LR1). He prepared the fluorescence micrographs showing MT assembly stimulation by Mal3, and disruption of MT assembly by the plus end blocked mutant of αβ-tubulin (LR1). He performed the phenotypical assays on Tub2 and MT spindown assays using the plus end blocked αβ-tubulin (LR1). He also performed the GTP binding assays.

Patrick Huddleston performed the MT assembly experiment to calculate the critical concentration for MT assembly.

I worked on the design and cloning of the minus end blocked αβ-tubulin mutants. I performed the TOG1 gel filtration binding experiments using WT, plus end and minus end blocked mutants of αβ-tubulin. I also performed the phenotypical assays on Tub1 and MT spindown assays using the minus end blocked αβ-tubulin (LR5). I did the comparative CD experiments using wild type and plus end blocked αβ-tubulin.